iScience

CellPress
OPEN ACCESS

Article

Virtual metabolic human dynamic model for pathological analysis and therapy design for diabetes

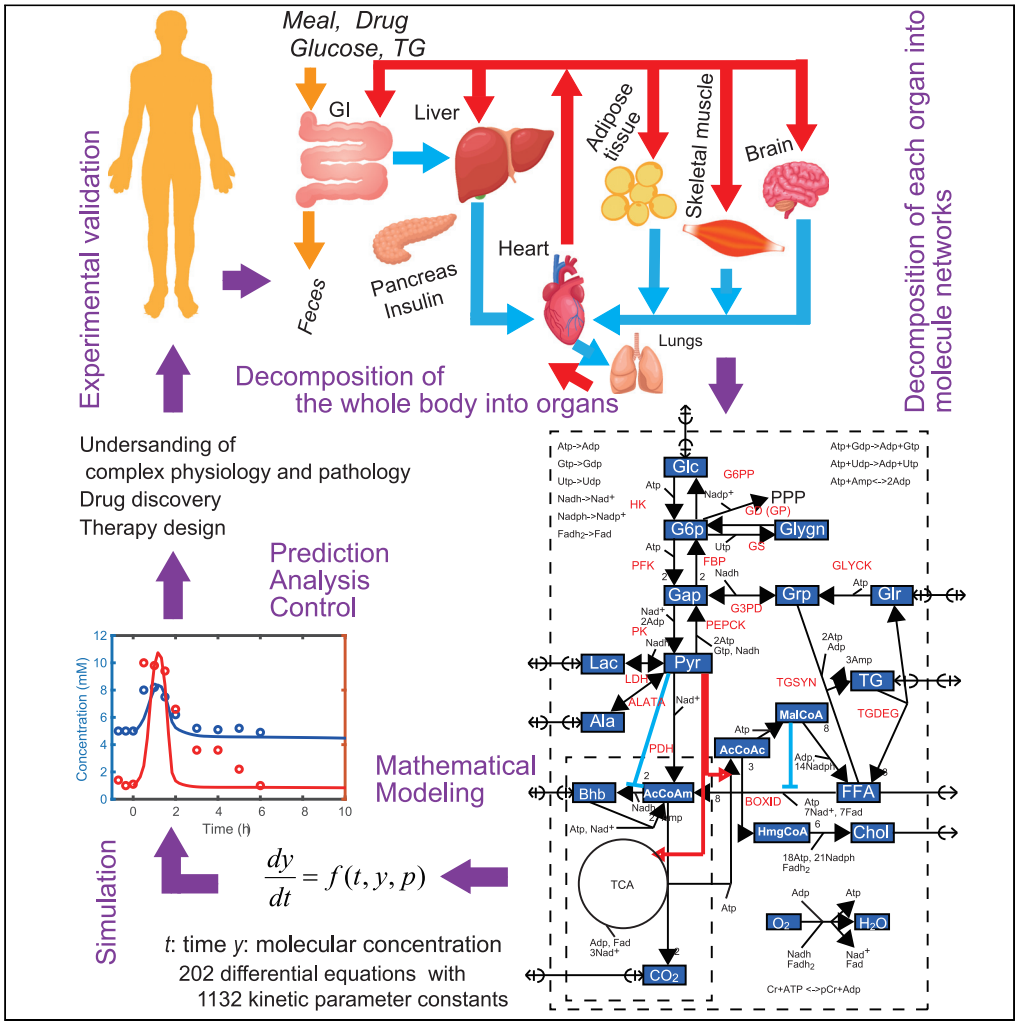

Hiroyuki Kurata

kurata@bio.kyutech.ac.jp

HIGHLIGHTS

A standard of virtual metabolic human dynamic models is proposed

It integrates the three scales of molecules, organs, and whole body

It gets insight into pathological mechanisms of type 1 and type 2 diabetes

It enables the computer-aided design of medication treatment for diabetes

Kurata, iScience 24, 102101
February 19, 2021
https://doi.org/10.1016/j.isci.2021.102101

iScience

CellPress
OPEN ACCESS

Article

Virtual metabolic human dynamic model for pathological analysis and therapy design for diabetes

Hiroyuki Kurata[1,2,*]

SUMMARY

A virtual metabolic human model is a valuable complement to experimental biology and clinical studies, because *in vivo* research involves serious ethical and technical problems. I have proposed a multi-organ and multi-scale kinetic model that formulates the reactions of enzymes and transporters with the regulation of hormonal actions at postprandial and postabsorptive states. The computational model consists of 202 ordinary differential equations for metabolites with 217 reaction rates and 1,140 kinetic parameter constants. It is the most comprehensive, largest, and highly predictive model of the whole-body metabolism. Use of the model revealed the mechanisms by which individual disorders, such as steatosis, β cell dysfunction, and insulin resistance, were combined to cause diabetes. The model predicted a glycerol kinase inhibitor to be an effective medicine for type 2 diabetes, which not only decreased hepatic triglyceride but also reduced plasma glucose. The model also enabled us to rationally design combination therapy.

INTRODUCTION

Virtual metabolic human is an attractive goal for synthetic biology, systems biology, and bioinformatics, which greatly contributes to advances in medicine and life science. Many scientists have raised its concepts and have been developing computational frameworks based on genome-scale gene networks and whole-body-scale omics data (Thiele et al., 2013, 2020; Viceconti and Hunter, 2016; Yugi et al., 2014). In 2019, the virtual metabolic human database has been presented to facilitate computational modeling by linking genome-scale networks of human metabolism to diseases and nutrition (Noronha et al., 2019). On the other hand, multi-scale, large-scale dynamic models have been developed to understand human metabolism (Ashworth et al., 2016; Berndt et al., 2018a, 2018b; Berndt and Holzhutter, 2018; Kim et al., 2007; Konig et al., 2012; Li et al., 2010; Sluka et al., 2016).

Metabolism plays a critical role in human health and diseases (Frayn, 2010). Perturbation of genetics and changes in lifestyle habitats, including excessive diet and inactivity, result in the development and progression of complex metabolic diseases, such as hyperglycemia, hyperlipidemia, obesity, non-alcoholic fatty liver disease (Kitade et al., 2017; Xia et al., 2019), and diabetes (Ashcroft and Rorsman, 2012; Perry et al., 2014; Saltiel, 2001; Xia et al., 2019). A systems approach is necessary to elucidate the molecular mechanisms causing such metabolic dysfunctions and to propose the strategies for the prevention and treatment of them (Kitano, 2010). As *in vivo* studies of human metabolism are hampered with serious ethical and technical problems, computational models are required to complement the *in vivo* studies (Eissing et al., 2011; Iyengar et al., 2012; Maldonado et al., 2018).

So far various types of mathematical models have simulated human metabolism. Early models extensively simulated glucose-insulin metabolism to analyze the effect of insulin secretion on glucose homeostasis (Berger and Rodbard, 1989; Cobelli et al., 1984; Insel et al., 1975; Sherwin et al., 1974). Such extensive efforts achieved the Food and Drug Administration-approved computational model that was implemented by the artificial pancreas for type 1 diabetes mellitus (T1DM) (Cobelli et al., 2011; Visentin et al., 2018). Most of the early models used the compartment models that regarded particular metabolites as the representatives responsible for their associated functions such as glycolysis, gluconeogenesis, glycogenolysis, glycogenesis, and triglyceride (TG) synthesis/degradation. Compartment models simulated the

[1]Department of Bioscience and Bioinformatics, Kyushu Institute of Technology, 680-4 Kawazu, Iizuka, Fukuoka 820-8502, Japan

[2]Lead contact

*Correspondence: kurata@bio.kyutech.ac.jp

https://doi.org/10.1016/j.isci.2021.102101

glucagon/insulin-controlled glucose homeostasis by linking the liver to other organ compartments (Hetherington et al., 2012; Pearson et al., 2014) and suggested the mechanisms by which changes in the ratio of carbohydrate to lipid alter hepatic TG synthesis through insulin action and generate different types of diabetes (Hassell Sweatman, 2020; Pratt et al., 2015).

As those compartment models were coarse-grained and not always based on molecular mechanisms, their applications were limited to an understanding of very specific functions according to their purpose. To overcome this limitation, biochemistry-based mechanistic models were constructed that assigned a rate equation to each metabolic reaction within a cell of the liver and skeletal muscle while considering allosteric effectors, enzyme activity regulation, and hormone-dependent reversible phosphorylation (Berndt et al., 2018a; Konig et al., 2012; Li et al., 2010). The kinetics was measured by means of *in vitro* assays. In 2019, Berndt et al. developed a genome-scale, detailed kinetic model of hepatic cells that formulated thousands of enzymes, transporters, and hormone-dependent regulations (Berndt et al., 2018a).

Those biochemistry-based models mainly pay attention to cells of the liver and skeletal muscle, although it is important to consider the rest of the human body because organs are tightly connected with each other through blood (Ashworth et al., 2016; Sluka et al., 2016; Xu et al., 2011). Xu et al. integrated hepatic glycogen regulation with extra-hepatic fuel metabolism after a meal in the whole-body context (Xu et al., 2011). Sluka et al. proposed a liver-centric model for acetaminophen pharmacology and metabolism (Sluka et al., 2016). They integrated three-scale modules of enzyme reactions within a cell, physiologically based pharmacokinetics of acetaminophen at organs, and its distribution at the whole-body level. Ashworth et al. developed a spatial kinetic model of hepatic glucose and lipid metabolism and treated the sinusoidal tissue units instead of the single hepatocyte (Ashworth et al., 2016). They identified critical differences between periportal and pericentral cells, indicating high susceptibility to pericentral steatosis during the development of steatosis. Berndt et al. also presented a dynamic model of the sinusoidal tissue units to suggest that structural properties, enzymatic properties, and regional blood flows are equally important for an understanding of liver functionality (Berndt and Holzhutter, 2018; Berndt et al., 2018b). Kim et al. proposed a whole-body computational model to simulate hormonal control over plasma glucose and TG under a limited condition of physical exercise (Kim et al., 2007). They decomposed the whole body into several organs and assigned each major metabolite within organs to an ordinary differential equation. Palumbo et al. added details of subjects' characteristics to the Kim's model to simulate the effects on personal metabolic homeostasis during exercise (Palumbo et al., 2018).

Construction of whole-body metabolic models has just started. The existing models are fit for specific purposes, which is quite reasonable, but their purposes are relatively limited. A more comprehensive model is required that is applicable to a broad range of functions including pathological analysis and medication. At present a virtual metabolic human model that integrates molecular mechanisms for each organ is highly expected not only to reproduce a variety of physiological and metabolic functions but also to analyze pathology and design therapy while considering side effects. To satisfy these requirements, I have first proposed a virtual metabolic human dynamic model or the multi-organ and multi-scale kinetic model that accurately simulates the dynamics in key metabolites of glucose, lactate, pyruvate, glycerol, alanine, glycogen, free fatty acid (FFA), and TG after a meal. To enhance the accuracy and applicability, the model incorporated nucleotide cofactors that are critically responsible for global regulations and energy balance, while conserving essential reaction pathways of carbohydrates and lipids for each organ. Use of the model revealed the pathological mechanisms by which the individual disorders of steatosis, β cell dysfunction, and insulin resistance (IR) are combined to cause diabetes. The model successfully predicted a glycerol kinase inhibitor to be a new medicine for type 2 diabetes mellitus (T2DM) and enabled us to rationally design combination therapy.

RESULTS

Model construction

A schematic diagram of the whole body is shown in Figure 1. It consists of the blood, pancreas, liver, skeletal muscle, adipose tissue, gastrointestinal (GI) tract, heart, and brain. I constructed the union of all the metabolic networks of the organs based on biochemistry (see Methods), as shown Figure 2. All the organ metabolic networks except the pancreas were built by selecting organ-specific reactions from the union network (Figure S1). The pancreas module was simplified as the controller that releases insulin in response to a change in plasma glucose. The insulin kinetics is given by Equations (S3–S6 and S220 in Data S1). The

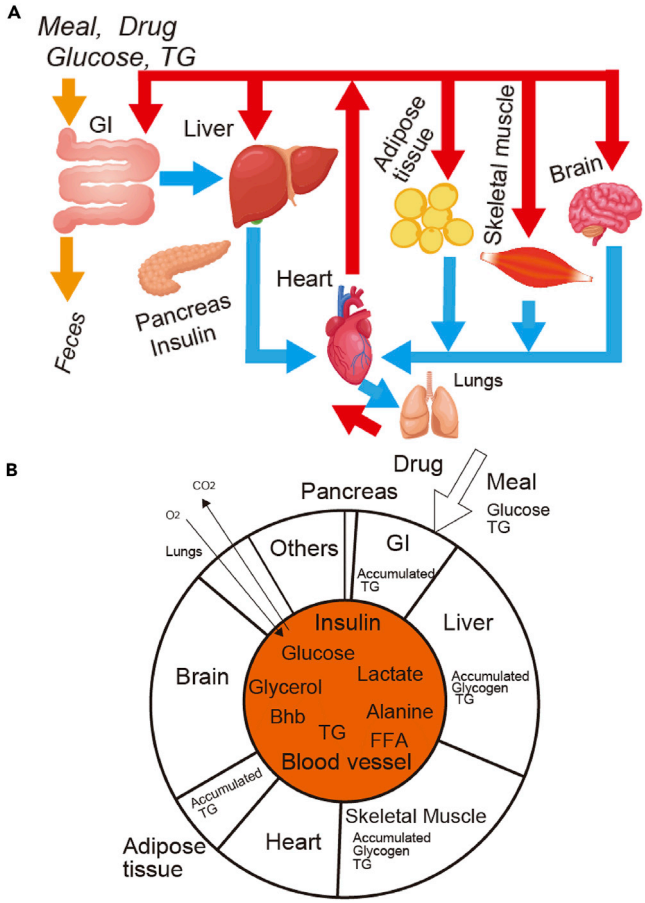

Figure 1. Schematic diagram of the human whole-body metabolism

(A) Realistic multi-organ model. The red and blue arrows indicate arterial and venous blood flows, respectively.

(B) Perfect mixing model of the whole-body metabolism.

Oxygen and carbon dioxide concentrations are assumed to be constant in the whole body, thus the kinetic model excludes the gas exchange in the lungs. The slice portion indicates the energy budget consumed by each organ at postabsorptive state.

values of the kinetic parameters were adjusted to reproduce the experimental insulin secretion rate (Figure S2) and the insulin response with respect to plasma glucose (Figure S3). The glucagon kinetics is given by Equations (S12–S16), assuming that the glucagon kinetics is opposite to the insulin kinetics (Vance et al., 1968). The glucagon response to plasma glucose was well reproduced (Figure S4). I built the kinetic models of the other organs, and then assembled them, as shown in Methods. The resultant kinetic model consists of 202 ordinary differential equations for metabolites with 217 reaction rates and 1,140 kinetic parameter constants, as shown in Data S1 (Equations (S1–S421)), Tables S1, and S2. Abbreviations of the kinetic parameter constants are defined in Table S3.

Experimental model validation under healthy condition

The proposed kinetic model simulated the time course of plasma insulin, plasma glucose, plasma lactate, plasma glycerol, plasma FFA, and plasma TG and liver/skeletal muscle glycogen after an overnight fast and following a single meal, as shown in Figures 3A–3C. The simulated results were mostly consistent with the clinical data of multiple healthy subjects (Bickerton et al., 2008; Frayn, 2010; Frayn et al., 1993; Meyer et al., 2002; Taylor et al., 1996). The simulated plasma glucose concentration increased to a peak around 60 min, and then decreased to approximately 5 mM. An increase in plasma glucose triggered the insulin secretion from the pancreas to enhance the uptake of plasma glucose by the organs of liver, skeletal muscle, GI, and adipose tissue. The plasma insulin concentration rapidly increased to a peak, which was caused by an

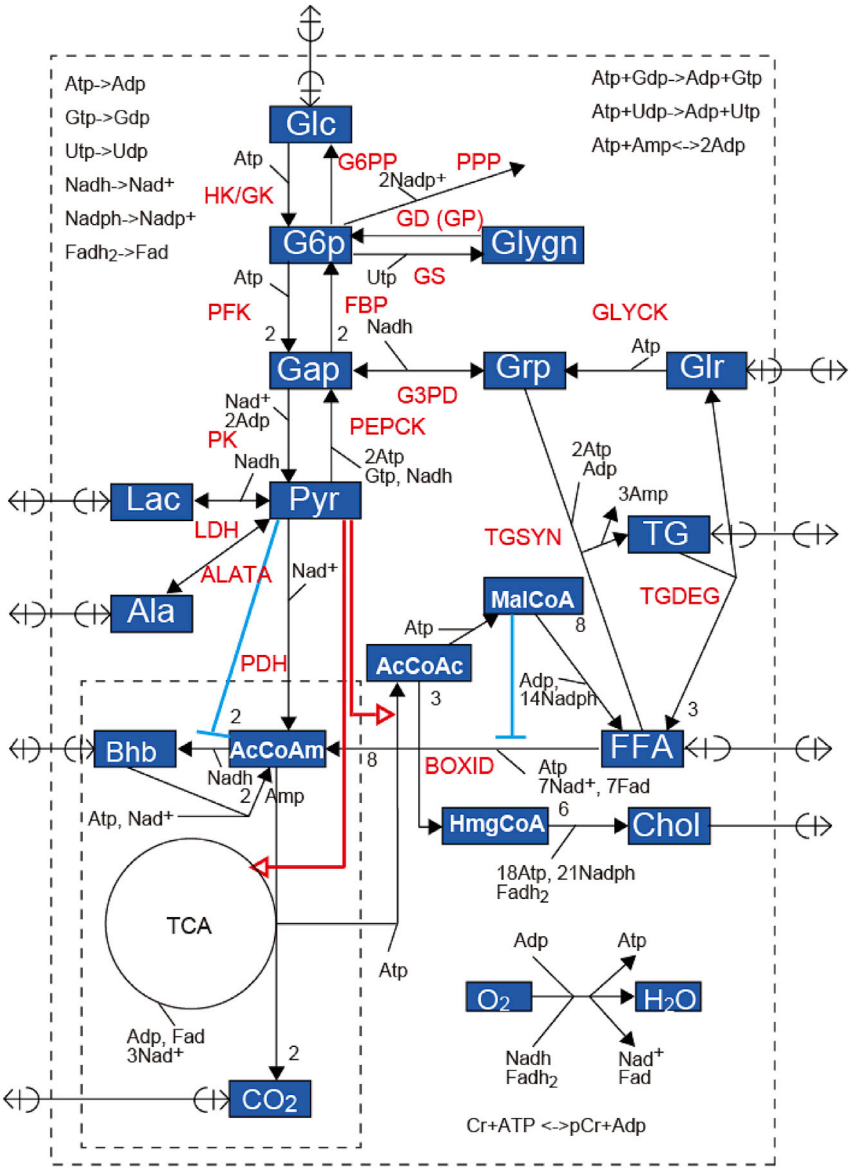

Figure 2. Union map of all organ metabolic networks

increase in plasma glucose, and then decreased with a decrease in plasma glucose. Plasma lactate increased to a peak after the meal and then decreased, as indicated by Frayn et al. (1993). The simulated plasma glycerol was kept to be low, as indicated by the experimental data (Meyer et al., 2002). Plasma FFA decreased after the meal, showing a dump, and then gradually increased, as indicated by Frayn et al. (1993). The dump may be caused by the decreased FFA release from the adipose tissue into blood, which results from the insulin-induced TG synthesis in the adipose tissue. Plasma TG, ingredient of chylomicrons slowly increased after a meal, and then decreased, as indicated by the experimental data (Bickerton et al., 2008; Karpe et al., 1992). In the liver and skeletal muscle, the glycogen concentrations increased due to insulin action after a meal, as shown by the experimental data (Taylor et al., 1996). And then liver glycogen was degraded into glucose (glyocogenolysis), which was released into blood. Skeletal muscle glycogen remained to be degraded, as suggested by Jensen et al. (2011).

As shown in Figure 3D, the simulated exchange fluxes between each organ and blood at postabsorptive state were consistent with the experimental data (Kim et al., 2007). The skeletal muscle released alanine and lactate; the adipose tissue released glycerol and lactate. The skeletal muscle and adipose tissue

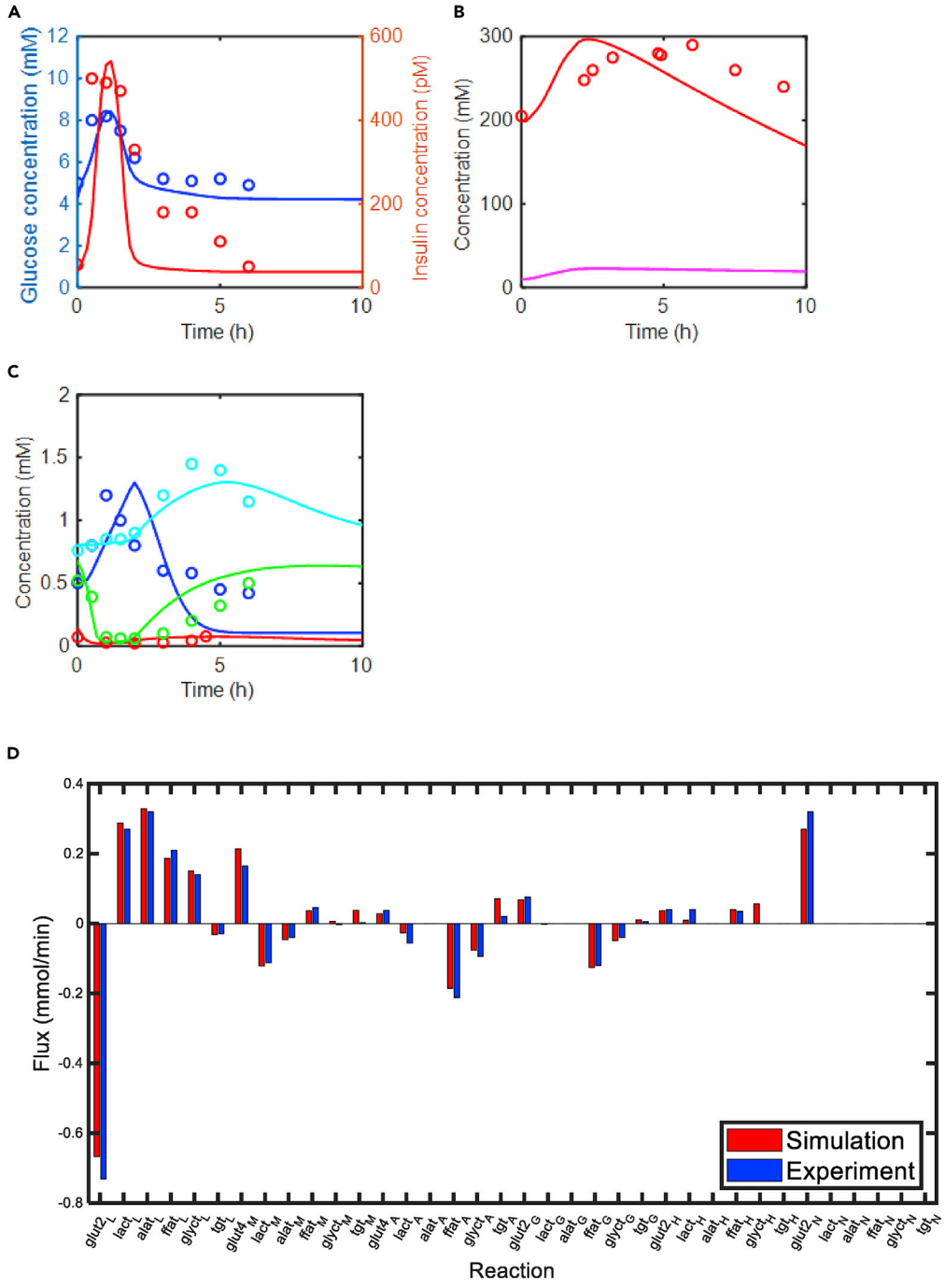

Figure 3. Experimental validation of the virtual metabolic human dynamic model

(A–C) Time course of key metabolite concentrations after an overnight fast and following a single meal of 87 g carbohydrate and 33 g fat. The circles and lines indicate the experimental and simulated concentrations, respectively. (A) Plasma glucose (blue); plasma insulin (red). (B) Liver glycogen (red); skeletal muscle glycogen (magenta) (no experimental data). (C) Plasma lactate (blue); plasma FFA (green); plasma TG (cyan); plasma glycerol (red).

(D) Transport/exchange fluxes at postabsorptive state between blood and each organ. The red and blue bars indicate the simulated and experimental fluxes, respectively.

converted a part of the utilized glucose into lactose and released it into blood. The liver utilized the three carbon metabolites of lactate, glycerol, and alanine to synthesize glucose (gluconeogenesis) and released it into blood. I confirmed that the liver took up glycerol to convert it into glyceraldehyde-3-phosphate (Gap) through glycerol 3-phosphate (Grp), or that plasma glycerol is used for gluconeogenesis (Figure S5). Thus, the computational model well reproduced the glucose-lactate/glycerol/alanine cycles. The liver synthesized TG, and then released it into blood. The heart utilized glucose, lactate, and FFA. The GI took up plasma glucose and degraded stored TG into plasma FFA and glycerol. The adipose tissue took up plasma glucose and TG; it released lactate, FFA, and glycerol. Plasma TG was utilized mainly by the adipose tissue. The brain exclusively utilized plasma glucose.

Model validation under healthy and diseases conditions

To further validate the dynamic model, I compared the simulated results with the experimental data under healthy and diseases (IR and T2DM) conditions (the IR and T2DM are defined in Methods). As shown in Figure S6, the computational model reproduced the time course of plasma glucose, insulin, β-hydroxybutyrate (Bhb), FFA, and TG for healthy subjects and subjects with IR. The model captured the experimental features (Bickerton et al., 2008): (1) IR increased plasma insulin, (2) IR a little increased plasma glucose and plasma TG, and (3) IR decreased plasma Bhb. As shown in Figure S7, the computational model simulated the time course of plasma glucose, insulin, lactate, and FFA for healthy, mild T2DM, and severe T2DM. The model reproduced the experimental features (Reaven et al., 1988): (1) the plasma insulin increased for mild T2DM, whereas it greatly decreased for severe T2DM due to β cell dysfunction; (2) the plasma glucose increased in the order of healthy, mild T2DM, and severe T2DM; and (3) the severe T2DM loosened the dent of the plasma FFA.

To verify each organ module model, I characterized the simulated exchange fluxes between each organ and the blood. Figure S8 indicated the remarkable metabolic shift that insulin changed the liver status between glucose utilization and production, as indicated by Frayn (2010). After a meal, the glucose uptake flux rapidly increased, whereas the FFA/lactate/alanine uptake and TG release decreased, indicating substrate storage. And then the glucose/TG release increased, the FFA uptake increased, and the lactose/alanine/glycerol uptake increased. The liver took up lactate, alanine, and glycerol to produce hepatic glucose through gluconeogenesis, as well as the experimental data (Figure 3D). This further supported the typical feature of the glucose-lactose and glucose-alanine cycles. Figure S9 verified that the computational model well reproduced the hepatic glucose production, gluconeogenesis, and glycogenolysis fluxes for healthy subjects and those with T2DM. The model captured some important features of the experimental data (Magnusson et al., 1992): (1) the T2DM increased the total glucose production and gluconeogenesis fluxes and (2) gluconeogenesis played a major role in glucose production compared with glycogenolysis. Figure S10 confirmed that the computational model reproduced the experimental uptake fluxes of glucose, FFA, and TG by the skeletal muscle for healthy subjects and those with T2DM (Bickerton et al., 2008) (Frayn et al., 1993). The model captured the important experimental features: an insulin-induced peak response of the glucose uptake flux and the levels of glucose, FFA, and TG uptake fluxes. Figure S11 verified that the computational model reproduced the experimental uptake fluxes of glucose, FFA, and TG by the adipose tissue for healthy subjects and subjects with T2DM (Bickerton et al., 2008). The model captured the typical experimental features: an insulin-induced peak response of the glucose uptake flux and the level of FFA and TG uptake fluxes. The model showed an insulin-induced fast response of FFA and TG, whereas the experimental data indicated a gradual response. Insulin may not be a unique factor for the enhanced TG synthesis from FFA in the adipose tissue.

Finally, I used the simulation to characterize the other three organs due to lack of experimental data. According to the previous model (Kim et al., 2007; Pan and Hussain, 2012), my model assumed that the GI degrades the accumulated TG in its cytosols into FFA and glycerol to release them into plasma (Kim et al., 2007) (Figure S12).The heart took up various substrates of plasma glucose, lactate, glycerol, and FFA (Figure S13). After a meal, the glucose and lactate uptake increased due to their increased plasma concentrations (Figure 3); the FFA and glycerol uptake decreased due to their decreased plasma concentrations. The brain utilized the plasma glucose and liver-produced Bhb (Figure S14). After a meal, the glucose uptake increased due to its increased plasma concentration. The Bhb uptake occurred late, because its synthesis by the liver may need some fasting conditions.

Discrepancy between experimental data and simulation

I illustrated some discrepancies between experimental data and simulation (Figure 3). The simulated insulin pulse was sharper than the experimental pulse with a long tail. Although the simulated glycogen

concentration in liver increased to a peak 1 h after the glucose peak, the duration to achieve the peak was shorter than that of the experimental data (4–6 h). In other words, the simulated glycogen synthesis was faster than experimental data. In addition, the simulated glycogen decreased more rapidly than experimental data. The simulated plasma lactate increased to a peak at 2 h following the glucose peak, whereas the duration (2 h) to achieve the peak was longer than the experimental lactate data. These discrepancies will be discussed later.

Critically important features

The proposed model simulated the switching function between *de novo* lipogenesis (DNL) and Bhb synthesis with respect to pyruvate in the liver, as shown in Figure 4A. A high concentration of pyruvate increased the DNL flux; a very low concentration of pyruvate induced Bhb synthesis flux. The β-oxidation flux gradually decreased with an increase in pyruvate, whereas the DNL flux and pyruvate dehydrogenase (PDH) flux increased. It corresponded to the observation of the reverse relationships between DNL and β-oxidation and between glycolysis and β-oxidation (Frayn, 2010).

I performed dynamic sensitivity analysis of metabolite concentrations with respect to specific kinetic parameters, as shown in Figure 4B. The plasma glucose level was highly robust with respect to changes in the kinetic parameters except the insulin-related parameters including Km_inssyn_Glc_B, Km_Ins_B_L, and Km_Ins_B_M. The set-point of plasma glucose was controlled dominantly by insulin. Km_inssyn_Glc_B, which determines glucose-stimulated insulin secretion, was the most effective parameter that altered the set-point of plasma glucose. Km_Ins_B_L and Km_Ins_B_M, which determine the insulin-stimulated glucose uptake in the liver and skeletal muscle, were the second and third critical parameters, respectively. Km_Ins_B_A hardly affected the set-point, because the glucose uptake rate of the adipose tissue was much less than that by the skeletal muscle (Figure 3D). In addition to the insulin-related parameters, nucleotide cofactor synthesis-related parameters were suggested to be responsible for remarkable changes. It is because nucleotide cofactors simultaneously affect multiple reactions. Hepatic FFA and TG concentrations indicated high sensitivities with respect to Vmax_tgdeg_TG_A and Vmax_tgdeg_TG_G that determine the TG degradation rate in the adipose tissue and GI. It suggests that the adipose tissue and GI are closely connected to liver through TG.

Prediction of hidden mechanisms

As shown in Figure 5, the hepatic FFA synthesis consists of two phases: the former phase is the malonyl-CoA increasing phase (lipog1) of 0.5–1.8 h; the latter is its decreasing phase (lipog2) of 1.8–3.5 h. They corresponded to the glucose utilization and production phases, respectively. During the former phase, an increase in pyruvate enhanced malonyl-CoA production (Figure 2), whereas a decrease in glucose-6-phosphate (G6p) reduced the pentose phosphate pathway flux and NADPH production. As NADPH, which is required for the conversion from malonyl-CoA to FFA (lipog2), decreased, malonyl-CoA accumulated. During the latter phase, an increase in G6p enhanced the pentose phosphate pathway flux and NADPH production. The accumulated malonyl-CoA was converted into FFA using NADPH. As shown in Figure S15, the simulated Bhb concentration increased at the early phase of a fasted condition, as indicated by the experimental data (Owen et al., 1990), but it gradually decreased after 150 h with a decrease in plasma FFA, which was not consistent with the experimental data that gradually increased with time. The decrease in the simulated Bhb concentration in the late fasted phase may be caused by the decrease in plasma FFA. It suggests that some mechanisms are required that increase plasma FFA under the fasted condition.

Pathological analysis

Individual disorders

The proposed model was used to perform pathological analysis of metabolic diseases. I simulated the effects of the individual disorders on marker metabolites such as plasma glucose, plasma insulin, and hepatic TG, as shown in Figures 6A–6C. In general, high plasma glucose and hepatic TG accumulation develop or exacerbate metabolic diseases (Frayn, 2010; Samuel and Shulman, 2012). In the steatosis model, hepatic TG increased due to acceleration of lipogenesis (Ferre and Foufelle, 2010), whereas the dynamics of plasma insulin and plasma glucose hardly changed compared with the healthy condition. In β cell dysfunction of the pancreas, where glucose-stimulated insulin secretion is impaired or Km_inssyn_Glc_B is increased, the plasma insulin concentration decreased, compared with the healthy condition; the peak and set-point of plasma glucose greatly increased, as indicated by Lehmann and Deutsch (1992). Plasma glucose was less

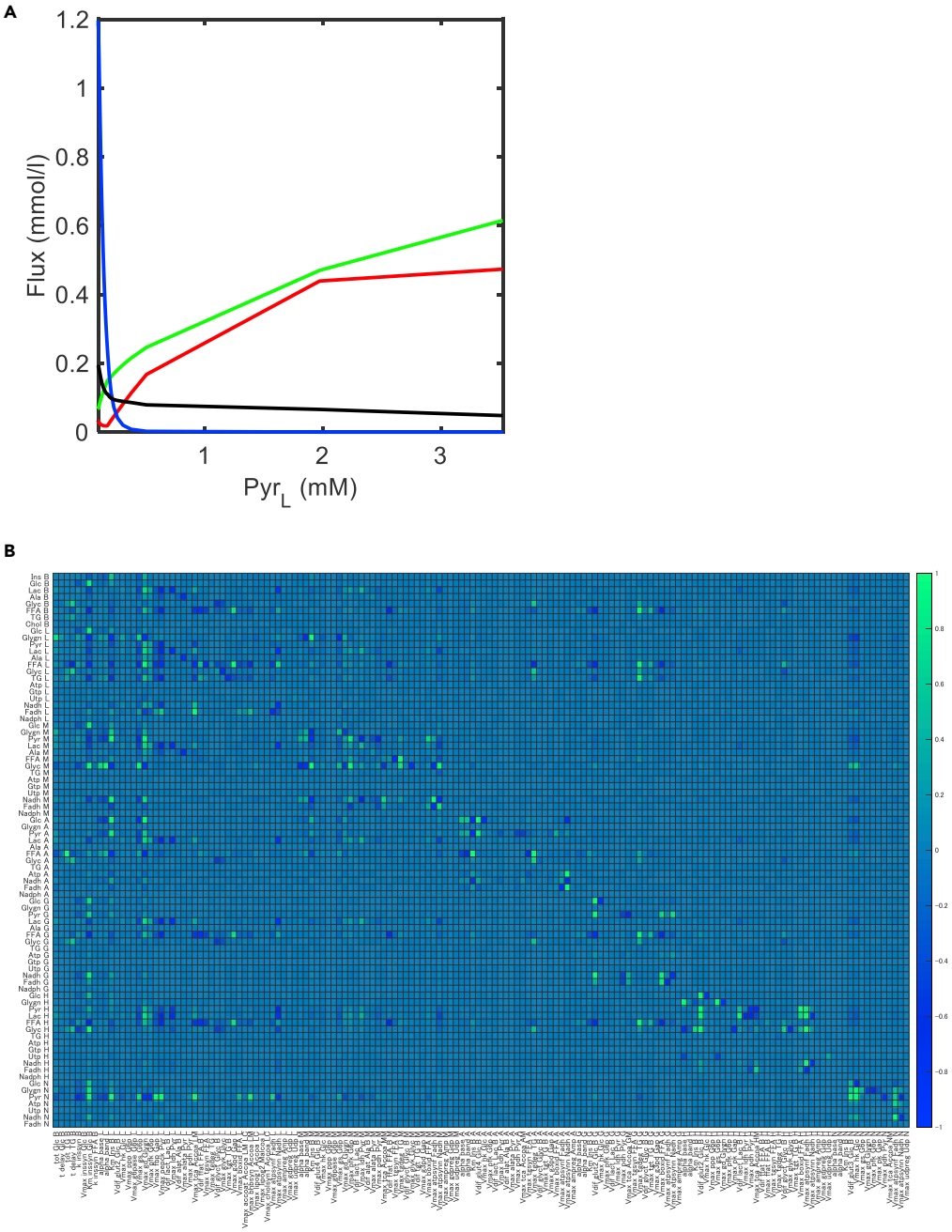

Figure 4. Critically important features of the virtual metabolic human dynamic model

The proposed model was simulated during 480 h after an overnight fast and following a single meal of 87 g carbohydrate and 33 g fat.

(A) Changes in the simulated fluxes of key reactions with respect to hepatic pyruvate. The four fluxes of the PDH reaction (red), DNL (green), Bhb synthesis (blue), and β-oxidation (black) were plotted with respect to pyruvate concentration in the liver.

(B) Dynamic sensitivity analysis of metabolite concentrations at postabsorptive state with respect to a single kinetic constant. The dynamic sensitivity was calculated at 10 h, where the value of a single kinetic parameter was changed by 1.1-fold.

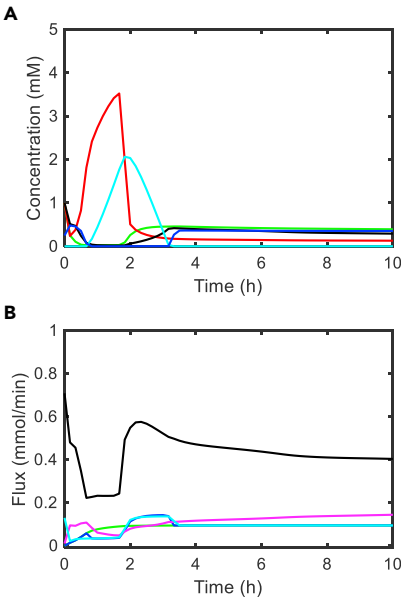

Figure 5. Prediction of a two-phase mechanism of *de novo* lipogenesis in the liver

The proposed model was simulated for 10 h after an overnight fast and following a single meal of 87 g carbohydrate and 33 g fat.

(A) The time course of G6p (green), pyruvate (red), acetyl-CoA (black), malonyl-CoA (cyan), and NADPH (blue) concentrations in the liver were simulated.

(B) The time course of TCA cycle (black), lipog1(green), lipog2 (blue), β-oxidation (magenta), and pentose phosphate pathway (cyan) fluxes in the liver were simulated. The lipog1 and lipog2 indicate the conversion from acetyl-CoA to malonyl-CoA and the conversion from malonyl-CoA to FFA, respectively.

utilized by the liver, skeletal muscle, and adipose tissue due to the impaired insulin secretion. Interestingly, hepatic TG decreased, which conflicted with the observation that the β cell dysfunction exacerbates the diseases (Cerf, 2013). T1DM is an extreme case of the β cell dysfunction, where Km_inssyn_Glc_B approaches to infinity or insulin is hardly produced in the pancreas. IR for the liver (IRL) increased the peak and set-point of plasma glucose. Hyperinsulinemia, which is a compensatory response to IR (Kasuga, 2006), was observed. Interestingly, IRL decreased hepatic TG, which presents a paradox that IRL recovers the hepatic steatosis that is a major cause of IRL, as suggested by Perry et al. (2014). IR for skeletal muscle (IRM) slightly increased the set-point of plasma glucose and plasma insulin, and also increased the hepatic TG, as suggested by the clinical observation (DeFronzo and Tripathy, 2009; Petersen et al., 2007). The skeletal muscle decreased the uptake of plasma glucose due to IRM, indicating hyperglycemia and hyperinsulinemia, whereas the liver utilized glucose to accumulate TG. It indicates that plasma glucose is diverted away from muscle glycogen storage to hepatic TG. IR for adipose tissue (IRA) hardly increased the set-point of plasma glucose, while increasing hepatic TG, as suggested by Perry et al. (2014) and Utzschneider and Kahn, (2006). It is because IRA decreases the insulin-induced TG synthesis in the adipose tissue, increasing FFA. The FFA is secreted into blood to enter the liver, increasing hepatic TG.

Combined disorders

The proposed model was applied to pathological analysis of T2DM. Particularly, I analyzed the effect of IR and β cell dysfunction on the progression of T2DM. I added the single disorders of IRM, IRA, IRL, and β cell dysfunction to the steatosis model, as shown in Figures 6D–F. Addition of IRM and IRA to the steatosis model slightly increased plasma insulin, and increased the peak and set-point of plasma glucose compared with those under the healthy condition, indicating hyperinsulinemia and hyperglycemia. While IRM and IRA cause hyperglycemia and enhance the release of FFA, respectively, the liver utilized plasma glucose and FFA to synthesize TG. When IRL was added to the steatosis with IRM and IRA, the plasma insulin and glucose increased, indicating typical IR symptom (Bickerton et al., 2008; Reaven et al., 1988), while decreasing hepatic TG, interestingly. Addition of β cell dysfunction greatly decreased plasma insulin, while increasing the peak and set-point of plasma glucose, indicating the severe T2DM symptom (Reaven et al., 1988).

Medication analysis

The proposed model was employed to investigate how three widely prescribed medicines for T2DM sulfonylurea, metformin, and thiazolidinedione and a glycerol kinase inhibitor medicine candidate recover T2DM, as shown in Figures 7A–7C. Sulfonylurea administration successfully decreased plasma glucose with an increase in plasma insulin, as shown by the experimental data (Aquilante, 2010), but increased

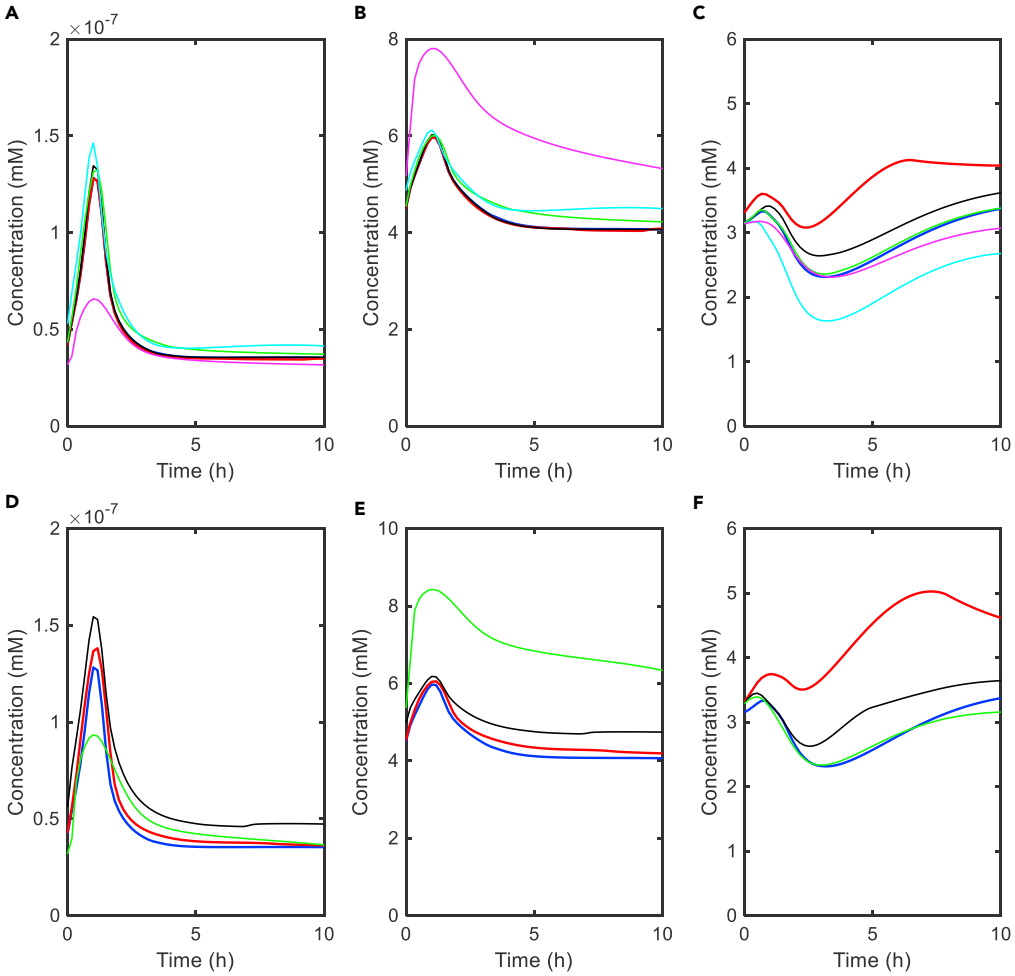

Figure 6. Pathological analysis using the virtual metabolic human model

(A–C) Single disorder. Time courses of plasma insulin (A), plasma glucose (B), and hepatic TG (C) for each disorder were simulated after an overnight fast and following a single meal of 40 g carbohydrate and 22 g fat. The colored lines indicate the healthy condition (blue), steatosis (red), IRA (black), IRM (green), IRL (cyan), and β cell dysfunction (magenta). Specifically, steatosis is built by multiplying Vmax_accoat_Accoa_LM_LC, Vmax_lipog1_Accoa_LC, Vmax_lipog2_Malcoa_L, and Vmax_tgsyn_FFA_L, Vmax_cholsyn1_Accoa_LC by 2. β cell dysfunction is built by multiplying Km_inssyn_Glc_B by 1.5. IRA is built by multiplying Km_Ins_B_A by 1.5. IRM is built by multiplying Km_Ins_B_M by 1.5. IRL is built by multiplying Km_Ins_B_L by 1.5.

(D–F) Combined disorders. Time courses of plasma insulin (D), plasma glucose (E), and hepatic TG (F) for each combined disorder model were simulated after an overnight fast and following a single meal of 40 g carbohydrate and 22 g fat. The colored lines indicate healthy condition (blue); the combination of steatosis, IRM, and IRA (red); the combination of steatosis, IRL, IRM, and IRA (black); and the combination of steatosis, IRL, IRM, IRA, and β cell dysfunction (green) (T2DM).

hepatic TG as an adverse effect, as suggested by Chen et al. (2015). Metformin acts not only on lactate dehydrogenase (LDH) but also on β-oxidation through AMP-activated protein kinase (AMPK). The LDH inhibition by metformin decreased plasma glucose and hepatic TG, while increasing plasma lactate (Figures S16), as indicated by the experimental data (Molavi et al., 2007; Natali and Ferrannini, 2006; Pernicova and Korbonits, 2014). Activation of β-oxidation by metformin decreased hepatic TG. Thiazolidinedione decreased hepatic plasma glucose and TG, as shown by the experimental data (Natali and Ferrannini, 2006). It is because thiazolidinedione enhances the glucose uptake in the skeletal muscle and activates TG synthesis in the adipose tissue, reducing plasma FFA (Natali and Ferrannini, 2006). Administration of a glycerol kinase inhibitor was found to decrease hepatic TG accumulation. Interestingly, it successfully decreased plasma glucose. It will be discussed later. The glycerol kinase inhibitor was referred to as a drug candidate for T2DM.

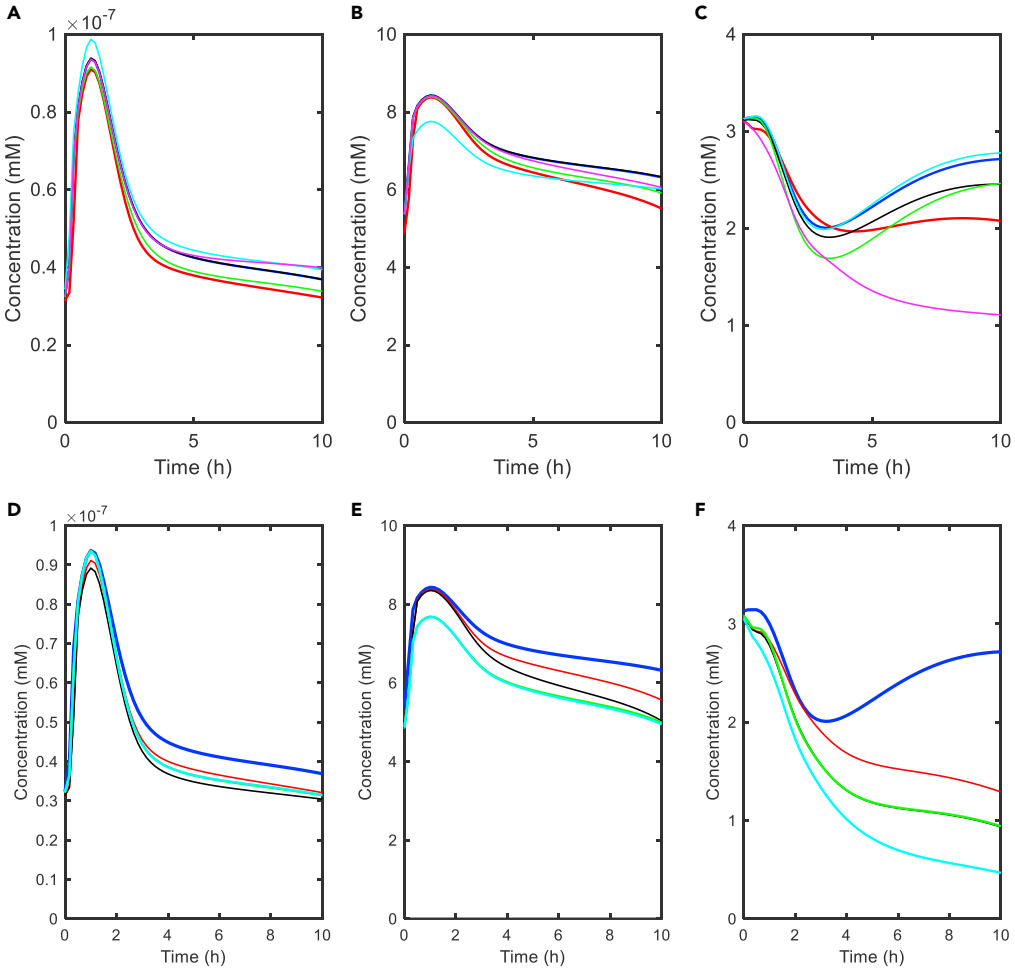

Figure 7. Single medication analysis and prediction of combination therapy for T2DM by using the virtual metabolic human model.

(A–C) Single medication: Time courses of the concentration of plasma insulin (A), plasma glucose (B), and hepatic TG (C) for T2DM were simulated after an overnight fast and following a single meal of 40 g carbohydrate and 22 g fat. The colored lines indicate the T2DM model without any medication (blue), LDH inhibition by metformin (red), β-oxidation activation by metformin (black), thiazolidinedione (green), sulfonylurea (cyan), and glycerol kinase inhibitor (magenta). Specifically, metformin reduces Vmax_ldh_Pyr_L to zero and multiplies Vmax_boxid_FFA_L by 2. Thiazolidinedione multiplies Vmax_tgsyn_FFA_A by 2. Sulfonylurea multiples Vmax_inssyn_Glc_B by 2. Glycerol kinase inhibitor reduces Vmax_glyk_Glyc_L to 0.

(D–F) Combination therapy: Time courses of the concentration of plasma insulin (D), plasma glucose (E), and hepatic TG (F) for T2DM were simulated after an overnight fast and following a single meal of 40 g carbohydrate and 22 g fat. The colored lines indicate no medication (T2DM) (blue); metformin therapy (red); the combination therapy of metformin and thiazolidinedione (black); the combination therapy of metformin, thiazolidinedione, and sulfonylurea (green); and the combination therapy of metformin, thiazolidinedione, sulfonylurea, and glycerol kinase inhibitor (cyan).

Design of combination therapy

To investigate the feasibility of combination therapy, I employed three medicines (metformin, thiazolidinedione, and sulfonylurea) and a glycerol kinase inhibitor. Figures 7D–F show the simulation results of three combination therapies. Expectedly metformin decreased plasma glucose and hepatic TG. The combination of metformin and thiazolidinedione was simulated to additively decrease plasma glucose, as shown by the experimental data (Fonseca et al., 2000). The combination of the three drugs (metformin, thiazolidinedione, and sulfonylurea) was simulated to be additively effective in reducing plasma glucose, as indicated by the experimental data (Yale et al., 2001) (Inzucchi, 2002). Addition of the glycerol kinase inhibitor to the aforementioned three medicines further decreased hepatic TG with a little decrease in plasma glucose; it hardly changed the insulin concentration. These simulation results revealed that the

combination therapy is effective in reducing plasma glucose and hepatic TG. The combination therapy presented explicitly additive effects, suggesting that the four medicines acted on different reactions.

DISCUSSION

Modular model construction

I have constructed a dynamic model that integrated eight organ modules and formulated the whole-body metabolism at the three scales of body, organ, and molecule. The resultant model consists of 202 ordinary differential equations with 217 reaction rates and 1,140 kinetic parameter constants. It is the most comprehensive, largest, and highly predictive kinetic model of the whole-body metabolism. The divide and conquer strategy at the organ scale allows us to run the individual organs separately and to exchange the organ module without any extensive rework. This modular dynamic model accurately reproduced the dynamics of experimental data of insulin, glucose, lactate, FFA, and TG concentrations and transport/exchange fluxes between blood and the other organs at postabsorptive state. In addition, the model also reproduced the typical features of subjects with metabolic diseases (IR and T2DM) and the effects of medicines on T2DM recovery. This model captured key features of human whole-body metabolism: lactate-glucose, alanine-glucose, glycerol-glucose cycles between the liver and other organs. The model reproduced the two typical features: the enhanced DNL suppressing β-oxidation and the enhanced glycolysis or PDH reaction decreasing β-oxidation. The former is effective in avoiding their futile cycles; the latter is effective in adjusting the energy balance between glycolysis and β-oxidation. In addition, the model presented a critical switching function between the DNL and Bhb synthesis with respect to pyruvate in the liver (Figure 4). Pyruvate played a key role in determining the entry of acetyl-CoA (AcCoA) into tricarboxylic acid (TCA) cycle, DNL or synthesis of FFA from citrate (CIT), and Bhb synthesis. As the entry reaction of the TCA cycle in mitochondria is presented by oxaloacetate (OAA)+ AcCoA → CIT, OAA that derives from pyruvate is essential to drive the TCA cycle. Under a fasted condition a low glucose concentration causes shortage of pyruvate, suppressing the entry reaction of the TCA cycle. In this case, β-oxidation-produced AcCoA is not consumed by the TCA cycle, but is utilized for the synthesis of Bhb. On the other hand, at high plasma glucose, abundant pyruvate activates the TCA cycle, enhancing CIT production in the mitochondria. CIT is transported into the cytoplasm, and converted into AcCoA to synthesize FFA. In a word, high plasma glucose enhances DNL.

Model validity

I discuss some discrepancies between the experimental data and simulation. This model reproduced the experimental plasma glucose pulse, but did not exactly reproduce the experimental insulin pulse. It was inevitable because the insulin dynamics was tightly coupled with the glucose pulse (Equation S4). Some factors other than glucose, e.g., amino acids, may induce insulin secretion. The simulated glycogen concentration in the liver increased to a peak 2–3 h before the experimental peak, and it decreased more rapidly than experimental data. The glycogen synthesis peak results from the assumption that the glycogen synthesis is tightly coupled with insulin dynamics in the proposed model. In the simulation model, the fast glycogenolysis (Figure 3) was definitely required to release glucose for plasma glucose homeostasis. If gluconeogenesis or glucose production is increased in the rest of the body, the hepatic glycogenolysis rate can be gradual or slow, reproducing the experimental observation more accurately. The present model does not consider the kidney module that converts plasma glutamine and lactate into glucose (Alsahli and Gerich, 2017), which underestimates the gluconeogenesis in the whole body. The fast glycogenolysis would be caused by the fact that the computational model excludes the gluconeogenesis by the kidney.

The experimental data employed in this study were a collection of different references, i.e., the experimental data were not obtained under the exactly same conditions. For example, the time course data of plasma insulin, plasma glucose, and plasma lactate derived from Frayn et al. (1993), whereas the experimental data of their transport fluxes came from Kim et al. (2007). The proposed model did not insist on the exact fitting, but pursued capturing critical metabolic features. In human metabolism studies, direct measurements of *in vivo* kinetics are very hard and *in vivo* experiments are seriously limited due to ethical issues. As it is difficult to obtain a sufficient amount of data for kinetic modeling at present and in the near future, we have to manage fragmental, heterogeneous quantitative data, qualitative features, and biological knowledge to build a mathematical model (Maeda et al., 2013, 2019). The important thing is not to precisely measure or evaluate the exact values of kinetic parameters, but to capture essential functions

underlying metabolic networks without insisting on the exact values *in vivo* or on complexity in detailed biochemistry (Kurata et al., 2003, 2005).

I derived the rate equations from precise chemical reaction equations (Swainston et al., 2016) when the experimentally validated rate equations are not available. Owing to shortage of measured data, I did not uniquely determine the kinetic parameter values. However, the existing experimental data including *in vitro* measured kinetic constants, qualitative data, and biological information rather constrained the parameter space of the kinetic model. They were feasible enough for constructing kinetic models, for understanding the mechanisms by which the metabolic networks generate physiological functions and robustness, and for performing pathological and medication analysis. The resolution of the model would be appropriate enough for the given experimental data and biological information. It may be no use to build much more detailed mathematical equations, if there is little experimental data to validate them.

Robustness

Generally, high sensitivity-indicating parameters point out critical mechanisms such as ultrasensitivity, positive feedback loop, and bottleneck reactions. The insulin-related kinetic parameters of Km_inssyn_Glc_B, Km_Ins_B_L, and Km_Ins_B_M, which were employed by Hill equations with ultrasensitivity (Konig et al., 2012), showed high sensitivity. Such ultrasensitivity makes it possible for insulin to induce the distinct shift between glucose utilization and production. Coenzyme (ATP, GTP, UTP, NADH, NADPH, and $FADH_2$) synthesis-related parameters greatly affected the major pathways of β-oxidation, TCA cycle, and PDH reaction, whereas previous whole-body models hardly considered nucleotide cofactors (Kim et al., 2007; Palumbo et al., 2018; Xu et al., 2011). NAD^+ affects the reactions of TCA cycle, β-oxidation, LDH, and glyceraldehyde-3-phosphate dehydrogenase (G3PD). G3PD is the critically responsible enzyme for linking glycolysis to TG synthesis. NADH, which is produced through glycolysis, β-oxidation, and TCA cycle, is essential to generate ATP through oxidative phosphorylation. NADPH, which is produced in the pentose phosphate pathway, is utilized for DNL. UTP, which is essential for glycogen synthesis, is regenerated by the nucleotide diphosphate kinase reaction ATP + UDP→ ADP + UTP. GTP, which is necessary for gluconeogenesis (Figure 2), is also regenerated by the nucleotide diphosphate kinase reaction of ATP + GDP→ ADP + GTP. Those nucleotide cofactors conjugate multiple cofactor-coupled reactions to form global feedback loops, which is exemplified by glycolysis pathways with TCA cycle and oxidative phosphorylation (Kurata, 2019; Teusink et al., 1998). Glycolysis requires ATP at the initial step (hexokinase [HK], glucokinase [GK], phosphofructokinase [PFK]) (Figure 2). An increase in the glycolysis flux enhances the TCA cycle with oxidative phosphorylation to further produce ATP, which activates the initial step of glycolysis in a positive feedback manner. This ATP amplification is called turbo-design or self-replenishment cycle (Kurata, 2019; Teusink et al., 1998). It accelerates the glucose utilization (HK, GK, PFK) to reduce plasma glucose. β-oxidation in each organ and Bhb degradation in the brain also employ the similar positive feedback loops. Thus, incorporation of nucleotide cofactors is effective in understanding the mechanisms of global metabolic changes.

While the insulin-related parameters including Km_inssyn_Glc_B, Km_Ins_B_L, and Km_Ins_B_M played a critical role in changing the set-point (5mM) of plasma glucose concentration, the set-point provided a highly robust property against changes in the other kinetic parameters. The set-point of plasma glucose is dominantly controlled by insulin. The robustness of the plasma glucose set-point is achieved by the insulin-based feedback switching between the hepatic glucose utilization and production. In addition, nucleotide cofactors conjugate multiple cofactor-coupled reactions to generate global negative feedback loops. The negative feedback loops control the balances of NADH redox energy and ATP energy. For example, an increase in NADH suppresses the β-oxidation and PDH reaction due to the decreased NAD^+, which deactivates the NADH-synthesizing TCA cycle. Excess ATP would be utilized to promote the synthesis of TG and cholesterol.

Prediction of hidden mechanism

The proposed model suggested a two-phase mechanism of FFA synthesis in the liver, which consists of an initial malonyl-CoA accumulation phase and a later malonyl-CoA decreasing phase (Figure 5). This separation is caused by the fact that NADPH synthesis in the pentose phosphate pathways is coupled with DNL (Figure 2). Malonyl-CoA is a key intermediate metabolite for the FFA synthesis. During the former phase, G6p in the liver decreases, which decreases the pentose phosphate pathway flux and NADPH. Malonyl-CoA accumulated due to shortage of NADPH. During the latter phase, G6p increases, which

enhances the flux of the pentose phosphate pathways with NADPH synthesis. The accumulated malonyl-CoA is converted with NADPH into FFA. The two phases correspond to the glucose production and utilization phases. Consequently, the DNL occurs shortly after the glucose pulse.

Pathological analysis

A computer model takes an advantage in analysis of the individual disorders and in understanding the mechanisms by which the individual ones are combined to cause complex pathologies. Metabolic diseases take a matter of years to develop, but short-term simulation is effective in considering some signs of such diseases and in capturing typical pathological features.

The proposed kinetic model was applied to pathological analysis for diabetes (Ashworth et al., 2016; Utzschneider and Kahn, 2006). In T1DM, little or no insulin is produced by the pancreas. T2DM is characterized by steatosis, IR, and β cell dysfunction. Of course steatosis is the underlying disease. I investigated the effect of IR and β cell dysfunction on diabetes progression. IRA alone hardly increased the plasma glucose set-point. The set-point increased in the order of IRM, IRL, and β cell dysfunction. An increase in the plasma glucose set-point by IRM reflects that skeletal muscle accounts for 80% of the whole insulin-mediated glucose uptake (Saltiel and Kahn, 2001; Stump et al., 2006; Thong et al., 2005). The β cell dysfunction is the first principal contribution to hyperglycemia, the IRL is the second one, and the IRM is the third one. β cell dysfunction and IRL greatly increased plasma glucose, inducing serious progression (Reaven et al., 1988). Quantitative analysis of mechanisms responsible for the insulin-controlled glucose uptake is useful to understand the contribution of each disorder to T2DM. The simulation results were consistent with the widely recognized experimental data that IRM and IRA promote hepatic TG synthesis (Perry et al., 2014; Petersen et al., 2007). On the other hand, Figure 6 suggests a paradox or conflict that β cell dysfunction and IRL, which are known to exacerbate diabetes (Cerf, 2013) (Perry et al., 2014), recover the steatosis that is a major cause of IR. I solve the paradox as follows. When IR occurs, hepatic TG accumulation may be no longer controlled by insulin (Doege et al., 2008; Kim et al., 2001), but be transformed into a chronic or irreversible state through oxidation, endoplasmic reticulum (ER) stress, and inflammation (Ferre and Foufelle, 2010; Samuel and Shulman, 2012).

Medication and combination therapy

Medication is a very popular way to treat T2DM. Out of many medications, I employed the three existing medicines (metformin, thiazolidinedione, and sulfonylurea) and a glycerol kinase inhibitor. Curative remedies are to reduce plasma glucose and to decrease ectopic TG accumulation. The three compounds metformin, thiazolidinedione, sulfonylurea were simulated to be effective in reducing plasma glucose, which was consistent with the experimental data (DeFronzo and Goodman, 1995; Inzucchi, 2002). The model demonstrated the adverse effect of metformin that increases plasma lactate as lactic acidosis (Figure S16), as indicated by the experimental data (Molavi et al., 2007; Pernicova and Korbonits, 2014). Interestingly, the proposed model uncovered that the glycerol kinase inhibitor decreased not only hepatic TG but also plasma glucose. The reduced plasma glucose results from the shortage of Grp due to the inhibited glycerol kinase in the liver. Specifically, the shortage of Grp decreases the backward reaction from Grp to Gap, which results in reduced gluconeogenesis. The glycerol kinase inhibitor is found to be a promising medicine for T2DM. Out of the several medications, activation of β-oxidation, which burns FFA, can be a powerful remedy of T2DM, because it has an advantage in removing not only TG but also its precursors. Metformin acts on β-oxidation through AMPK activation, although its action is marginal. Thus, new medicines should be developed that effectively activate β-oxidation. Sulfonylurea successfully reduced plasma glucose, but increased hepatic TG as an adverse effect, as suggested by Chen et al. (2015). The model not only accurately predicted the essential results of medications but also achieved a rational design of combination therapy. The combination therapy of metformin, thiazolidinedione, sulfonylurea, and glycerol kinase inhibitor was found to be a novel therapy to reduce plasma glucose and hepatic TG. The successful combination results from the fact that the four compounds act on different reactions.

Limitations of the study

IR can be caused by ectopic TG accumulation. Specifically, a lipid metabolite of diacylglycerol activates protein kinase C isoforms, impairing insulin signaling in organs (Cerf, 2013; Perry et al., 2014). In addition, the ratio of saturated FFA to monounsaturated FFA plays a major role in disease progression (Alkhouri et al., 2009). Saturated FFA leads to inflammation, ER stress, and apoptosis. As the proposed model is not able to consider DAG or saturated FFA, more detailed models are necessary that consider the IR-inducing mechanisms. The present model seems a mono-stable model (I have not found any bistability yet in the model), whereas real disorders are often chronic and irreversible. Actually, accumulated TG may be

aggregated and denatured due to inflammation, oxidation, and ER stress to cause chronic and irreversible dysfunctions (Perry et al., 2014). Such irreversible disorders should be considered in the next model.

Resource availability

Lead contact

Hiroyuki Kurata (kurata@bio.kyutech.ac.jp)

Materials availability

Not applicable.

Data and code availability

The program is freely available at http://www.cadlive.jp/cadlive_main/Softwares/vmh/dynamic_model.html.

METHODS

All methods can be found in the accompanying Transparent Methods supplemental file.

SUPPLEMENTAL INFORMATION

Supplemental information can be found online at https://doi.org/10.1016/j.isci.2021.102101.

ACKNOWLEDGMENTS

This work was supported by the Grant-in-Aid for Scientific Research (B) (19H04208) from Japan Society for the Promotion of Science and partially supported by the developing key technologies for discovering and manufacturing pharmaceuticals used for next-generation treatments and diagnoses from Japan Agency for Medical Research and Development (AMED). I am grateful of K. Horimoto, K, Ogata, K. Nasu, H. Shikita, and R. Yoshimori performing computer simulation and system analysis. The organ illustrations in Figure 1A are provided by freepik (https://jp.freepik.com) and ac-illust (https://www.ac-illust.com/).

AUTHOR CONTRIBUTIONS

H.K. did everything.

DECLARATION OF INTERESTS

The author declares no competing interests.

Received: September 17, 2020
Revised: December 21, 2020
Accepted: January 20, 2021
Published: February 19, 2021

REFERENCES

Alkhouri, N., Dixon, L.J., and Feldstein, A.E. (2009). Lipotoxicity in nonalcoholic fatty liver disease: not all lipids are created equal. Expert Rev. Gastroenterol. Hepatol. *3*, 445–451.

Alsahli, M., and Gerich, J.E. (2017). Renal glucose metabolism in normal physiological conditions and in diabetes. Diabetes Res. Clin. Pract. *133*, 1–9.

Aquilante, C.L. (2010). Sulfonylurea pharmacogenomics in Type 2 diabetes: the influence of drug target and diabetes risk polymorphisms. Expert Rev. Cardiovasc. Ther. *8*, 359–372.

Ashcroft, F.M., and Rorsman, P. (2012). Diabetes mellitus and the beta cell: the last ten years. Cell *148*, 1160–1171.

Ashworth, W.B., Davies, N.A., and Bogle, I.D. (2016). A computational model of hepatic energy metabolism: understanding zonated damage and steatosis in NAFLD. PLoS Comput. Biol. *12*, e1005105.

Berger, M., and Rodbard, D. (1989). Computer simulation of plasma insulin and glucose dynamics after subcutaneous insulin injection. Diabetes Care *12*, 725–736.

Berndt, N., Bulik, S., Wallach, I., Wunsch, T., Konig, M., Stockmann, M., Meierhofer, D., and Holzhutter, H.G. (2018a). HEPATOKIN1 is a biochemistry-based model of liver metabolism for applications in medicine and pharmacology. Nat. Commun. *9*, 2386.

Berndt, N., Horger, M.S., Bulik, S., and Holzhutter, H.G. (2018b). A multiscale modelling approach to assess the impact of metabolic zonation and microperfusion on the hepatic carbohydrate metabolism. PLoS Comput. Biol. *14*, e1006005.

Berndt, N., and Holzhutter, H.G. (2018). Dynamic metabolic zonation of the hepatic glucose metabolism is accomplished by sinusoidal plasma gradients of nutrients and hormones. Front. Physiol. *9*, 1786.

Bickerton, A.S., Roberts, R., Fielding, B.A., Tornqvist, H., Blaak, E.E., Wagenmakers, A.J., Gilbert, M., Humphreys, S.M., Karpe, F., and Frayn, K.N. (2008). Adipose tissue fatty acid metabolism in insulin-resistant men. Diabetologia *51*, 1466–1474.

Cerf, M.E. (2013). Beta cell dysfunction and insulin resistance. Front. Endocrinol. (Lausanne) *4*, 37.

Chen, Y.H., Du, L., Geng, X.Y., Peng, Y.L., Shen, J.N., Zhang, Y.G., Liu, G.J., and Sun, X. (2015). Effects of sulfonylureas on lipids in type 2 diabetes mellitus: a meta-analysis of randomized controlled trials. J. Evid. Based Med. *8*, 134–148.

Cobelli, C., Renard, E., and Kovatchev, B. (2011). Artificial pancreas: past, present, future. Diabetes *60*, 2672–2682.

Cobelli, C., Toffolo, G., and Ferrannini, E. (1984). A model of glucose kinetics and their control by insulin, compartmental and noncompartmental approaches. Math. Biosciences *72*, 291–315.

DeFronzo, R.A., and Goodman, A.M. (1995). Efficacy of metformin in patients with non-insulin-dependent diabetes mellitus. The Multicenter Metformin Study Group. N. Engl. J. Med. *333*, 541–549.

DeFronzo, R.A., and Tripathy, D. (2009). Skeletal muscle insulin resistance is the primary defect in type 2 diabetes. Diabetes Care *32*, S157–S163.

Doege, H., Grimm, D., Falcon, A., Tsang, B., Storm, T.A., Xu, H., Ortegon, A.M., Kazantzis, M., Kay, M.A., and Stahl, A. (2008). Silencing of hepatic fatty acid transporter protein 5 in vivo reverses diet-induced non-alcoholic fatty liver disease and improves hyperglycemia. J. Biol. Chem. *283*, 22186–22192.

Eissing, T., Kuepfer, L., Becker, C., Block, M., Coboeken, K., Gaub, T., Goerlitz, L., Jaeger, J., Loosen, R., Ludewig, B., et al. (2011). A computational systems biology software platform for multiscale modeling and simulation: integrating whole-body physiology, disease biology, and molecular reaction networks. Front. Physiol. *2*, 4.

Ferre, P., and Foufelle, F. (2010). Hepatic steatosis: a role for de novo lipogenesis and the transcription factor SREBP-1c. Diabetes Obes. Metab. *12*, 83–92.

Fonseca, V., Rosenstock, J., Patwardhan, R., and Salzman, A. (2000). Effect of metformin and rosiglitazone combination therapy in patients with type 2 diabetes mellitus: a randomized controlled trial. JAMA *283*, 1695–1702.

Frayn, K.N. (2010). Metabolic Regulation: A Human Perspective (Willey-Blackwell).

Frayn, K.N., Coppack, S.W., Humphreys, S.M., Clark, M.L., and Evans, R.D. (1993). Periprandial regulation of lipid metabolism in insulin-treated diabetes mellitus. Metabolism *42*, 504–510.

Hassell Sweatman, C.Z.W. (2020). Mathematical model of diabetes and lipid metabolism linked to diet, leptin sensitivity, insulin sensitivity and VLDLTG clearance predicts paths to health and type II diabetes. J. Theor. Biol. *486*, 110037.

Hetherington, J., Sumner, T., Seymour, R.M., Li, L., Rey, M.V., Yamaji, S., Saffrey, P., Margoninski, O., Bogle, I.D., Finkelstein, A., et al. (2012). A composite computational model of liver glucose homeostasis. I. Building the composite model. J. R. Soc. Interf. *9*, 689–700.

Insel, P.A., Liljenquist, J.E., Tobin, J.D., Sherwin, R.S., Watkins, P., Andres, R., and Berman, M. (1975). Insulin control of glucose metabolism in man: a new kinetic analysis. J. Clin. Invest. *55*, 1057–1066.

Inzucchi, S.E. (2002). Oral antihyperglycemic therapy for type 2 diabetes: scientific review. JAMA *287*, 360–372.

Iyengar, R., Zhao, S., Chung, S.W., Mager, D.E., and Gallo, J.M. (2012). Merging systems biology with pharmacodynamics. Sci. Transl Med. *4*, 126ps127.

Jensen, J., Rustad, P.I., Kolnes, A.J., and Lai, Y.C. (2011). The role of skeletal muscle glycogen breakdown for regulation of insulin sensitivity by exercise. Front. Physiol. *2*, 112.

Karpe, F., Olivecrona, T., Walldius, G., and Hamsten, A. (1992). Lipoprotein lipase in plasma after an oral fat load: relation to free fatty acids. J. Lipid Res. *33*, 975–984.

Kasuga, M. (2006). Insulin resistance and pancreatic beta cell failure. J. Clin. Invest. *116*, 1756–1760.

Kim, J., Saidel, G.M., and Cabrera, M.E. (2007). Multi-scale computational model of fuel homeostasis during exercise: effect of hormonal control. Ann. Biomed. Eng. *35*, 69–90.

Kim, J.K., Fillmore, J.J., Chen, Y., Yu, C., Moore, I.K., Pypaert, M., Lutz, E.P., Kako, Y., Velez-Carrasco, W., Goldberg, I.J., et al. (2001). Tissue-specific overexpression of lipoprotein lipase causes tissue-specific insulin resistance. Proc. Natl. Acad. Sci. U S A *98*, 7522–7527.

Kitade, H., Chen, G., Ni, Y., and Ota, T. (2017). Nonalcoholic fatty liver disease and insulin resistance: new insights and potential new treatments. Nutrients *9*, 387.

Kitano, H. (2010). Grand challenges in systems physiology. Front. Physiol. *1*, 3.

Konig, M., Bulik, S., and Holzhutter, H.G. (2012). Quantifying the contribution of the liver to glucose homeostasis: a detailed kinetic model of human hepatic glucose metabolism. PLoS Comput. Biol. *8*, e1002577.

Kurata, H. (2019). Self-replenishment cycles generate a threshold response. Sci. Rep. *9*, 17139.

Kurata, H., Masaki, K., Sumida, Y., and Iwasaki, R. (2005). CADLIVE dynamic simulator: direct link of biochemical networks to dynamic models. Genome Res. *15*, 590–600.

Kurata, H., Matoba, N., and Shimizu, N. (2003). CADLIVE for constructing a large-scale biochemical network based on a simulation-directed notation and its application to yeast cell cycle. Nucleic Acids Res. *31*, 4071–4084.

Lehmann, E.D., and Deutsch, T. (1992). A physiological model of glucose-insulin interaction in type 1 diabetes mellitus. J. Biomed. Eng. *14*, 235–242.

Li, Y., Solomon, T.P., Haus, J.M., Saidel, G.M., Cabrera, M.E., and Kirwan, J.P. (2010). Computational model of cellular metabolic dynamics: effect of insulin on glucose disposal in human skeletal muscle. Am. J. Physiol. Endocrinol. Metab. *298*, E1198–E1209.

Maeda, K., Minamida, H., Yoshida, K., and Kurata, H. (2013). Flux module decomposition for parameter estimation in a multiple-feedback loop model of biochemical networks. Bioproc. Biosyst Eng. *36*, 333–344.

Maeda, K., Westerhoff, H.V., Kurata, H., and Boogerd, F.C. (2019). Ranking network mechanisms by how they fit diverse experiments and deciding on E. coli's ammonium transport and assimilation network. NPJ Syst. Biol. Appl. *5*, 14.

Magnusson, I., Rothman, D.L., Katz, L.D., Shulman, R.G., and Shulman, G.I. (1992). Increased rate of gluconeogenesis in type II diabetes mellitus. A 13C nuclear magnetic resonance study. J. Clin. Invest. *90*, 1323–1327.

Maldonado, E.M., Fisher, C.P., Mazzatti, D.J., Barber, A.L., Tindall, M.J., Plant, N.J., Kierzek, A.M., and Moore, J.B. (2018). Multi-scale, whole-system models of liver metabolic adaptation to fat and sugar in non-alcoholic fatty liver disease. NPJ Syst. Biol. Appl. *4*, 33.

Meyer, C., Dostou, J.M., Welle, S.L., and Gerich, J.E. (2002). Role of human liver, kidney, and skeletal muscle in postprandial glucose homeostasis. Am. J. Physiol. Endocrinol. Metab. *282*, E419–E427.

Molavi, B., Rassouli, N., Bagwe, S., and Rasouli, N. (2007). A review of thiazolidinediones and metformin in the treatment of type 2 diabetes with focus on cardiovascular complications. Vasc. Health Risk Manag. *3*, 967–973.

Natali, A., and Ferrannini, E. (2006). Effects of metformin and thiazolidinediones on suppression of hepatic glucose production and stimulation of glucose uptake in type 2 diabetes: a systematic review. Diabetologia *49*, 434–441.

Noronha, A., Modamio, J., Jarosz, Y., Guerard, E., Sompairac, N., Preciat, G., Danielsdottir, A.D., Krecke, M., Merten, D., Haraldsdottir, H.S., et al. (2019). The Virtual Metabolic Human database: integrating human and gut microbiome metabolism with nutrition and disease. Nucleic Acids Res. *47*, D614–D624.

Owen, O.E., Tappy, L., Mozzoli, M.A., and Smalley, K.J. (1990). Acute starvation. In The Metabolic and Molecular Basis of Acquired Disease, R.D. Cohen, B. Lewis, K.G.M.M. Alberti, and A.M. Denman, eds. (Bailliere Tindall), pp. 550–570.

Palumbo, M.C., Morettini, M., Tieri, P., Diele, F., Sacchetti, M., and Castiglione, F. (2018). Personalizing physical exercise in a computational model of fuel homeostasis. PLoS Comput. Biol. *14*, e1006073.

Pan, X., and Hussain, M.M. (2012). Gut triglyceride production. Biochim. Biophys. Acta *1821*, 727–735.

Pearson, T., Wattis, J.A., King, J.R., MacDonald, I.A., and Mazzatti, D.J. (2014). A mathematical model of the human metabolic system and metabolic flexibility. Bull Math. Biol. *76*, 2091–2121.

Pernicova, I., and Korbonits, M. (2014). Metformin–mode of action and clinical implications for diabetes and cancer. Nat. Rev. Endocrinol. *10*, 143–156.

Perry, R.J., Samuel, V.T., Petersen, K.F., and Shulman, G.I. (2014). The role of hepatic lipids in hepatic insulin resistance and type 2 diabetes. Nature *510*, 84–91.

Petersen, K.F., Dufour, S., Savage, D.B., Bilz, S., Solomon, G., Yonemitsu, S., Cline, G.W., Befroy, D., Zemany, L., Kahn, B.B., et al. (2007). The role of skeletal muscle insulin resistance in the pathogenesis of the metabolic syndrome. Proc. Natl. Acad. Sci. U S A *104*, 12587–12594.

Pratt, A.C., Wattis, J.A., and Salter, A.M. (2015). Mathematical modelling of hepatic lipid metabolism. Math. Biosci. *262*, 167–181.

Reaven, G.M., Hollenbeck, C., Jeng, C.Y., Wu, M.S., and Chen, Y.D. (1988). Measurement of plasma glucose, free fatty acid, lactate, and insulin for 24 h in patients with NIDDM. Diabetes *37*, 1020–1024.

Saltiel, A.R. (2001). New perspectives into the molecular pathogenesis and treatment of type 2 diabetes. Cell *104*, 517–529.

Saltiel, A.R., and Kahn, C.R. (2001). Insulin signalling and the regulation of glucose and lipid metabolism. Nature *414*, 799–806.

Samuel, V.T., and Shulman, G.I. (2012). Mechanisms for insulin resistance: common threads and missing links. Cell *148*, 852–871.

Sherwin, R.S., Kramer, K.J., Tobin, J.D., Insel, P.A., Liljenquist, J.E., Berman, M., and Andres, R. (1974). A model of the kinetics of insulin in man. J. Clin. Invest. *53*, 1481–1492.

Sluka, J.P., Fu, X., Swat, M., Belmonte, J.M., Cosmanescu, A., Clendenon, S.G., Wambaugh, J.F., and Glazier, J.A. (2016). A liver-centric multiscale modeling framework for xenobiotics. PLoS One *11*, e0162428.

Stump, C.S., Henriksen, E.J., Wei, Y., and Sowers, J.R. (2006). The metabolic syndrome: role of skeletal muscle metabolism. Ann. Med. *38*, 389–402.

Swainston, N., Smallbone, K., Hefzi, H., Dobson, P.D., Brewer, J., Hanscho, M., Zielinski, D.C., Ang, K.S., Gardiner, N.J., Gutierrez, J.M., et al. (2016). Recon 2.2: from reconstruction to model of human metabolism. Metabolomics *12*, 109.

Taylor, R., Magnusson, I., Rothman, D.L., Cline, G.W., Caumo, A., Cobelli, C., and Shulman, G.I. (1996). Direct assessment of liver glycogen storage by 13C nuclear magnetic resonance spectroscopy and regulation of glucose homeostasis after a mixed meal in normal subjects. J. Clin. Invest. *97*, 126–132.

Teusink, B., Walsh, M.C., van Dam, K., and Westerhoff, H.V. (1998). The danger of metabolic pathways with turbo design. Trends Biochem. Sci. *23*, 162–169.

Thiele, I., Sahoo, S., Heinken, A., Hertel, J., Heirendt, L., Aurich, M.K., and Fleming, R.M. (2020). Personalized whole-body models integrate metabolism, physiology, and the gut microbiome. Mol. Syst. Biol. *16*, e8982.

Thiele, I., Swainston, N., Fleming, R.M., Hoppe, A., Sahoo, S., Aurich, M.K., Haraldsdottir, H., Mo, M.L., Rolfsson, O., Stobbe, M.D., et al. (2013). A community-driven global reconstruction of human metabolism. Nat. Biotechnol. *31*, 419–425.

Thong, F.S., Dugani, C.B., and Klip, A. (2005). Turning signals on and off: GLUT4 traffic in the insulin-signaling highway. Physiology (Bethesda) *20*, 271–284.

Utzschneider, K.M., and Kahn, S.E. (2006). Review: the role of insulin resistance in nonalcoholic fatty liver disease. J. Clin. Endocrinol. Metab. *91*, 4753–4761.

Vance, J.E., Buchanan, K.D., Challoner, D.R., and Williams, R.H. (1968). Effect of glucose concentration on insulin and glucagon release from isolated islets of Langerhans of the rat. Diabetes *17*, 187–193.

Viceconti, M., and Hunter, P. (2016). The virtual physiological human: ten years after. Annu. Rev. Biomed. Eng. *18*, 103–123.

Visentin, R., Campos-Nanez, E., Schiavon, M., Lv, D., Vettoretti, M., Breton, M., Kovatchev, B.P., Dalla Man, C., and Cobelli, C. (2018). The UVA/padova type 1 diabetes simulator goes from single meal to single day. J. Diabetes Sci. Technol. *12*, 273–281.

Xia, M.F., Bian, H., and Gao, X. (2019). NAFLD and diabetes: two sides of the same coin? Rationale for gene-based personalized NAFLD treatment. Front. Pharmacol. *10*, 877.

Xu, K., Morgan, K.T., Todd Gehris, A., Elston, T.C., and Gomez, S.M. (2011). A whole-body model for glycogen regulation reveals a critical role for substrate cycling in maintaining blood glucose homeostasis. PLoS Comput. Biol. *7*, e1002272.

Yale, J.F., Valiquett, T.R., Ghazzi, M.N., Owens-Grillo, J.K., Whitcomb, R.W., and Foyt, H.L. (2001). The effect of a thiazolidinedione drug, troglitazone, on glycemia in patients with type 2 diabetes mellitus poorly controlled with sulfonylurea and metformin. A multicenter, randomized, double-blind, placebo-controlled trial. Ann. Intern. Med. *134*, 737–745.

Yugi, K., Kubota, H., Toyoshima, Y., Noguchi, R., Kawata, K., Komori, Y., Uda, S., Kunida, K., Tomizawa, Y., Funato, Y., et al. (2014). Reconstruction of insulin signal flow from phosphoproteome and metabolome data. Cell Rep. *8*, 1171–1183.

iScience, Volume *24*

Supplemental Information

Virtual metabolic human dynamic model for pathological analysis and therapy design for diabetes

Hiroyuki Kurata

Transparent Methods

Mathematical model

Model overview

A schematic diagram of the whole body is shown in **Figure 1**. I constructed the union of all the metabolic networks of the organs based on biochemistry, as shown **Figure 2**. I lumped associated enzyme reactions into chemical reaction equations based on Recon2.2 (Swainston et al., 2016). Each organ network was built by selecting organ-specific reactions from the union network. The whole-body model formulates the metabolic enzyme and transporter reactions with regulation of enzyme activities and hormonal actions for all the organs. A meal of glucose and triglyceride (TG) is inputted into blood through the gastrointestinal (GI) tract. The model focuses on insulin hormone (Yugi et al., 2014), assuming that glucagon effect is approximately opposite to insulin (Kawamori et al., 2009). Note that detailed kinetics of glucagon *in vivo* remains to be measured. The model takes account for glucose, lactate, glycerol, alanine, β-hydroxybutyrate (Bhb), TG, free fatty acid (FFA) and insulin in blood, assuming the perfect mixing that there is no spatial gradient of metabolites, oxygen and carbon dioxide in each organ. In this study alanine represents the gluconeogenic amino acids and Bhb represents ketone bodies. Notably, the nucleotide cofactors of ATP, GTP, UTP, NADH, NADPH, and $FADH_2$ are incorporated to reflect realistic metabolic changes. The resultant model consists of 202 ordinary differential equations for metabolites with 217 reaction rates and 1141 kinetic parameter constants, as shown in **Equation S1-S421**, **Table S1**, and **Table S2**. Abbreviations of the kinetic parameter constants are defined in **Table S3**. The differential equations are integrated with ode15s (MATLAB R2019a, The MathWorks, Inc.) to simulate their dynamics.

Module decomposition

A divide and conquer strategy is employed for model construction (Karr et al., 2012; Kurata et al., 2007). The whole body is decomposed into blood (B) and eight distinct tissue/organ modules (**Figure 1**): liver (L), skeletal muscle (M) adipose tissue (A), GI tract (G), heart (H), brain (N), pancreas (P), and other tissues (T). Blood acts as the principal transport/exchange medium for metabolites between the different organs. Glucose and TG are inputted to blood through the GI tract, following ingestion of a meal (**Equations S1**, **S2**). Insulin secretion from the pancreas is controlled by plasma glucose and FFA concentrations (Yaney and Corkey, 2003) (**Equations S4**, **S5**). The pancreas is simplified as an insulin controller. In the liver, many rate equations are derived from several previous works (Ashworth et al., 2016; Berndt et al., 2018a; Berndt et al., 2018b; Kim et al., 2007; Pearson et al., 2014). I lump multiple associated enzyme reactions and simplify signal transduction pathways including glucose-controlled insulin secretion, phosphorylation of enzymes, and gene regulations by carbohydrate responsive element binding protein (ChREBP) and sterol-regulatory element binding protein 1c (SREBP-1c). When no experimental rate equation is available, I derive plain Michaelis-Menten type equations based on chemical reaction equations and then estimate the value of Vmax of rate equations. The parameter estimation is carried by genetic algorithms (Maeda et al., 2013; Maeda et al., 2019) so that the model can reproduce the

experimental transport/exchange fluxes at postabsorptive state between blood and each organ (Kim et al., 2007) without changing the experimental values of the Michaelis and dissociation constants. In the other organs, where little measured kinetic data is available, I estimate Vmax of rate equations so as to reproduce the experimental transport fluxes at postabsorptive state (Kim et al., 2007), while fixing the experimental values the Michaelis and dissociation constants. I assume that gene expression profiles depend on organs but the employed enzymes are common to all the organs. The other tissue has no specific regulation.

Module assembly

I combine all the organ modules. To connect blood to each organ, I define α_X and β_X $(X = L, M, A, G, H)$ as the insulin and glucagon factors for each organ, respectively, which alters the activity of insulin- and glucagon-controlled enzymes (**Equations S7-S16**). Organs of B, N, P, and T do not have the insulin/glucagon factors. I connect the liver module to the blood module. Subsequently, I add the skeletal muscle, adipose tissue, GI, heart and brain modules. The values of the insulin-related kinetic parameters are estimated so that the model can reproduce the experimental time course data of plasma insulin, plasma glucose, plasma lactate (Frayn et al., 1993), plasma glycerol (Meyer et al., 2002), plasma TG (Bickerton et al., 2008), plasma FFA, and hepatic glycogen (Taylor et al., 1996).

Dynamic sensitivity analysis

To investigate the robustness of the model, the relative change of metabolite concentrations with respect to a change in a kinetic constant were evaluated. Sensitivity analysis explores some mechanisms by which a system of interest generates robustness and remarkable changes (Masunaga et al., 2017). The dynamic sensitivity of target parameter *y* with respect to a change in specific constant parameter *p* is given by:

$$Sensitivity = \frac{\Delta y}{\Delta p}\frac{p}{y}.$$

Pathological analysis

A long-term excess supply of glucose develops steatosis, lipotoxicity, or ectopic TG accumulation by increasing synthesis of ChREBP, a transcription factor whose expression is more exclusively regulated by sugars than insulin (Mandarino et al., 1993, 1996). It also leads to the synthesis of SREBP-1c, which is stimulated by insulin under metabolically healthy conditions. In steatosis, the activities of enzymes regarding *de novo* lipogenesis (DNL) (synthesis from acetyl-CoA to TG) and cholesterol synthesis abnormally increase in the liver. Steatosis or ectopic TG accumulation can cause metabolic diseases, such as hyperglycemia, hyperlipidemia, hyperinsulinemia, obesity, NAFLD and type 2 diabetes mellitus (T2DM) (Friedman, 2002; Guebre-Egziabher et al., 2013; Kitade et al., 2017; Molavi et al., 2007). Chronic exposure to high plasma glucose and obesity, leading to oxidative stress and inflammation, induce changes in the regulation of gene expression that converge on impaired glucose-stimulated insulin secretion (Gilbert and Liu, 2012) and insulin resistance (IR). β cell dysfunction in the pancreas suppresses glucose-stimulated insulin secretion.

Individual disorder decomposition

While complex mechanisms of metabolic diseases may not be exactly defined, I conveniently decomposed the diseases into individual disorders to perform pathological analysis. Diabetes was decomposed into steatosis, β cell dysfunction, and IR. Steatosis is the underlying disease. β Cell dysfunction of pancreas is a major cause of shifting a set-point of plasma glucose concentration (Ashcroft and Rorsman, 2012; Cerf, 2013). IR is further classified with respect to each organ of the liver, skeletal muscle, and adipose tissue. IR of each organ is also a major cause. To build a steatosis model, I increased the values of kinetic parameters regarding the DNL and cholesterol synthesis in the liver. Specifically, steatosis is built by multiplying Vmax_accoat_Accoa_LM_LC, Vmax_lipog1_Accoa_LC, Vmax_lipog2_Malcoa_L, and Vmax_tgsyn_FFA_L, Vmax_cholsyn1_Accoa_LC by 2. β-cell dysfunction is built by multiplying Km_inssyn_Glc_B by 1.5. IRA is built by multiplying Km_Ins_B_A by 1.5. IRM is built by multiplying Km_Ins_B_M by 1.5. IRL is built by multiplying Km_Ins_B_L by 1.5.

Diabetes reconstruction

T2DM consists of steatosis, β cell dysfunction and IR (Ashcroft and Rorsman, 2012; Saltiel, 2001; Xia et al., 2019). To build a T2DM model, insulin resistance for the liver (IRL), insulin resistance for the skeletal muscle (IRM) or insulin resistance for the adipose tissue (IRA) was added to the steatosis and β cell dysfunction model. Type 1 diabetes mellitus (T1DM), once known as juvenile diabetes or insulin-dependent diabetes, is the extreme case of β cell dysfunction in which the pancreas produces little or no insulin. Differing from T2DM, T1DM results from genetic defects or some viruses and it has no cure.

Medication analysis

I used three types of widely prescribed T2DM medicines: sulfonylurea, metformin and thiazolidinedione to perform medication analysis. In addition to the three medicines, a glycerol kinase inhibitor was used to inhibit TG synthesis (Seltzer et al., 1986). Sulfonylurea promotes insulin secretion by the pancreas (Aquilante, 2010). Metformin is active in the suppression of hepatic gluconeogenesis. (DeFronzo et al 1991; Stumvoll et al 1995) (Molavi et al., 2007). Specifically, it suppresses lactate dehydrogenase (LDH) in the liver, accompanied by lactic acidosis (Pernicova and Korbonits, 2014). It also activates AMP-activated protein kinase (AMPK) that regulates energy homeostasis (Fullerton et al., 2013; Pernicova and Korbonits, 2014) or activate β-oxidation. Thiazolidinediones are a family of drugs that have been used in the treatment of T2DM since the late 1990s (Molavi et al., 2007). The thiazolidinedione derivatives, pioglitazone and rosiglitazone, are synthetic ligands for peroxisome proliferative-activated receptor γ (PPARγ) that improve insulin sensitivity. PPARγ is mainly expressed in the adipose tissue; PPARγ agonists promote adipocyte differentiation and promote the FFA uptake and storage in the subcutaneous adipose tissue rather than visceral sites (Rasouli et al., 2005). In addition, thiazolidinedione is known to enhance the glucose uptake in the skeletal muscle (Natali and Ferrannini, 2006). Specifically, metformin reduces Vmax_ldh_Pyr_L to zero and multiplies Vmax_boxid_FFA_L by 2. Thiazolidinedione multiplies Vmax_tgsyn_FFA_A by 2. Sulfonylurea multiples Vmax_inssyn_Glc_B by 2.

Glycerol kinase inhibitor reduces Vmax_glyk_Glyc_L to zero.

Experimental data and subjects

The model targets a healthy young adult man with 70 kg body weight. The exchange fluxes between blood and each organ at postabsorptive state were derived from the previous work (Kim et al., 2007). The time course data of plasma insulin, plasma glucose, plasma lactate, plasama FFA, and plasma TG were measured for 6 h after an overnight fast and following a single meal of 87 g carbohydrate and 33 g fat (Time = 0) for 8 healthy subjects (Frayn et al., 1993) (Bickerton et al., 2008). The plasma lactate and liver glycogen were measured after an overnight fast and following a meal containing 98 g carbohydrate and 14 g fat for 8 healthy subjects (Taylor et al., 1996). The plasma glycerol and alanine were measured after an overnight fast and following a meal containing 75 g carbohydrate for 10 healthy subjects (Meyer et al., 2002).

Homeostasis of metabolites in blood

Glucose and hormone

Plasma glucose in human is controlled at a set-point of 5 mM by hormones of insulin and glucagon (Frayn, 2010). Insulin is the only hormone that decreases the plasma glucose concentration, while multiple glucose increasing hormones are known. Glucagon is a counter partner of insulin. The plasma concentrations of insulin and glucagon directly respond to changes in plasma glucose. The plasma glucose concentration is maintained in a narrow range between a minimum value of 3 mM after prolonged fasting or exercise and a maximum value of 9 mM after a meal (Nuttall et al., 2008). Glucose enters blood in three ways: absorption from the intestine, glycogenolysis in the liver, and gluconeogenesis in the liver and kidney. After an overnight fast, 95% of glucose production comes from the liver (Kim et al., 2007). The liver produces glucose through glycogenolysis and gluconeogenesis with almost equal contribution at postabsorptive state. Lactate, pyruvate, alanine and glycerol are the major gluconeogenic precursors. Fifty percentages of glucose at postabsorptive state is utilized by the brain, while the skeletal muscle uses 20%. The gastrointestinal (GI) tract consumes only 10% of glucose. The organs except the brain use FFA as metabolic fuels to save glucose.

Lactate, pyruvate and alanine

The liver and heart primarily consume plasma lactate, while the skeletal muscle, adipose tissue and other tissues, including inactive upper body muscles and red blood cells, produce lactate. Pyruvate exchange occurs primarily between the skeletal muscle and other tissues. Plasma pyruvate concentration is very small or negligible. Only the liver consumes amino acids, especially alanine, for gluconeogenesis, while the skeletal muscle is the main source of alanine and the inactive muscle in other tissues is an additional source.

FFA, glycerol and triglyceride (TG)

FFA and glycerol are mainly produced from lipolysis of TG in the adipose tissue. The liver uptakes FFA from blood and utilizes FFA as a main fuel. A half of the liver-taken FFA is oxidized; the half is re-esterified into TG (Frayn, 2010; Kim et al., 2007). Since the adipose tissue lacks glycerol phosphorylase, lipolysis-produced

glycerol is not utilized for TG synthesis in the adipose tissue. The liver uptakes the glycerol released from the adipose tissue and utilize it as a gluconeogenic precursor, i.e., a substrate for TG synthesis.

Ketone body

Ketone bodies including β-hydroxybutyrate (Bhb) are synthesized from acetyl-CoA produced through β-oxidation. Synthesis of ketone bodies are stimulated mainly by glucagon in the liver under a fasted condition. Ketone bodies are utilized exclusively by the brain.

Metabolic reactions of each organ

Liver and pancreas

The liver plays a central role in buffering or controlling plasma glucose. Switching between the glucose utilization (glycolysis and glycogenesis) and glucose production (gluconeogenesis and glycogenolysis) is dependent on the plasma glucose level. The glucose utilization occurs at glucose concentration exceeding a critical threshold value; the glucose production occurs below the critical concentration. Insulin alters the phosphorylation state of multiple key interconvertible enzymes of hexokinase (HK), glycogen synthase (GS), glycogen phosphorylase (GP), phosphofructokinase (PFK), fructose-1,6-bisphosphatase (FBP), pyruvate kinase (PK) and pyruvate dehydrogenase (PDH) to shift a remarkable metabolic state. The liver temporally stores substantial amounts of glucose as glycogen, synthesizes glucose from small carbohydrates, including lactate, pyruvate, glycerol and alanine, and converts excess glucose into FFA. It also synthesizes TG and cholesterol and secretes them into blood. Under a fasted condition, the liver synthesizes Bhb from acetyl-CoA as a metabolic fuel for the brain. In the pancreas β cells serve as a controller of insulin synthesis and release in response to a plasma glucose concentration.

Skeletal muscle and heart

Insulin activates glucose transporter 4 (GLUT4) in the skeletal muscle to uptake glucose and to accumulate glycogen. To control substantially glucose uptake rates, a few key enzymes of HK, GS, and PDH are activated (Mandarino et al., 1993, 1996). In this study the skeletal muscle represents the lean muscles in the lower extremity. The skeletal muscle uptakes FFA as fuels and releases lactate and alanine into blood. Heart consists of specialized muscle cells (cardiomyocytes) and constantly uptakes metabolic fuels, including glucose, lactate, and FFA to generate ATP to maintain contractile function without any fatigue. In contrast to the skeletal muscle, GLUT1, which is not controlled by insulin, is dominant. The major metabolic fuel for the heart is FFA.

Adipose tissue and GI tract

The adipose tissues are producers and reservoirs of TG. Plasma TG is degraded by lipase on the adipose tissue surface into FFA and glycerol. FFA enters the adipose cells; glycerol returns to blood. Within the adipose tissue, FFA and glycerol-3-phosphate (Grp) are synthesized into TG. Since the adipose tissue lacks glycerol kinase, glycerol-3-P comes just from glucose-derived glycelaldehyde-3-phosphate (Gap). Insulin activates the TG synthesis and lipase reaction, facilitating TG accumulation. The GI tract includes the splanchnic region (stomach,

spleen, intestines) except the liver. It utilizes glucose, accumulates TG, and releases FFA and glycerol into blood.

Brain and other tissues

The brain constantly takes only glucose and Bhb as metabolic fuels, neither utilizes FFA nor TG, because the blood-brain barrier prevents such large-size molecules from entering the brain. It has Bhb degradation pathways to degrade Bhb into acetyl-CoA for energy. The other tissue compartment includes kidney, upper extremity muscles, and the rest of tissues.

References

Aquilante, C.L. (2010). Sulfonylurea pharmacogenomics in Type 2 diabetes: the influence of drug target and diabetes risk polymorphisms. Expert Rev Cardiovasc Ther *8*, 359-372.

Ashcroft, F.M., and Rorsman, P. (2012). Diabetes mellitus and the beta cell: the last ten years. Cell *148*, 1160-1171.

Ashworth, W.B., Davies, N.A., and Bogle, I.D. (2016). A Computational Model of Hepatic Energy Metabolism: Understanding Zonated Damage and Steatosis in NAFLD. PLoS Comput Biol *12*, e1005105.

Berndt, N., Bulik, S., Wallach, I., Wunsch, T., Konig, M., Stockmann, M., Meierhofer, D., and Holzhutter, H.G. (2018a). HEPATOKIN1 is a biochemistry-based model of liver metabolism for applications in medicine and pharmacology. Nat Commun *9*, 2386.

Berndt, N., Horger, M.S., Bulik, S., and Holzhutter, H.G. (2018b). A multiscale modelling approach to assess the impact of metabolic zonation and microperfusion on the hepatic carbohydrate metabolism. PLoS Comput Biol *14*, e1006005.

Bickerton, A.S., Roberts, R., Fielding, B.A., Tornqvist, H., Blaak, E.E., Wagenmakers, A.J., Gilbert, M., Humphreys, S.M., Karpe, F., and Frayn, K.N. (2008). Adipose tissue fatty acid metabolism in insulin-resistant men. Diabetologia *51*, 1466-1474.

Cerf, M.E. (2013). Beta cell dysfunction and insulin resistance. Front Endocrinol (Lausanne) *4*, 37.

Frayn, K.N. (2010). Metabolic regulation: A human perspective (UK: Willey-Blackwell).

Frayn, K.N., Coppack, S.W., Humphreys, S.M., Clark, M.L., and Evans, R.D. (1993). Periprandial regulation of lipid metabolism in insulin-treated diabetes mellitus. Metabolism *42*, 504-510.

Friedman, J. (2002). Fat in all the wrong places. Nature *415*, 268-269.

Fullerton, M.D., Galic, S., Marcinko, K., Sikkema, S., Pulinilkunnil, T., Chen, Z.P., O'Neill, H.M., Ford, R.J., Palanivel, R., O'Brien, M., *et al.* (2013). Single phosphorylation sites in Acc1 and Acc2 regulate lipid homeostasis and the insulin-sensitizing effects of metformin. Nat Med *19*, 1649-1654.

Gilbert, E.R., and Liu, D. (2012). Epigenetics: the missing link to understanding beta-cell dysfunction in the pathogenesis of type 2 diabetes. Epigenetics *7*, 841-852.

Guebre-Egziabher, F., Alix, P.M., Koppe, L., Pelletier, C.C., Kalbacher, E., Fouque, D., and Soulage, C.O. (2013). Ectopic lipid accumulation: A potential cause for metabolic disturbances and a contributor to the alteration of kidney function. Biochimie *95*, 1971-1979.

Karr, J.R., Sanghvi, J.C., Macklin, D.N., Gutschow, M.V., Jacobs, J.M., Bolival, B., Jr., Assad-Garcia, N., Glass, J.I., and Covert, M.W. (2012). A whole-cell computational model predicts phenotype from genotype. Cell *150*, 389-401.

Kawamori, D., Kurpad, A.J., Hu, J., Liew, C.W., Shih, J.L., Ford, E.L., Herrera, P.L., Polonsky, K.S., McGuinness, O.P., and Kulkarni, R.N. (2009). Insulin signaling in alpha cells modulates glucagon secretion in vivo. Cell Metab *9*, 350-361.

Kim, J., Saidel, G.M., and Cabrera, M.E. (2007). Multi-scale computational model of fuel homeostasis during exercise: effect of hormonal control. Ann Biomed Eng *35*, 69-90.

Kitade, H., Chen, G., Ni, Y., and Ota, T. (2017). Nonalcoholic Fatty Liver Disease and Insulin Resistance: New Insights and Potential New Treatments. Nutrients *9*.

Kurata, H., Inoue, K., Maeda, K., Masaki, K., Shimokawa, Y., and Zhao, Q. (2007). Extended CADLIVE: a novel graphical notation for design of biochemical network maps and computational pathway analysis. Nucleic Acids Res *35*, e134.

Maeda, K., Minamida, H., Yoshida, K., and Kurata, H. (2013). Flux module decomposition for parameter estimation in a multiple-feedback loop model of biochemical networks. Bioprocess Biosyst Eng *36*, 333-344.

Maeda, K., Westerhoff, H.V., Kurata, H., and Boogerd, F.C. (2019). Ranking network mechanisms by how they fit diverse experiments and deciding on E. coli's ammonium transport and assimilation network. NPJ Syst Biol Appl *5*, 14.

Mandarino, L.J., Consoli, A., Jain, A., and Kelley, D.E. (1993). Differential regulation of intracellular glucose metabolism by glucose and insulin in human muscle. Am J Physiol *265*, E898-905.

Mandarino, L.J., Consoli, A., Jain, A., and Kelley, D.E. (1996). Interaction of carbohydrate and fat fuels in human skeletal muscle: impact of obesity and NIDDM. Am J Physiol *270*, E463-470.

Masunaga, H., Sugimoto, Y., Magi, S., Itasaki, R., Okada-Hatakeyama, M., and Kurata, H. (2017). Robustness analysis of the detailed kinetic model of an ErbB signaling network by using dynamic sensitivity. PLoS One *12*, e0178250.

Meyer, C., Dostou, J.M., Welle, S.L., and Gerich, J.E. (2002). Role of human liver, kidney, and skeletal muscle in postprandial glucose homeostasis. Am J Physiol Endocrinol Metab *282*, E419-427.

Molavi, B., Rassouli, N., Bagwe, S., and Rasouli, N. (2007). A review of thiazolidinediones and metformin in the treatment of type 2 diabetes with focus on cardiovascular complications. Vasc Health Risk Manag *3*, 967-973.

Natali, A., and Ferrannini, E. (2006). Effects of metformin and thiazolidinediones on suppression of hepatic glucose production and stimulation of glucose uptake in type 2 diabetes: a systematic review. Diabetologia *49*, 434-441.

Nuttall, F.Q., Ngo, A., and Gannon, M.C. (2008). Regulation of hepatic glucose production and the role of gluconeogenesis in humans: is the rate of gluconeogenesis constant? Diabetes Metab Res Rev *24*, 438-458.

Pearson, T., Wattis, J.A., King, J.R., MacDonald, I.A., and Mazzatti, D.J. (2014). A mathematical model of the human metabolic system and metabolic flexibility. Bull Math Biol *76*, 2091-2121.

Pernicova, I., and Korbonits, M. (2014). Metformin--mode of action and clinical implications for diabetes and cancer. Nat Rev Endocrinol *10*, 143-156.

Rasouli, N., Raue, U., Miles, L.M., Lu, T., Di Gregorio, G.B., Elbein, S.C., and Kern, P.A. (2005). Pioglitazone improves insulin sensitivity through reduction in muscle lipid and redistribution of lipid into adipose tissue. Am J Physiol Endocrinol Metab *288*, E930-934.

Saltiel, A.R. (2001). New perspectives into the molecular pathogenesis and treatment of type 2 diabetes. Cell *104*, 517-529.

Seltzer, W.K., Dhariwal, G., McKelvey, H.A., and McCabe, E.R. (1986). 1-Thioglycerol: inhibitor of glycerol kinase activity in vitro and in situ. Life Sci *39*, 1417-1424.

Swainston, N., Smallbone, K., Hefzi, H., Dobson, P.D., Brewer, J., Hanscho, M., Zielinski, D.C., Ang, K.S., Gardiner, N.J., Gutierrez, J.M.*, et al.* (2016). Recon 2.2: from reconstruction to model of human metabolism. Metabolomics *12*, 109.

Taylor, R., Magnusson, I., Rothman, D.L., Cline, G.W., Caumo, A., Cobelli, C., and Shulman, G.I. (1996). Direct assessment of liver glycogen storage by 13C nuclear magnetic resonance spectroscopy and regulation of glucose homeostasis after a mixed meal in normal subjects. J Clin Invest *97*, 126-132.

Xia, M.F., Bian, H., and Gao, X. (2019). NAFLD and Diabetes: Two Sides of the Same Coin? Rationale for Gene-Based Personalized NAFLD Treatment. Front Pharmacol *10*, 877.

Yaney, G.C., and Corkey, B.E. (2003). Fatty acid metabolism and insulin secretion in pancreatic beta cells. Diabetologia *46*, 1297-1312.

Yugi, K., Kubota, H., Toyoshima, Y., Noguchi, R., Kawata, K., Komori, Y., Uda, S., Kunida, K., Tomizawa, Y., Funato, Y.*, et al.* (2014). Reconstruction of insulin signal flow from phosphoproteome and metabolome data. Cell Rep *8*, 1171-1183.

Data S1 Mathematical equations, Related to Figures 3-7

Dietary input flux

$$v_{meal}^{Glc_B} = Glc_B^{meal} \frac{t}{T_{delay}^{Glc_B 2}} \exp(-\frac{t^2}{2T_{delay}^{Glc_B 2}}) \quad \text{(S1)}$$

$$v_{meal}^{TG_B} = TG_B^{meal} \frac{t}{T_{delay}^{TG_B 2}} \exp(-\frac{t^2}{2T_{delay}^{TG_B 2}}) \quad \text{(S2)}$$

where t is time. (Pearson et al., 2014)

Insulin flux

The insulin synthesis rate is described by Hill equation for plasma glucose (Konig et al., 2012; Pearson et al., 2014).

$$v_{inssyn}^{B} = k_{inssyn}^{B} \quad \text{(S3)}$$

$$v_{inssyn}^{Glc_B} = Vmax_{inssyn}^{Glc_B} \frac{Glc_B^{n_{inssyn}^{Glc_B}}}{K_{minssyn}^{Glc_B n_{inssyn}^{Glc_B}} + Glc_B^{n_{inssyn}^{Glc_B}}} \quad \text{(S4)}$$

$$v_{inssyn}^{FFA_B} = k_{inssyn}^{FFA_B} FFA_B \quad \text{(S5)}$$

$$v_{insdeg}^{Ins_B} = k_{insdeg}^{Ins_B} Ins_B \quad \text{(S6)}$$

Insulin and glucagon activities in organs

Insulin-regulated enzyme activity factor in liver is defined as α_L, which is determined by plasma insulin concentration, depending on each organ.

$$\alpha_L = \alpha_L^{Base} + \alpha_L^{Band} \frac{Ins_B^{n^{Ins_{BL}}}}{Km^{Ins_{BL} n^{Ins_{BL}}} + Ins_B^{n^{Ins_{BL}}}} \quad \text{(S7)}$$

$$\alpha_M = \alpha_M^{Base} + \alpha_M^{Band} \frac{Ins_B^{n^{Ins_{BM}}}}{Km^{Ins_{BM} n^{Ins_{BM}}} + Ins_B^{n^{Ins_{BM}}}} \quad \text{(S8)}$$

$$\alpha_A = \alpha_A^{Base} + \alpha_A^{Band} \frac{Ins_B^{n^{Ins_{BA}}}}{Km^{Ins_{BA} n^{Ins_{BA}}} + Ins_B^{n^{Ins_{BA}}}} \quad \text{(S9)}$$

$$\alpha_G = \alpha_G^{Base} + \alpha_G^{Band} \frac{Ins_B^{n^{Ins_{BG}}}}{Km^{Ins_{BG} n^{Ins_{BG}}} + Ins_B^{n^{Ins_{BG}}}} \quad \text{(S10)}$$

$$\alpha_H = \alpha_H^{Base} + \alpha_H^{Band} \frac{Ins_B^{n^{Ins_{BH}}}}{Km^{Ins_{BH}\, n^{Ins_{BH}}} + Ins_B^{n^{Ins_{BH}}}} \tag{S11}$$

Glucagon-regulated enzyme activity factor is given by

$$\beta_L = 1 - \alpha_L \tag{S12}$$

$$\beta_M = 1 - \alpha_M \tag{S13}$$

$$\beta_A = 1 - \alpha_A \tag{S14}$$

$$\beta_G = 1 - \alpha_G \tag{S15}$$

$$\beta_H = 1 - \alpha_H \tag{S16}$$

Subscripts: *L*, *M*, *A*, *G*, *H*, *N* and *T* indicate liver, skeletal muscle, adipose tissue, GI, heart, brain, and other tissue, respectively.

Flux in liver

Glucose transporter (GLUT2) (Ashworth et al., 2016; Berndt et al., 2018b; Zheng et al., 1995)

$$v_{glut2}^{Glc_{BL}} = Vdif_{glut2}^{Glc_{BL}} \frac{Glc_B - Glc_L}{1 + \frac{Glc_B}{Kdif_{glut2}^{Glc_{BL}}} + \frac{Glc_L}{Kdif_{glut2}^{Glc_L}}} \tag{S17}$$

Hexokinase (HK) (Berndt et al., 2018b)

$$v_{hk}^{Glc_L} = \alpha_L \cdot Vmax_{hk}^{Glc_L} \frac{Glc_L}{Glc_L + Km_{hk}^{Glc_L}(1 + \frac{G6p_L}{Ki_{hk}^{G6p_L}})} \cdot \frac{Atp_L}{Atp_L + Km_{hk}^{Atp_L}(1 + \frac{G6p_L}{Ki_{hk}^{Atp_L}})} \tag{S18}$$

Glucokinase (GK) (Ashworth et al., 2016)

$$v_{hk}^{Glc_L} = \alpha_L \cdot Vmax_{gk}^{Glc_L} \cdot \frac{Glc_L^{n_{1gk}^{Glc_L}}}{Glc_L^{n_{1gk}^{Glc_L}} + Km_{1gk}^{Glc_L\, n_{1gk}^{Glc_L}}} \cdot \frac{Glc_L^{n_{2gk}^{Glc_L}}}{Glc_L^{n_{2gk}^{Glc_L}} + Km_{2gk}^{Glc_L\, n_{2gk}^{Glc_L}}} \frac{Atp_L}{Atp_L + Km_{gk}^{Atp_L}} (1 - \frac{G6p_L^{n_{gk}^{G6p_L}}}{G6p_L^{n_{gk}^{G6p_L}} + Ki_{gk}^{G6p_L\, n_{gk}^{G6p_L}}}) \tag{S19}$$

Pentose phosphate pathway (PPP)

$$v_{ppp}^{G6p_X} = Vmax_{g6pase}^{G6p_L} \frac{G6p_L}{G6p_L + Km_{ppp}^{G6p_L}} \frac{Nadp_L}{Nadp_L + Km_{ppp}^{Nadp_L}} \tag{S20}$$

G6Pase (Ashworth et al., 2016)

$$v_{g6pase}^{G6p_L} = Vmax_{g6pase}^{G6p_L} \frac{G6p_L}{G6p_L + Km_{g6pase}^{G6p_L}} \quad \text{(S21)}$$

Glycogen synthase (GS) (Ashworth et al., 2016)

$$v_{gs}^{G6p_X} = \alpha_L \cdot Vmax_{gs}^{G6p_L} \frac{G6p_L^{n_{gs}^{G6pL}}}{G6p_X^{n_{gs}^{G6pX}} + Km_{gs}^{G6p_X n_{gs}^{G6pX}}} \cdot \frac{(Glygn_L^{\max} - Glygn_L)}{(Glygn_L^{\max} - Glygn_L) + Km_{gs}^{Glygn_L}} \cdot \frac{Utp_L}{Utp_L + Km_{gs}^{Utp_L}} \quad \text{(S22)}$$

$Glygn_L^{\max}$ denotes the maximum amount of glycogen that liver can store (Pearson et al., 2014).

Glycogen degradation (GD) by glycogen phosphorylase (GP) (Ashworth et al., 2016)

$$v_{gd}^{Glygn_L} = \beta_L \cdot Vmax_{gd}^{Glygn_L} \frac{Glygn_L}{Glygn_L + Km_{gd}^{Glygn_L}} \frac{Phos_L}{Phos_L + Km_{gd}^{Phos_L}} \quad \text{(S23)}$$

Phosphofructokinase (PFK) (Ashworth et al., 2016)

$$v_{pfk}^{G6p_L} = \alpha_L \cdot Vmax_{pfk}^{G6p_L} \frac{G6p_L}{G6p_L + Km_{pfk}^{G6p_L}} \cdot \frac{Atp_L}{Atp_L + Km_{pfk}^{Atp_L}} \cdot \frac{Ki_{pfk}^{Atp_L}}{Atp_L + Ki_{pfk}^{Atp_L}} \cdot \frac{Adp_L}{Adp_L + Km_{pfk}^{Adp_L}} \cdot (1 - b_{pfk}^{Gap_L} \frac{Gap_L}{Gap_L + Ki_{pfk}^{Gap_L}}) \quad \text{(S24)}$$

Fructose-1,6-bisphosphatase (FBP) (Ashworth et al., 2016)

$$v_{fbp}^{Gap_L} = \beta_L \cdot Vmax_{fbp}^{Gap_L} \frac{Gap_L}{Gap_L + Km_{fbp}^{Gap_L}} \quad \text{(S25)}$$

Pyruvate kinase (PK) (Ashworth et al., 2016)

$$v_{pk}^{Gap_L} = \alpha_L \cdot Vmax_{pk}^{Gap_L} \cdot \frac{Gap_L}{Gap_L + Km_{pk}^{Gap_L}} \cdot (1 - b_{pk}^{Accoa_{LM}} \frac{Accoa_{LM}}{Accoa_{LM} + Ki_{pk}^{Accoa_{LM}}}) \cdot \frac{Adp_L}{Adp_L + Km_{pk}^{Adp_L}} \quad \text{(S26)}$$

Phosphoenolpyruvate carboxykinase (PEPCK) (Ashworth et al., 2016)

$$v_{pepck}^{Pyr_L} = \beta_L \cdot Vmax_{pepck}^{Pyr_L} \cdot \frac{Pyr_L}{Pyr_L + Km_{pepck}^{Pyr_X}} \cdot \frac{Atp_L}{Atp_L + Km_{pepck}^{Atp_L}} \cdot \frac{Gtp_L}{Gtp_L + Km_{pepck}^{Gtp_L}} \quad \text{(S27)}$$

Pyruvate transporter (PYRT) (Berndt et al., 2018b)

$$v_{pyrt}^{Pyr_{BL}} = Vdif_{pyrt}^{Pyr_{BL}} \frac{Pyr_B - Pyr_L}{1 + \frac{Pyr_B}{Kdif_{pyrt}^{Pyr_{BL}}} + \frac{Pyr_L}{Kdif_{pyrt}^{Pyr_L}}} \quad \text{(S28)}$$

Lactate transporter (LACT) (Berndt et al., 2018b)

$$v_{lact}^{Lac_{BL}} = Vdif_{lact}^{Lac_{BL}} \frac{Lac_B - Lac_L}{1 + \frac{Lac_B}{Kdif_{lact}^{Lac_{BL}}} + \frac{Lac_L}{Kdif_{lact}^{Lac_L}}} \quad \text{(S29)}$$

Lactate dehydrogenase (LDH) (Berndt et al., 2018b)

$$v_{ldh}^{Pyr_L} = Vmax_{ldh}^{Pyr_L} \cdot \frac{Pyr_L \cdot Nadh_L - Lac_L \cdot Nad_L / Keq_{ldh}^{Lac_L}}{(1 + \frac{Pyr_L}{Km_{ldh}^{Pyr_L}}) \cdot (1 + \frac{Nadh_L}{Km_{ldh}^{Nadh_L}}) + (1 + \frac{Lac_L}{Km_{ldh}^{Lac_L}}) \cdot (1 + \frac{Nad_L}{Km_{ldh}^{Nad_L}}) - 1} \quad \text{(S30)}$$

Alanine transporter (ALAT)

$$v_{alat}^{Ala_{BL}} = Vdif_{alat}^{Ala_{BL}} \frac{Ala_B - Ala_L}{1 + \frac{Ala_B}{Kdif_{alat}^{Ala_B}} + \frac{Ala_L}{Kdif_{alat}^{Ala_L}}} \quad \text{(S31)}$$

Alanine transaminase (ALAT)

$$v_{alata}^{Pyr_L} = Vmax_{alata}^{Pyr_L} \cdot \frac{Pyr_L - Ala_L / Keq_{alata}^{Ala_L}}{(1 + \frac{Pyr_L}{Km_{alata}^{Pyr_L}}) + (1 + \frac{Ala_L}{Km_{alata}^{Ala_L}}) - 1} \quad \text{(S32)}$$

Pyruvate dehydrogenase (PDH) (Ashworth et al., 2016)

$$v_{pdh}^{Pyr_L} = \alpha_L \cdot Vmax_{pdh}^{Pyr_L} \cdot \frac{Pyr_L}{Pyr_L + Km_{pdh}^{Pyr_L}} \cdot \frac{Nad_L}{Nad_L + Km_{pdh}^{Nad_L}} \cdot \frac{Km_{pdh}^{Accoa_{LM}}}{Accoa_{LM} + Km_{pdh}^{Accoa_{LM}}} \quad \text{(S33)}$$

TCA cycle (TCA)

$$v_{tca}^{Accoa_{LM}} = Vmax_{tca}^{Accoa_{LM}} \cdot \frac{Accoa_{LM}}{Accoa_{LM} + Km_{tca}^{Accoa_{LM}}} \cdot \frac{Adp_L}{Adp_L + Km_{tca}^{Adp_L}} \cdot \frac{Nad_L}{Nad_L + Km_{tca}^{Nad_L}} \cdot \frac{Fad_L}{Fad_L + Km_{tca}^{Fad_L}} \cdot \frac{Phos_L}{Phos_L + Km_{tca}^{Phos_L}} \cdot \frac{Pyr_L}{Pyr_L + Km_{tca}^{Pyr_L}} \quad \text{(S34)}$$

FFA transporter (FFAT) (Ashworth et al., 2016)

$$v_{ffat}^{FFA_{BL}} = v_{ffat\_d}^{FFA_{BL}} + v_{ffat\_a}^{FFA_{BL}} \quad \text{(S35)}$$

$$v_{ffat\_d}^{FFA_{BL}} = Vdif_{ffat}^{FFA_{BL}} \frac{FFA_B - FFA_L}{1 + \frac{FFA_B}{Kdif_{ffat}^{FFA_{BL}}} + \frac{FFA_L}{Kdif_{ffat}^{FFA_L}}} \quad \text{(S36)}$$

$$v_{ffat\_a}^{FFA_{BL}} = Vmax_{ffat}^{FFA_{BL}} \frac{FFA_B}{FFA_B + Km_{ffat}^{FFA_{BL}}} \quad \text{(S37)}$$

TG synthesis (TGSYN) (Ashworth et al., 2016)

$$v_{tgsyn}^{FFA_L} = \alpha_L \cdot Vmax_{tgsyn}^{FFA_L} \frac{FFA_L}{FFA_L + Km_{tgsyn}^{FFA_L}} \cdot \frac{Glycp_L}{Glycp_L + Km_{tgsyn}^{Glycp_L}} \cdot \frac{Atp_L}{Atp_L + Km_{tgsyn}^{Atp_L}} \quad \text{(S38)}$$

TG degradation (TGDEG) (Ashworth et al., 2016)

$$v_{tgdeg}^{TG_L} = \beta_L Vmax_{tgdeg}^{TG_L} \frac{TG_L}{TG_L + Km_{tgdeg}^{TG_L}} \quad \text{(S39)}$$

Glycerol transporter (GLYCT) (Ashworth et al., 2016)

$$v_{glyct}^{Glyc_{BL}} = Vdif_{glyct}^{Glyc_{BL}} \frac{Glyc_B - Glyc_L}{1 + \frac{Glyc_B}{Kdif_{glyct}^{Glyc_{BL}}} + \frac{Glyc_L}{Kdif_{glyct}^{Glyc_L}}} \quad \text{(S40)}$$

Glycerol kinase (GLYK) (Berndt et al., 2018a)

$$v_{glyk}^{Glyc_L} = Vmax_{glyk}^{Glyc_L} \frac{Glyc_L}{Glyc_L + Km_{glyk}^{Glyc_L}(1 + \frac{Gap_L}{Ki_{glyk}^{Gap_L}})} \frac{Atp_L}{Atp_L + Km_{glyk}^{Atp_L}} \quad \text{(S41)}$$

TG transporter (TGT) (Ashworth et al., 2016)

$$v_{tgt}^{TG_{BL}} = v_{tgt\_a}^{TG_L} + v_{tgt\_d}^{TG_L} \tag{S42}$$

$$v_{tgt\_d}^{TG_{BL}} = Vdif_{tgt}^{TG_{BL}} \frac{TG_B - TG_L \Big/ Keq_{tgt}^{TG_L}}{TG_B + Kdif_{tgt}^{TG_{BL}} + \dfrac{TG_L}{Keq_{tgt}^{TG_L}}} \tag{S43}$$

$$v_{tgt\_a}^{TG_{BL}} = -\beta_L \cdot Vmax_{tgt}^{TG_L} \frac{TG_L}{TG_L + Km_{tgt}^{TG_L}} \tag{S44}$$

Glycerol-3-phosphate dehydrogenase (G3PD) (Berndt et al., 2018a)

$$v_{g3pd}^{Gap_L} = Vmax_{g3pd}^{Gap_L} \frac{Gap_L Nadh_L - \dfrac{Glycp_L}{Keq_{g3pd}^{Glycp_L}} Nad_L}{(1+\dfrac{Gap_L}{Km_{g3pd}^{Gap_L}})(1+\dfrac{Nadh_L}{Km_{g3pd}^{Nadh_L}}) + (1+\dfrac{Glycp_L}{Km_{g3pd}^{Glycp_L}})(1+\dfrac{Nad_L}{Km_{g3pd}^{Nad_L}}) - 1} \tag{S45}$$

β-oxidation (BOXID) (Ashworth et al., 2016)

$$v_{boxid}^{FFA_L} = Vmax_{boxid}^{FFA_L} \frac{FFA_L}{FFA_L + Km_{boxid}^{FFA_L}} \cdot \frac{Atp_L}{Atp_L + Km_{boxid}^{Atp_L}} \cdot \frac{Nad_L}{Nad_L + Km_{boxid}^{Nad_L}} \cdot \frac{Fad_L}{Fad_L + Km_{boxid}^{Fad_L}} \cdot \frac{Ki_{boxid}^{Accoa_{LM}}}{Accoa_{LM} + Ki_{boxid}^{Accoa_{LM}}} \cdot \frac{Ki_{boxid}^{Malcoa_L}}{Malcoa_L + Ki_{boxid}^{Malcoa_L}} \tag{S46}$$

AcCoA release into cytoplasm for FFA synthesis (ACCOAT)

$$v_{accoat}^{Accoa_{LMLC}} = Vmax_{accoat}^{Accoa_{LMLC}} \frac{Accoa_{LM}}{Accoa_{LM} + Km_{accoat}^{Accoa_{LM}}} \cdot \frac{Atp_L}{Atp_L + Km_{accoat}^{Atp_L}} \cdot \frac{Pyr_L}{Pyr_L + Km_{accoat}^{Pyr_L}} \tag{S47}$$

β-hydroxybutyrate synthesis (BHBSYN)

$$v_{bhbsyn}^{Accoa_{LM}} = \beta_L \cdot Vmax_{bhbsyn}^{Accoa_{LM}} \frac{Accoa_{LM}}{Accoa_{LM} + Km_{bhbsyn}^{Accoa_{LM}}} \frac{Nadh_L}{Nadh_L + Km_{bhbsyn}^{Nadh_L}} \cdot \frac{Ki_{bhbsyn}^{Pyr_L\ n_{bhbsyn}^{Pyr_L}}}{Pyr_L^{\ n_{bhbsyn}^{Pyr_L}} + Ki_{bhbsyn}^{Pyr_L\ n_{bhbsyn}^{Pyr_L}}} \tag{S48}$$

β-hydroxybutyrate transporter (BHBT)

$$v_{bhbt}^{Bhb_{BL}} = Vdif_{bhbt}^{Bhb_{BL}} \frac{Bhb_B - Bhb_L}{1 + \dfrac{Bhb_B}{Kdif_{bhbt}^{Bhb_{BL}}} + \dfrac{Bhb_L}{Kdif_{bhbt}^{Bhb_L}}} \tag{S49}$$

Lipogenesis 1 (LIPOG1)

$$v_{lipog1}^{Accoa_{LC}} = Vmax_{lipog1}^{Accoa_{LC}} \frac{Accoa_{LC}}{Accoa_{LC} + Km_{lipog1}^{Accoa_{LC}}} \cdot \frac{Atp_L}{Atp_L + Km_{lipog1}^{Atp_L}} \quad \text{(S50)}$$

Lipogenesis 2 (LIPOG2)

$$v_{lipog2}^{Malcoa_L} = Vmax_{lipog2}^{Malcoa_L} \frac{Malcoa_L}{Malcoa_L + Km_{lipog2}^{Malcoa_L}} \cdot \frac{Adp_L}{Adp_L + Km_{lipog2}^{Adp_L}} \cdot \frac{Nadph_L}{Nadph_L + Km_{lipog2}^{Nadph_L}} \quad \text{(S51)}$$

Cholesterol synthesis 1 (CHOLSYN1)

$$v_{cholsyn1}^{Accoa_{LC}} = Vmax_{cholsyn1}^{Accoa_{LC}} \frac{Accoa_{LC}}{Accoa_{LC} + Km_{cholsyn1}^{Accoa_{LC}}} \quad \text{(S52)}$$

Cholesterol synthesis 2 (CHOLSYN2)

$$v_{cholsyn2}^{Hmgcoa_L} = Vmax_{cholsyn2}^{Hmgcoa_L} \frac{Hmgcoa_L}{Hmgcoa_L + Km_{cholsyn2}^{Hmgcoa_L}} \cdot \frac{Atp_L}{Atp_L + Km_{cholsyn2}^{Atp_L}} \cdot \frac{Fadh_L}{Fadh_L + Km_{cholsyn2}^{Fadh_L}} \cdot \frac{Nadph_L}{Nadph_L + Km_{cholsyn2}^{Nadph_L}} \quad \text{(S53)}$$

Cholesterol transporter (CHOLT)

$$v_{cholt}^{Chol_{BL}} = -Vmax_{cholt}^{Chol_{BL}} \frac{Chol_L}{Chol_L + Km_{cholt}^{Chol_L}} \quad \text{(S54)}$$

ATP synthesis from FADH (ATPSYNF)

$$v_{atpsynf}^{Fadh_L} = Vmax_{atpsynf}^{Fadh_L} \frac{Fadh_L}{Fadh_L + Km_{atpsynf}^{Fadh_L}} \cdot \frac{Adp_L}{Adp_L + Km_{atpsynf}^{Adp_L}} \quad \text{(S55)}$$

ATP synthesis from NADH (ATPSYNN)

$$v_{atpsynn}^{Nadh_L} = Vmax_{atpsynn}^{Nadh_L} \frac{Nadh_L}{Nadh_L + Km_{atpsynn}^{Nadh_L}} \cdot \frac{Adp_L}{Adp_L + Km_{atpsynn}^{Adp_L}} \quad \text{(S56)}$$

ATP utilization (ATPUSE)

$$v_{atpuse}^{Atp_L} = Vmax_{atpuse}^{Atp_L} \frac{Atp_L}{Atp_L + Km_{atpuse}^{Atp_L}} \quad \text{(S57)}$$

Adenosine kinase (AMP regeneration into ADP (AMPREG)) (Ashworth et al., 2016)

$$v_{ampreg}^{Amp_L} = Vmax_{ampreg}^{Amp_L} \left(\frac{Amp_L}{Amp_L + Km_{ampreg}^{Amp_L}} \frac{Atp_L}{Atp_L + Km_{ampreg}^{Atp_L}} - \frac{Adp_L}{Adp_L + Km_{ampreg}^{Adp_L}} \frac{Adp_L}{Adp_L + Km_{ampreg}^{Adp_L}} \right) \quad \text{(S58)}$$

Guanosine diphosphate kinase (GDP regeneration to GTP (GDPREG) (Berndt et al., 2018a; Berndt et al., 2018b)

$$v_{gdpreg}^{Gdp_L} = Vmax_{gdpreg}^{Gdp_L} \frac{Gdp_L Atp_L - \frac{Gtp_L Adp_L}{Keq_{gdpreg}^{Gtp_L}}}{(1 + \frac{Gdp_L}{Km_{gdpreg}^{Gdp_L}})(1 + \frac{Atp_L}{Km_{gdpreg}^{Atp_L}}) + (1 + \frac{Gtp_L}{Km_{gdpreg}^{Gtp_L}})(1 + \frac{Adp_L}{Km_{gdpreg}^{Adp_L}}) - 1} \quad \text{(S59)}$$

Uridine diphosphate kinase (UDP regeneration to UDP (UDPREG))(Berndt et al., 2018a; Berndt et al., 2018b)

$$v_{udpreg}^{Udp_L} = Vmax_{udpreg}^{Udp_L} \frac{Udp_L Atp_L - \frac{Utp_L Adp_L}{Keq_{udpreg}^{Utp_L}}}{(1 + \frac{Udp_L}{Km_{udpreg}^{Udp_L}})(1 + \frac{Atp_L}{Km_{udpreg}^{Atp_L}}) + (1 + \frac{Utp_L}{Km_{udpreg}^{Utp_L}})(1 + \frac{Adp_L}{Km_{udpreg}^{Adp_L}}) - 1} \quad \text{(S60)}$$

NADH kinase (NADHK)

$$v_{nadhk}^{Nadh_L} = Vmax_{nadhk}^{Nadh_L} \frac{Nadh_L}{Nadh_L + Km_{nadhk}^{Nadh_L}} \frac{Atp_L}{Atp_L + Km_{nadhk}^{Atp_L}} \quad \text{(S61)}$$

UTP utilization (UTPUSE)

$$v_{utpuse}^{Utp_L} = Vmax_{utpuse}^{Utp_L} \frac{Utp_L}{Utp_L + Km_{utpuse}^{Utp_L}} \quad \text{(S62)}$$

GTP utilization (GTPUSE)

$$v_{gtpuse}^{Gtp_L} = Vmax_{gtpuse}^{Gtp_L} \frac{Gtp_L}{Gtp_L + Km_{gtpuse}^{Gtp_L}} \quad \text{(S63)}$$

NADH utilization (NADHUSE)

$$v_{nadhuse}^{Nadh_L} = Vmax_{nadhuse}^{Nadh_L} \frac{Nadh_L}{Nadh_L + Km_{nadhuse}^{Nadh_L}} \quad \text{(S64)}$$

NADPH utilization (NADPHUSE)

$$v_{nadphuse}^{Nadph_L} = Vmax_{nadphuse}^{Nadph_L} \frac{Nadph_L}{Nadph_L + Km_{nadphuse}^{Nadph_L}} \quad \text{(S65)}$$

FADH utilization (FADHUSE)

$$v_{fadhuse}^{Fadh_L} = Vmax_{fadhuse}^{Fadh_L} \frac{Fadh_L}{Fadh_L + Km_{fadhuse}^{Fadh_L}} \quad \text{(S66)}$$

Creatine kinase (CK) (Kim et al., 2007)

$$v_{ck}^{Cre_L} = Vmax_{ck}^{Cre_L} \cdot \frac{Cre_L \cdot Atp_L - Crep_L \cdot Adp_L / Keq_{ck}^{Crep_L}}{(1+\frac{Cre_L}{Km_{ck}^{Cre_L}}) \cdot (1+\frac{Atp_L}{Km_{ck}^{Atp_L}}) + (1+\frac{Crep_L}{Km_{ck}^{Crep_L}}) \cdot (1+\frac{Adp_L}{Km_{ck}^{Adp_L}}) - 1} \quad \text{(S67)}$$

Flux in skeletal muscle

Glucose transporter (GLUT4)

$$v_{glut4}^{Glc_{BM}} = \alpha_M \cdot Vdif_{glut4}^{Glc_{BM}} \frac{Glc_B - Glc_M}{1 + \frac{Glc_B}{Kdif_{glut4}^{Glc_{BM}}} + \frac{Glc_M}{Kdif_{glut4}^{Glc_M}}} \quad \text{(S68)}$$

Hexokinase (HK)

$$v_{hk}^{Glc_M} = \alpha_M \cdot Vmax_{hk}^{Glc_M} \frac{Glc_M}{Glc_M + Km_{hk}^{Glc_M}(1+\frac{G6p_M}{Ki_{hk}^{G6p_M}})} \frac{Atp_M}{Atp_M + Km_{hk}^{Atp_M}(1+\frac{G6p_M}{Ki_{hk}^{Atp_M}})} \quad \text{(S69)}$$

Glycogen synthase (GS)

$$v_{gs}^{G6p_M} = \alpha_M \cdot Vmax_{gs}^{G6p_M} \frac{G6p_M^{n_{gs}^{G6pM}}}{G6p_M^{n_{gs}^{G6pM}} + Km_{gs}^{G6p_M n_{gs}^{G6pM}}} \frac{(Glygn_M^{\max} - Glygn_M)}{(Glygn_M^{\max} - Glygn_M) + Km_{gs}^{Glygn_L}} \frac{Utp_M}{Utp_M + Km_{gs}^{Utp_M}}$$

(S70)

$Glygn_M^{\max}$ denotes the maximum amount of glycogen that skeletal muscle can store.

Glycogen degradation (GD) by glycogen phosphorylase (GP)

$$v_{gd}^{Glygn_M} = Vmax_{gd}^{Glygn_M} \frac{Glygn_M}{Glygn_M + Km_{gd}^{Glygn_M}} \frac{Phos_M}{Phos_M + Km_{gd}^{Phos_M}} \quad \text{(S71)}$$

Phosphofructokinase (PFK)

$$v_{pfk}^{G6p_M} = \alpha_M \cdot Vmax_{pfk}^{G6p_M} \frac{G6p_M}{G6p_M + Km_{pfk}^{G6p_M}} \frac{Atp_M}{Atp_M + Km_{pfk}^{Atp_M}} \cdot \frac{Ki_{pfk}^{Atp_M}}{Atp_M + Ki_{pfk}^{Atp_M}} \frac{Adp_M}{Adp_M + Km_{pfk}^{Adp_M}} (1 - b_{pfk}^{Gap_M} \frac{Gap_M}{Gap_M + Ki_{pfk}^{Gap_M}}) \quad \text{(S72)}$$

Pyruvate kinase (PK)

$$v_{pk}^{Gap_M} = \alpha_M \cdot Vmax_{pk}^{Gap_M} \frac{Gap_M}{Gap_M + Km_{pk}^{Gap_M}} (1 - b_{pk}^{Accoa_{MM}} \frac{Accoa_{MM}}{Accoa_{MM} + Ki_{pk}^{Accoa_{MM}}}) \frac{Adp_M}{Adp_M + Km_{pk}^{Adp_M}} \quad \text{(S73)}$$

Pyruvate transporter (PYRT)

$$v_{pyrt}^{Pyr_{BM}} = Vdif_{pyrt}^{Pyr_{BM}} \frac{Pyr_B - Pyr_M}{1 + \frac{Pyr_B}{Kdif_{pyrt}^{Pyr_{BM}}} + \frac{Pyr_M}{Kdif_{pyrt}^{Pyr_M}}} \quad \text{(S74)}$$

Lactate transporter (LACT)

$$v_{lact}^{Lac_{BM}} = Vdif_{lact}^{Lac_{BM}} \frac{Lac_B - Lac_M}{1 + \frac{Lac_B}{Kdif_{lact}^{Lac_{BM}}} + \frac{Lac_M}{Kdif_{lact}^{Lac_M}}} \quad \text{(S75)}$$

Lactate dehydrogenase (LDH)

$$v_{ldh}^{Pyr_M} = Vmax_{ldh}^{Pyr_M} \frac{Pyr_M \cdot Nadh_M - Lac_M \cdot Nad_M \,/\, Keq_{ldh}^{Lac_M}}{(1+\frac{Pyr_M}{Km_{ldh}^{Pyr_M}})(1+\frac{Nadh_M}{Km_{ldh}^{Nadh_M}}) + (1+\frac{Lac_M}{Km_{ldh}^{Lac_M}})(1+\frac{Nad_M}{Km_{ldh}^{Nad_M}}) - 1} \quad \text{(S76)}$$

Alanine transporter (ALAT)

$$v_{alat}^{Ala_{BM}} = Vdif_{alat}^{Ala_{BM}} \frac{Ala_B - Ala_M}{1+\frac{Ala_B}{Kdif_{alat}^{Ala_{BM}}} + \frac{Ala_M}{Kdif_{alat}^{Ala_M}}} \quad \text{(S77)}$$

Alanine transaminase (ALAT)

$$v_{alata}^{Pyr_M} = Vmax_{alata}^{Pyr_M} \cdot \frac{Pyr_M - Ala_M \,/\, Keq_{alata}^{Ala_M}}{(1+\frac{Pyr_M}{Km_{alata}^{Pyr_M}}) + (1+\frac{Ala_M}{Km_{alata}^{Ala_M}}) - 1} \quad \text{(S78)}$$

Pyruvate dehydrogenase (PDH)

$$v_{pdh}^{Pyr_M} = \alpha_M \cdot Vmax_{pdh}^{Pyr_M} \frac{Pyr_M}{Pyr_M + Km_{pdh}^{Pyr_M}} \frac{Nad_M}{Nad_M + Km_{pdh}^{Nad_M}} \frac{Km_{pdh}^{Accoa_{MM}}}{Accoa_{MM} + Km_{pdh}^{Accoa_{MM}}} \quad \text{(S79)}$$

TCA cycle (TCA)

$$v_{tca}^{Accoa_{MM}} = Vmax_{tca}^{Accoa_{MM}} \frac{Accoa_{MM}}{Accoa_{MM} + Km_{tca}^{Accoa_{MM}}} \frac{Adp_M}{Adp_M + Km_{tca}^{Adp_M}} \frac{Nad_M}{Nad_M + Km_{tca}^{Nad_M}} \frac{Fad_M}{Fad_M + Km_{tca}^{Fad_M}} \frac{Phos_M}{Phos_M + Km_{tca}^{Phos_M}} \frac{Pyr_M}{Pyr_M + Km_{tca}^{Pyr_M}} \quad \text{(S80)}$$

FFA transporter (FFAT)

$$v_{ffat}^{FFA_{BM}} = v_{ffat\_d}^{FFA_{BM}} + v_{ffat\_a}^{FFA_{BM}} \quad \text{(S81)}$$

$$v_{ffat\_d}^{FFA_{BM}} = Vdif_{ffat}^{FFA_{BM}} \frac{FFA_B - FFA_M}{1+\frac{FFA_B}{Kdif_{ffat}^{FFA_{BM}}} + \frac{FFA_M}{Kdif_{ffat}^{FFA_M}}} \quad \text{(S82)}$$

$$v_{ffat\_a}^{FFA_{BM}} = Vmax_{ffat}^{FFA_{BM}} \frac{FFA_B}{FFA_B + Km_{ffat}^{FFA_{BM}}} \quad \text{(S83)}$$

TG synthesis (TGSYN)

$$v_{tgsyn}^{FFA_M} = Vmax_{tgsyn}^{FFA_M} \frac{FFA_M}{FFA_M + Km_{tgsyn}^{FFA_M}} \frac{Glycp_M}{Glycp_M + Km_{tgsyn}^{Glycp_M}} \frac{TG_M^{\max} - TG_M}{(TG_M^{\max} - TG_M) + Km_{tgsyn}^{TG_M}} \frac{Atp_M}{Atp_M + Km_{tgsyn}^{Atp_M}} \quad \text{(S84)}$$

TG degradation (TGDEG)

$$v_{tgdeg}^{TG_L} = \beta_L Vmax_{tgdeg}^{TG_L} \frac{TG_L}{TG_L + Km_{tgdeg}^{TG_L}} \quad \text{(S85)}$$

Glycerol transporter (GLYCT)

$$v_{glyct}^{Glyc_{BM}} = Vdif_{glyct}^{Glyc_{BM}} \frac{Glyc_B - Glyc_M}{1 + \frac{Glyc_B}{Kdif_{glyct}^{Glyc_{BM}}} + \frac{Glyc_M}{Kdif_{glyct}^{Glyc_M}}} \quad \text{(S86)}$$

Glycerol kinase (GLYK)

$$v_{glyk}^{Glyc_M} = Vmax_{glyk}^{Glyc_M} \frac{Glyc_M}{Glyc_M + Km_{glyk}^{Glyc_M}(1 + \frac{Gap_M}{Ki_{glyk}^{Gap_M}})} \frac{Atp_M}{Atp_M + Km_{glyk}^{Atp_M}} \quad \text{(S87)}$$

TG transporter (TGT)

$$v_{tgt}^{TG_{BM}} = v_{tgt\_a}^{TG_{BM}} + v_{tgt\_d}^{TG_{BM}} \quad \text{(S80)}$$

$$v_{tgt\_d}^{TG_{BM}} = Vdif_{tgt}^{TG_{BM}} \frac{TG_B - TG_M / Keq_{tgt}^{TG_M}}{TG_B + Kdif_{tgt}^{TG_{BM}} + \frac{TG_M}{Keq_{tgt}^{TG_M}}} \quad \text{(S88)}$$

$$v_{tgt\_a}^{TG_{BM}} = Vmax_{tgt}^{TG_{BM}} \frac{TG_B}{TG_B + Km_{tgt}^{TG_M}} \quad \text{(S89)}$$

Glycerol-3-phosphate dehydrogenase (G3PD)

$$v_{g3pd}^{Gap_M} = Vmax_{g3pd}^{Gap_M} \frac{Gap_M Nadh_M - \frac{Glycp_M}{Keq_{g3pd}^{Glycp_M}} Nad_M}{(1+\frac{Gap_M}{Km_{g3pd}^{Gap_M}})(1+\frac{Nadh_M}{Km_{g3pd}^{Nadh_M}}) + (1+\frac{Glycp_M}{Km_{g3pd}^{Glycp_M}})(1+\frac{Nad_M}{Km_{g3pd}^{Nad_M}}) - 1} \quad \text{(S90)}$$

β-oxidation (BOXID)

$$v_{boxid}^{FFA_M} = Vmax_{boxid}^{FFA_M} \frac{FFA_M}{FFA_M + Km_{boxid}^{FFA_M}} \frac{Atp_M}{Atp_M + Km_{boxid}^{Atp_M}} \frac{Nad_M}{Nad_M + Km_{boxid}^{Nad_M}} \frac{Fad_M}{Fad_M + Km_{boxid}^{Fad_M}} \cdot \frac{Ki_{boxid}^{Accoa_{MM}}}{Accoa_{MM} + Ki_{boxid}^{Accoa_{MM}}} \frac{Ki_{boxid}^{Malcoa_M}}{Malcoa_M + Ki_{boxid}^{Malcoa_M}} \quad \text{(S91)}$$

ATP synthesis from FADH (ATPSYNF)

$$v_{atpsynf}^{Fadh_M} = Vmax_{atpsynf}^{Fadh_M} \frac{Fadh_M}{Fadh_M + Km_{atpsynf}^{Fadh_M}} \frac{Adp_M}{Adp_M + Km_{atpsynf}^{Adp_M}} \quad \text{(S92)}$$

ATP synthesis from NADH (ATPSYNN)

$$v_{atpsynn}^{Nadh_M} = Vmax_{atpsynn}^{Nadh_M} \frac{Nadh_M}{Nadh_M + Km_{atpsynn}^{Nadh_M}} \frac{Adp_M}{Adp_M + Km_{atpsynn}^{Adp_M}} \quad \text{(S93)}$$

ATP utilization (ATPUSE)

$$v_{atpuse}^{Atp_M} = Vmax_{atpuse}^{Atp_M} \frac{Atp_M}{Atp_M + Km_{atpuse}^{Atp_M}} \quad \text{(S94)}$$

Adenosine kinase (AMP regeneration into ADP (AMPREG))

$$v_{ampreg}^{Amp_M} = Vmax_{ampreg}^{Amp_M} \left(\frac{Amp_M}{Amp_M + Km_{ampreg}^{Amp_M}} \frac{Atp_M}{Atp_M + Km_{ampreg}^{Atp_M}} - \frac{Adp_M}{Adp_M + Km_{ampreg}^{Adp_M}} \frac{Adp_M}{Adp_M + Km_{ampreg}^{Adp_M}} \right) \quad \text{(S95)}$$

Uridine diphosphate kinase (UDP regeneration to UDP (UDPREG))

$$v_{udpreg}^{Udp_M} = Vmax_{udpreg}^{Udp_M} \frac{Udp_M Atp_M - \frac{Utp_M Adp_M}{Keq_{udpreg}^{Utp_M}}}{(1+\frac{Udp_M}{Km_{udpreg}^{Udp_M}})(1+\frac{Atp_M}{Km_{udpreg}^{Atp_M}}) + (1+\frac{Utp_M}{Km_{udpreg}^{Utp_M}})(1+\frac{Adp_M}{Km_{udpreg}^{Adp_M}}) - 1} \quad \text{(S96)}$$

UTP utilization (UTPUSE)

$$v_{utpuse}^{Utp_M} = Vmax_{utpuse}^{Utp_M} \frac{Utp_M}{Utp_M + Km_{utpuse}^{Utp_M}} \quad \text{(S97)}$$

NADH utilization (NADHUSE)

$$v_{nadhuse}^{Nadh_M} = Vmax_{nadhuse}^{Nadh_M} \frac{Nadh_M}{Nadh_M + Km_{nadhuse}^{Nadh_M}} \quad \text{(S98)}$$

NADPH utilization (NADPHUSE)

$$v_{nadphuse}^{Nadph_L} = Vmax_{nadphuse}^{Nadph_L} \frac{Nadph_L}{Nadph_L + Km_{nadphuse}^{Nadph_L}} \quad \text{(S99)}$$

FADH utilization (FADHUSE)

$$v_{fadhuse}^{Fadh_M} = Vmax_{fadhuse}^{Fadh_M} \frac{Fadh_M}{Fadh_M + Km_{fadhuse}^{Fadh_M}} \quad \text{(S100)}$$

Creatine kinase (CK)

$$v_{ck}^{Cre_M} = Vmax_{ck}^{Cre_M} \cdot \frac{Cre_M \cdot Atp_M - Crep_M \cdot Adp_M / Keq_{ck}^{Crep_M}}{(1+\frac{Cre_M}{Km_{ck}^{Cre_M}})(1+\frac{Atp_M}{Km_{ck}^{Atp_M}}) + (1+\frac{Crep_M}{Km_{ck}^{Crep_M}})(1+\frac{Adp_M}{Km_{ck}^{Adp_M}}) - 1} \quad \text{(S101)}$$

Flux in adipose tissue

Glucose transporter (GLUT4)

$$v_{glut4}^{Glc_{BA}} = \alpha_A \cdot Vdif_{glut4}^{Glc_{BA}} \frac{Glc_B - Glc_A}{1 + \frac{Glc_B}{Kdif_{glut4}^{Glc_{BA}}} + \frac{Glc_A}{Kdif_{glut4}^{Glc_A}}} \quad \text{(S102)}$$

Hexokinase (HK)

$$v_{hk}^{Glc_A} = \alpha_A \cdot Vmax_{hk}^{Glc_A} \frac{Glc_A}{Glc_A + Km_{hk}^{Glc_A}(1+\frac{G6p_A}{Ki_{hk}^{G6p_A}})} \frac{Atp_A}{Atp_A + Km_{hk}^{Atp_A}(1+\frac{G6p_A}{Ki_{hk}^{Atp_A}})} \quad \text{(S103)}$$

Phosphofructokinase (PFK)

$$v_{pfk}^{G6p_A} = \alpha_A \cdot Vmax_{pfk}^{G6p_A} \frac{G6p_A}{G6p_A + Km_{pfk}^{G6p_A}} \frac{Atp_A}{Atp_A + Km_{pfk}^{Atp_A}} \cdot \frac{Ki_{pfk}^{Atp_A}}{Atp_A + Ki_{pfk}^{Atp_A}} \frac{Adp_A}{Adp_A + Km_{pfk}^{Adp_A}}(1 - b_{pfk}^{Gap_A} \frac{Gap_A}{Gap_A + Ki_{pfk}^{Gap_A}}) \quad \text{(S104)}$$

Pyruvate kinase (PK)

$$v_{pk}^{Gap_A} = \alpha_A \cdot Vmax_{pk}^{Gap_A} \frac{Gap_A}{Gap_A + Km_{pk}^{Gap_A}}(1 - b_{pk}^{Accoa_{AM}} \frac{Accoa_{AM}}{Accoa_{AM} + Ki_{pk}^{Accoa_{AM}}}) \frac{Adp_A}{Adp_A + Km_{pk}^{Adp_A}} \quad \text{(S105)}$$

Pyruvate transporter (PYRT)

$$v_{pyrt}^{Pyr_{BA}} = Vdif_{pyrt}^{Pyr_{BA}} \frac{Pyr_B - Pyr_A}{1 + \frac{Pyr_B}{Kdif_{pyrt}^{Pyr_{BM}}} + \frac{Pyr_A}{Kdif_{pyrt}^{Pyr_A}}} \quad \text{(S106)}$$

Lactate transporter (LACT)

$$v_{lact}^{Lac_{BA}} = Vdif_{lact}^{Lac_{BA}} \frac{Lac_B - Lac_A}{1 + \frac{Lac_B}{Kdif_{lact}^{Lac_{BM}}} + \frac{Lac_A}{Kdif_{lact}^{Lac_A}}} \quad \text{(S107)}$$

Lactate dehydrogenase (LDH)

$$v_{ldh}^{Pyr_A} = Vmax_{ldh}^{Pyr_A} \frac{Pyr_A \cdot Nadh_A - Lac_A \cdot Nad_A / Keq_{ldh}^{Lac_A}}{(1+\frac{Pyr_A}{Km_{ldh}^{Pyr_A}})(1+\frac{Nadh_A}{Km_{ldh}^{Nadh_A}}) + (1+\frac{Lac_A}{Km_{ldh}^{Lac_A}})(1+\frac{Nad_A}{Km_{ldh}^{Nad_A}}) - 1} \quad \text{(S108)}$$

Alanine transporter (ALAT)

$$v_{alat}^{Ala_{BA}} = Vdif_{alat}^{Ala_{BA}} \frac{Ala_B - Ala_A}{1 + \frac{Ala_B}{Kdif_{alat}^{Ala_{BA}}} + \frac{Ala_A}{Kdif_{alat}^{Ala_A}}} \quad \text{(S109)}$$

Alanine transaminase (ALAT)

$$v_{alata}^{Pyr_A} = Vmax_{alata}^{Pyr_A} \cdot \frac{Pyr_A - Ala_A / Keq_{alata}^{Ala_A}}{(1 + \frac{Pyr_A}{Km_{alata}^{Pyr_A}}) + (1 + \frac{Ala_A}{Km_{alata}^{Ala_A}}) - 1} \quad \text{(S110)}$$

Pyruvate dehydrogenase (PDH)

$$v_{pdh}^{Pyr_A} = \alpha_A \cdot Vmax_{pdh}^{Pyr_A} \frac{Pyr_A}{Pyr_A + Km_{pdh}^{Pyr_A}} \frac{Nad_A}{Nad_A + Km_{pdh}^{Nad_A}} \frac{Km_{pdh}^{Accoa_{AM}}}{Accoa_{AM} + Km_{pdh}^{Accoa_{AM}}} \quad \text{(S111)}$$

TCA cycle (TCA)

$$v_{tca}^{Accoa_{AM}} = Vmax_{tca}^{Accoa_{AM}} \frac{Accoa_{AM}}{Accoa_{AM} + Km_{tca}^{Accoa_{AM}}} \frac{Adp_A}{Adp_A + Km_{tca}^{Adp_A}} \frac{Nad_A}{Nad_A + Km_{tca}^{Nad_A}} \frac{Fad_A}{Fad_A + Km_{tca}^{Fad_A}} \frac{Phos_A}{Phos_A + Km_{tca}^{Phos_A}} \frac{Pyr_A}{Pyr_A + Km_{tca}^{Pyr_A}} \quad \text{(S112)}$$

FFA transporter (FFAT)

$$v_{ffat}^{FFA_{BA}} = v_{ffat\_d}^{FFA_{BA}} + v_{ffat\_a}^{FFA_{BA}} \quad \text{(S113)}$$

$$v_{ffat\_d}^{FFA_{BA}} = Vdif_{ffat}^{FFA_{BA}} \frac{FFA_B - FFA_A}{1 + \frac{FFA_B}{Kdif_{ffat}^{FFA_{BA}}} + \frac{FFA_M}{Kdif_{ffat}^{FFA_M}}} \quad \text{(S114)}$$

$$v_{ffat\_a}^{FFA_{BA}} = -Vmax_{ffat}^{FFA_{BA}} \frac{FFA_A}{FFA_A + Km_{ffat}^{FFA_{BA}}} \quad \text{(S115)}$$

TG synthesis (TGSYN)

$$v_{tgsyn}^{FFA_A} = Vmax_{tgsyn}^{FFA_A} \frac{FFA_A}{FFA_A + Km_{tgsyn}^{FFA_A}} \frac{Glycp_A}{Glycp_A + Km_{tgsyn}^{Glycp_A}} \frac{TG_A^{\max} - TG_A}{(TG_A^{\max} - TG_A) + Km_{tgsyn}^{TG_A}} \frac{Atp_A}{Atp_A + Km_{tgsyn}^{Atp_A}} \quad \text{(S116)}$$

TG degradation (TGDEG)

$$v_{tgdeg}^{TG_A} = \beta_A Vmax_{tgdeg}^{TG_A} \frac{TG_A}{TG_A + Km_{tgdeg}^{TG_A}} \quad \text{(S117)}$$

Glycerol transporter (GLYCT)

$$v_{glyct}^{Glyc_{BA}} = Vdif_{glyct}^{Glyc_{BA}} \frac{Glyc_B - Glyc_A}{1 + \frac{Glyc_B}{Kdif_{glyct}^{Glyc_{BA}}} + \frac{Glyc_A}{Kdif_{glyct}^{Glyc_A}}} \quad \text{(S118)}$$

Glycerol kinase (GLYK)

$$v_{glyk}^{Glyc_A} = Vmax_{glyk}^{Glyc_A} \frac{Glyc_A}{Glyc_A + Km_{glyk}^{Glyc_A}(1 + \frac{Gap_A}{Ki_{glyk}^{Gap_A}})} \frac{Atp_A}{Atp_A + Km_{glyk}^{Atp_A}} \quad \text{(S119)}$$

TG transporter (TGT)

$$v_{tgt}^{TG_{BM}} = v_{tgt\_a}^{TG_{BM}} + v_{tgt\_d}^{TG_{BM}} \quad \text{(S120)}$$

$$v_{tgt\_a}^{TG_{BA}} = \alpha_A \cdot Vmax_{tgt}^{TG_{BA}} \frac{TG_B}{TG_B + Km_{tgt}^{TG_A}} \quad \text{(S121)}$$

$$v_{tgt\_d}^{TG_{BA}} = Vdif_{tgt}^{TG_{BA}} \frac{TG_B - TG_A / Keq_{tgt}^{TG_A}}{TG_B + Kdif_{tgt}^{TG_{BA}} + \frac{TG_A}{Keq_{tgt}^{TG_A}}} \quad \text{(S122)}$$

Glycerol-3-phosphate dehydrogenase (G3PD)

$$v_{g3pd}^{Gap_A} = Vmax_{g3pd}^{Gap_A} \frac{Gap_A Nadh_A - \frac{Glycp_A}{Keq_{g3pd}^{Glycp_A}} Nad_A}{(1 + \frac{Gap_A}{Km_{g3pd}^{Gap_A}})(1 + \frac{Nadh_A}{Km_{g3pd}^{Nadh_A}}) + (1 + \frac{Glycp_A}{Km_{g3pd}^{Glycp_A}})(1 + \frac{Nad_A}{Km_{g3pd}^{Nad_A}}) - 1} \quad \text{(S123)}$$

β-oxidation (BOXID)

$$v_{boxid}^{FFA_A} = Vmax_{boxid}^{FFA_A} \frac{FFA_A}{FFA_A + Km_{boxid}^{FFA_A}} \frac{Atp_A}{Atp_A + Km_{boxid}^{Atp_A}} \frac{Nad_A}{Nad_A + Km_{boxid}^{Nad_A}} \frac{Fad_A}{Fad_A + Km_{boxid}^{Fad_A}} \cdot \frac{Ki_{boxid}^{Accoa_{AM}}}{Accoa_{AM} + Ki_{boxid}^{Accoa_{AM}}} \frac{Ki_{boxid}^{Malcoa_A}}{Malcoa_A + Ki_{boxid}^{Malcoa_A}} \quad \text{(S124)}$$

ATP synthesis from FADH (ATPSYNF)

$$v_{atpsynf}^{Fadh_A} = Vmax_{atpsynf}^{Fadh_A} \frac{Fadh_A}{Fadh_A + Km_{atpsynf}^{Fadh_A}} \frac{Adp_A}{Adp_A + Km_{atpsynf}^{Adp_A}} \quad \text{(S125)}$$

ATP synthesis from NADH (ATPSYNN)

$$v_{atpsynn}^{Nadh_A} = Vmax_{atpsynn}^{Nadh_A} \frac{Nadh_A}{Nadh_A + Km_{atpsynn}^{Nadh_A}} \frac{Adp_A}{Adp_A + Km_{atpsynn}^{Adp_A}} \quad \text{(S126)}$$

ATP utilization (ATPUSE)

$$v_{atpuse}^{Atp_A} = Vmax_{atpuse}^{Atp_A} \frac{Atp_A}{Atp_A + Km_{atpuse}^{Atp_A}} \quad \text{(S127)}$$

Adenosine kinase (AMP regeneration into ADP (AMPREG))

$$v_{ampreg}^{Amp_A} = Vmax_{ampreg}^{Amp_A} \left(\frac{Amp_A}{Amp_A + Km_{ampreg}^{Amp_A}} \frac{Atp_A}{Atp_A + Km_{ampreg}^{Atp_A}} - \frac{Adp_A}{Adp_A + Km_{ampreg}^{Adp_A}} \frac{Adp_A}{Adp_A + Km_{ampreg}^{Adp_A}} \right) \quad \text{(S128)}$$

NADH utilization (NADHUSE)

$$v_{nadhuse}^{Nadh_A} = Vmax_{nadhuse}^{Nadh_A} \frac{Nadh_A}{Nadh_A + Km_{nadhuse}^{Nadh_A}} \quad \text{(S129)}$$

FADH utilization (FADHUSE)

$$v_{fadhuse}^{Fadh_A} = Vmax_{fadhuse}^{Fadh_A} \frac{Fadh_A}{Fadh_A + Km_{fadhuse}^{Fadh_A}} \quad \text{(S130)}$$

Creatine kinase (CK)

$$v_{ck}^{Cre_A} = Vmax_{ck}^{Cre_A} \cdot \frac{Cre_A \cdot Atp_A - Crep_A \cdot Adp_A / Keq_{ck}^{Crep_A}}{(1 + \frac{Cre_A}{Km_{ck}^{Cre_A}})(1 + \frac{Atp_A}{Km_{ck}^{Atp_A}}) + (1 + \frac{Crep_A}{Km_{ck}^{Crep_A}})(1 + \frac{Adp_A}{Km_{ck}^{Adp_A}}) - 1} \quad \text{(S131)}$$

Flux in GI tract

Glucose transporter (GLUT2)

$$v_{glut2}^{Glc_{BG}} = Vdif_{glut2}^{Glc_{BG}} \frac{Glc_B - Glc_G}{1 + \frac{Glc_B}{Kdif_{glut2}^{Glc_{BG}}} + \frac{Glc_G}{Kdif_{glut2}^{Glc_G}}} \quad \text{(S132)}$$

Hexokinase (HK)

$$v_{hk}^{Glc_G} = \alpha_G \cdot Vmax_{hk}^{Glc_G} \frac{Glc_G}{Glc_G + Km_{hk}^{Glc_G}(1 + \frac{G6p_G}{Ki_{hk}^{G6p_G}})} \frac{Atp_G}{Atp_G + Km_{hk}^{Atp_G}(1 + \frac{G6p_G}{Ki_{hk}^{Atp_G}})} \quad \text{(S133)}$$

Phosphofructokinase (PFK)

$$v_{pfk}^{G6p_G} = \alpha_G \cdot Vmax_{pfk}^{G6p_G} \frac{G6p_G}{G6p_G + Km_{pfk}^{G6p_G}} \frac{Atp_G}{Atp_G + Km_{pfk}^{Atp_G}} \cdot \frac{Ki_{pfk}^{Atp_G}}{Atp_G + Ki_{pfk}^{Atp_G}} \frac{Adp_G}{Adp_G + Km_{pfk}^{Adp_G}} (1 - b_{pfk}^{Gap_G} \frac{Gap_G}{Gap_G + Ki_{pfk}^{Gap_G}}) \quad \text{(S134)}$$

Pyruvate kinase (PK)

$$v_{pk}^{Gap_G} = \alpha_G \cdot Vmax_{pk}^{Gap_G} \frac{Gap_G}{Gap_G + Km_{pk}^{Gap_G}} (1 - b_{pk}^{Accoa_{GM}} \frac{Accoa_{GM}}{Accoa_{GM} + Ki_{pk}^{Accoa_{GM}}}) \frac{Adp_G}{Adp_G + Km_{pk}^{Adp_G}} \quad \text{(S135)}$$

Pyruvate transporter (PYRT)

$$v_{pyrt}^{Pyr_{BG}} = Vdif_{pyrt}^{Pyr_{BG}} \frac{Pyr_B - Pyr_G}{1 + \frac{Pyr_B}{Kdif_{pyrt}^{Pyr_{BG}}} + \frac{Pyr_G}{Kdif_{pyrt}^{Pyr_G}}} \quad \text{(S136)}$$

Lactate transporter (LACT)

$$v_{lact}^{Lac_{BA}} = Vdif_{lact}^{Lac_{BA}} \frac{Lac_B - Lac_A}{1 + \frac{Lac_B}{Kdif_{lact}^{Lac_{BM}}} + \frac{Lac_A}{Kdif_{lact}^{Lac_A}}} \quad \text{(S137)}$$

Lactate dehydrogenase (LDH)

$$v_{ldh}^{Pyr_G} = Vmax_{ldh}^{Pyr_G} \frac{Pyr_G \cdot Nadh_G - Lac_G \cdot Nad_G / Keq_{ldh}^{Lac_G}}{(1+\frac{Pyr_G}{Km_{ldh}^{Pyr_G}})(1+\frac{Nadh_G}{Km_{ldh}^{Nadh_G}}) + (1+\frac{Lac_G}{Km_{ldh}^{Lac_G}})(1+\frac{Nad_G}{Km_{ldh}^{Nad_G}}) - 1} \quad \text{(S138)}$$

Alanine transporter (ALAT)

$$v_{alat}^{Ala_{BG}} = Vdif_{alat}^{Ala_{BG}} \frac{Ala_B - Ala_G}{1+\frac{Ala_B}{Kdif_{alat}^{Ala_{BG}}} + \frac{Ala_G}{Kdif_{alat}^{Ala_G}}} \quad \text{(S139}$$

Alanine transaminase (ALAT)

$$v_{alata}^{Pyr_G} = Vmax_{alata}^{Pyr_G} \cdot \frac{Pyr_G - Ala_G / Keq_{alata}^{Ala_G}}{(1+\frac{Pyr_G}{Km_{alata}^{Pyr_G}}) + (1+\frac{Ala_G}{Km_{alata}^{Ala_G}}) - 1} \quad \text{(S140)}$$

Pyruvate dehydrogenase (PDH)

$$v_{pdh}^{Pyr_G} = \alpha_G \cdot Vmax_{pdh}^{Pyr_G} \frac{Pyr_G}{Pyr_G + Km_{pdh}^{Pyr_G}} \frac{Nad_G}{Nad_G + Km_{pdh}^{Nad_G}} \frac{Km_{pdh}^{Accoa_{GM}}}{Accoa_{GM} + Km_{pdh}^{Accoa_{GM}}} \quad \text{(S141)}$$

TCA cycle (TCA)

$$v_{tca}^{Accoa_{GM}} = Vmax_{tca}^{Accoa_{GM}} \frac{Accoa_{GM}}{Accoa_{GM} + Km_{tca}^{Accoa_{GM}}} \frac{Adp_G}{Adp_G + Km_{tca}^{Adp_G}} \frac{Nad_G}{Nad_G + Km_{tca}^{Nad_G}} \frac{Fad_G}{Fad_G + Km_{tca}^{Fad_G}} \frac{Phos_G}{Phos_G + Km_{tca}^{Phos_G}} \frac{Pyr_G}{Pyr_G + Km_{tca}^{Pyr_G}} \quad \text{(S142)}$$

FFA transporter (FFAT)

$$v_{ffat}^{FFA_{BG}} = v_{ffat\_d}^{FFA_{BG}} + v_{ffat\_a}^{FFA_{BG}} \quad \text{(S143)}$$

$$v_{ffat\_d}^{FFA_{BG}} = Vdif_{ffat}^{FFA_{BG}} \frac{FFA_B - FFA_G}{1+\frac{FFA_B}{Kdif_{ffat}^{FFA_{BG}}} + \frac{FFA_G}{Kdif_{ffat}^{FFA_G}}} \quad \text{(S144)}$$

$$v_{ffat\_a}^{FFA_{BG}} = -Vmax_{ffat}^{FFA_{BG}} \frac{FFA_G}{FFA_G + Km_{ffat}^{FFA_{BG}}} \quad \text{(S145)}$$

TG synthesis (TGSYN)

$$v_{tgsyn}^{FFA_G} = Vmax_{tgsyn}^{FFA_G} \frac{FFA_G}{FFA_G + Km_{tgsyn}^{FFA_G}} \frac{Glycp_G}{Glycp_G + Km_{tgsyn}^{Glycp_G}} \frac{TG_G^{\max} - TG_G}{(TG_G^{\max} - TG_G) + Km_{tgsyn}^{TG_G}} \frac{Atp_G}{Atp_G + Km_{tgsyn}^{Atp_G}} \quad \text{(S146)}$$

TG degradation (TGDEG)

$$v_{tgdeg}^{TG_G} = \beta_G Vmax_{tgdeg}^{TG_G} \frac{TG_G}{TG_G + Km_{tgdeg}^{TG_G}} \quad \text{(S147)}$$

Glycerol transporter (GLYCT)

$$v_{glyct}^{Glyc_{BG}} = Vdif_{glyct}^{Glyc_{BG}} \frac{Glyc_B - Glyc_G}{1 + \frac{Glyc_B}{Kdif_{glyct}^{Glyc_{BG}}} + \frac{Glyc_G}{Kdif_{glyct}^{Glyc_G}}} \quad \text{(S148)}$$

Glycerol kinase (GLYK)

$$v_{glyk}^{Glyc_G} = Vmax_{glyk}^{Glyc_G} \frac{Glyc_G}{Glyc_G + Km_{glyk}^{Glyc_G}(1 + \frac{Gap_G}{Ki_{glyk}^{Gap_G}})} \frac{Atp_G}{Atp_G + Km_{glyk}^{Atp_G}} \quad \text{(S149)}$$

TG transporter (TGT)

$$v_{tgt}^{TG_{BG}} = v_{tgt\_a}^{TG_{BG}} + v_{tgt\_d}^{TG_{BG}} \quad \text{(S150}$$

$$v_{tgt\_a}^{TG_{BG}} = \alpha_G \cdot Vmax_{tgt}^{TG_{BG}} \frac{TG_B}{TG_B + Km_{tgt}^{TG_G}} \quad \text{(S151)}$$

$$v_{tgt\_d}^{TG_{BG}} = Vdif_{tgt}^{TG_{BG}} \frac{TG_B - TG_G / Keq_{tgt}^{TG_G}}{TG_B + Kdif_{tgt}^{TG_{BG}} + \frac{TG_G}{Keq_{tgt}^{TG_G}}} \quad \text{(S152)}$$

Glycerol-3-phosphate dehydrogenase (G3PD)

$$v_{g3pd}^{Gap_G} = Vmax_{g3pd}^{Gap_G} \frac{Gap_G Nadh_G - \frac{Glycp_G}{Keq_{g3pd}^{Glycp_G}} Nad_G}{(1+\frac{Gap_G}{Km_{g3pd}^{Gap_G}})(1+\frac{Nadh_G}{Km_{g3pd}^{Nadh_G}}) + (1+\frac{Glycp_G}{Km_{g3pd}^{Glycp_G}})(1+\frac{Nad_G}{Km_{g3pd}^{Nad_G}}) - 1} \quad \text{(S153)}$$

β-oxidation (BOXID)

$$v_{boxid}^{FFA_G} = Vmax_{boxid}^{FFA_G} \frac{FFA_G}{FFA_G + Km_{boxid}^{FFA_G}} \frac{Atp_G}{Atp_G + Km_{boxid}^{Atp_G}} \frac{Nad_G}{Nad_G + Km_{boxid}^{Nad_G}} \frac{Fad_G}{Fad_G + Km_{boxid}^{Fad_G}} \cdot \frac{Ki_{boxid}^{Accoa_{GM}}}{Accoa_{GM} + Ki_{boxid}^{Accoa_{GM}}} \frac{Ki_{boxid}^{Malcoa_G}}{Malcoa_G + Ki_{boxid}^{Malcoa_G}} \quad \text{(S154)}$$

ATP synthesis from FADH (ATPSYNF)

$$v_{atpsynf}^{Fadh_G} = Vmax_{atpsynf}^{Fadh_G} \frac{Fadh_G}{Fadh_G + Km_{atpsynf}^{Fadh_G}} \frac{Adp_G}{Adp_G + Km_{atpsynf}^{Adp_G}} \quad \text{(S155)}$$

ATP synthesis from NADH (ATPSYNN)

$$v_{atpsynn}^{Nadh_G} = Vmax_{atpsynn}^{Nadh_G} \frac{Nadh_G}{Nadh_G + Km_{atpsynn}^{Nadh_G}} \frac{Adp_G}{Adp_G + Km_{atpsynn}^{Adp_G}} \quad \text{(S156)}$$

ATP utilization (ATPUSE)

$$v_{atpuse}^{Atp_G} = Vmax_{atpuse}^{Atp_G} \frac{Atp_G}{Atp_G + Km_{atpuse}^{Atp_G}} \quad \text{(S157)}$$

Adenosine kinase (AMP regeneration into ADP (AMPREG))

$$v_{ampreg}^{Amp_G} = Vmax_{ampreg}^{Amp_G} \left(\frac{Amp_G}{Amp_G + Km_{ampreg}^{Amp_G}} \frac{Atp_G}{Atp_G + Km_{ampreg}^{Atp_G}} - \frac{Adp_G}{Adp_G + Km_{ampreg}^{Adp_G}} \frac{Adp_G}{Adp_G + Km_{ampreg}^{Adp_G}} \right) \quad \text{(S158)}$$

NADH utilization (NADHUSE)

$$v_{nadhuse}^{Nadh_G} = Vmax_{nadhuse}^{Nadh_G} \frac{Nadh_G}{Nadh_G + Km_{nadhuse}^{Nadh_G}} \quad \text{(S159)}$$

FADH utilization (FADHUSE)

$$v_{fadhuse}^{Fadh_G} = Vmax_{fadhuse}^{Fadh_G} \frac{Fadh_G}{Fadh_G + Km_{fadhuse}^{Fadh_G}} \quad \text{(S160)}$$

Creatine kinase (CK)

$$v_{ck}^{Cre_G} = Vmax_{ck}^{Cre_G} \cdot \frac{Cre_G \cdot Atp_G - Crep_G \cdot Adp_G / Keq_{ck}^{Crep_G}}{(1+\frac{Cre_G}{Km_{ck}^{Cre_G}})(1+\frac{Atp_G}{Km_{ck}^{Atp_G}}) + (1+\frac{Crep_G}{Km_{ck}^{Crep_G}})(1+\frac{Adp_G}{Km_{ck}^{Adp_G}}) - 1} \quad \text{(S161)}$$

Flux in heart

Glucose transporter (GLUT2)

$$v_{glut2}^{Glc_{BH}} = Vdif_{glut2}^{Glc_{BH}} \frac{Glc_B - Glc_H}{1 + \frac{Glc_B}{Kdif_{glut2}^{Glc_{BH}}} + \frac{Glc_H}{Kdif_{glut2}^{Glc_H}}} \quad \text{(S162)}$$

Hexokinase (HK)

$$v_{hk}^{Glc_H} = Vmax_{hk}^{Glc_H} \frac{Glc_H}{Glc_H + Km_{hk}^{Glc_H}(1+\frac{G6p_H}{Ki_{hk}^{G6p_H}})} \frac{Atp_H}{Atp_H + Km_{hk}^{Atp_H}(1+\frac{G6p_H}{Ki_{hk}^{Atp_H}})} \quad \text{(S163)}$$

Glycogen synthase (GS)

$$v_{gs}^{G6p_H} = \alpha_H \cdot Vmax_{gs}^{G6p_H} \frac{G6p_H^{n_{gs}^{G6pH}}}{G6p_H^{n_{gs}^{G6pH}} + Km_{gs}^{G6p_H n_{gs}^{G6pH}}} \frac{(Glygn_H^{\max} - Glygn_H)}{(Glygn_H^{\max} - Glygn_H) + Km_{gs}^{Glygn_H}} \frac{Utp_H}{Utp_H + Km_{gs}^{Utp_H}} \quad \text{(S164)}$$

$Glygn_H^{\max}$ denotes the maximum amount of glycogen that heart can store.

Glycogen degradation (GD) by glycogen phosphorylase (GP)

$$v_{gd}^{Glygn_H} = \beta_H \cdot Vmax_{gd}^{Glygn_H} \frac{Glygn_H}{Glygn_H + Km_{gd}^{Glygn_H}} \frac{Phos_H}{Phos_H + Km_{gd}^{Phos_H}} \quad \text{(S165)}$$

Phosphofructokinase (PFK)

$$v_{pfk}^{G6p_H} = Vmax_{pfk}^{G6p_H} \frac{G6p_H}{G6p_H + Km_{pfk}^{G6p_H}} \frac{Atp_H}{Atp_H + Km_{pfk}^{Atp_H}} \cdot \frac{Ki_{pfk}^{Atp_H}}{Atp_H + Ki_{pfk}^{Atp_H}} \frac{Adp_H}{Adp_H + Km_{pfk}^{Adp_H}} (1 - b_{pfk}^{Gap_H} \frac{Gap_H}{Gap_H + Ki_{pfk}^{Gap_H}}) \quad \text{(S166)}$$

Pyruvate kinase (PK)

$$v_{pk}^{Gap_H} = Vmax_{pk}^{Gap_H} \frac{Gap_H}{Gap_H + Km_{pk}^{Gap_H}} (1 - b_{pk}^{Accoa_{HM}} \frac{Accoa_{HM}}{Accoa_{HM} + Ki_{pk}^{Accoa_{HM}}}) \frac{Adp_H}{Adp_H + Km_{pk}^{Adp_H}} \quad \text{(S167)}$$

Pyruvate transporter (PYRT)

$$v_{pyrt}^{Pyr_{BH}} = Vdif_{pyrt}^{Pyr_{BH}} \frac{Pyr_B - Pyr_H}{1 + \frac{Pyr_B}{Kdif_{pyrt}^{Pyr_{BH}}} + \frac{Pyr_H}{Kdif_{pyrt}^{Pyr_H}}} \quad \text{(S168)}$$

Lactate transporter (LACT)

$$v_{lact}^{Lac_{BH}} = Vdif_{lact}^{Lac_{BH}} \frac{Lac_B - Lac_H}{1 + \frac{Lac_B}{Kdif_{lact}^{Lac_{BH}}} + \frac{Lac_H}{Kdif_{lact}^{Lac_H}}} \quad \text{(S169)}$$

Lactate dehydrogenase (LDH)

$$v_{ldh}^{Pyr_H} = Vmax_{ldh}^{Pyr_H} \frac{Pyr_H \cdot Nadh_H - Lac_H \cdot Nad_H / Keq_{ldh}^{Lac_H}}{(1 + \frac{Pyr_H}{Km_{ldh}^{Pyr_H}})(1 + \frac{Nadh_H}{Km_{ldh}^{Nadh_H}}) + (1 + \frac{Lac_H}{Km_{ldh}^{Lac_H}})(1 + \frac{Nad_H}{Km_{ldh}^{Nad_H}}) - 1} \quad \text{(S170)}$$

Alanine transporter (ALAT)

$$v_{alat}^{Ala_{BH}} = Vdif_{alat}^{Ala_{BH}} \frac{Ala_B - Ala_H}{1 + \frac{Ala_B}{Kdif_{alat}^{Ala_{BH}}} + \frac{Ala_H}{Kdif_{alat}^{Ala_H}}} \quad \text{(S171)}$$

Alanine transaminase (ALAT)

$$v_{alata}^{Pyr_H} = Vmax_{alata}^{Pyr_H} \cdot \frac{Pyr_H - Ala_H / Keq_{alata}^{Ala_H}}{(1+\frac{Pyr_H}{Km_{alata}^{Pyr_H}})+(1+\frac{Ala_H}{Km_{alata}^{Ala_H}})-1} \quad \text{(S172)}$$

Pyruvate dehydrogenase (PDH)

$$v_{pdh}^{Pyr_H} = Vmax_{pdh}^{Pyr_H} \frac{Pyr_H}{Pyr_H + Km_{pdh}^{Pyr_H}} \frac{Nad_H}{Nad_H + Km_{pdh}^{Nad_H}} \frac{Km_{pdh}^{Accoa_{HM}}}{Accoa_{HM} + Km_{pdh}^{Accoa_{HM}}} \quad \text{(S173)}$$

TCA cycle (TCA)

$$v_{tca}^{Accoa_{HM}} = Vmax_{tca}^{Accoa_{HM}} \frac{Accoa_{HM}}{Accoa_{HM} + Km_{tca}^{Accoa_{HM}}} \frac{Adp_H}{Adp_H + Km_{tca}^{Adp_H}} \frac{Nad_H}{Nad_H + Km_{tca}^{Nad_H}} \frac{Fad_H}{Fad_H + Km_{tca}^{Fad_H}} \frac{Phos_H}{Phos_H + Km_{tca}^{Phos_H}} \frac{Pyr_H}{Pyr_H + Km_{tca}^{Pyr_H}} \quad \text{(S174)}$$

FFA transporter (FFAT)

$$v_{ffat}^{FFA_{BH}} = v_{ffat\_d}^{FFA_{BH}} + v_{ffat\_a}^{FFA_{BH}} \quad \text{(S175)}$$

$$v_{ffat\_d}^{FFA_{BH}} = Vdif_{ffat}^{FFA_{BH}} \frac{FFA_B - FFA_H}{1+\frac{FFA_B}{Kdif_{ffat}^{FFA_{BH}}}+\frac{FFA_H}{Kdif_{ffat}^{FFA_H}}} \quad \text{(S176)}$$

$$v_{ffat\_a}^{FFA_{BH}} = Vmax_{ffat}^{FFA_{BH}} \frac{FFA_B}{FFA_B + Km_{ffat}^{FFA_{BH}}} \quad \text{(S177)}$$

TG synthesis (TGSYN)

$$v_{tgsyn}^{FFA_H} = Vmax_{tgsyn}^{FFA_H} \frac{FFA_H}{FFA_H + Km_{tgsyn}^{FFA_H}} \frac{Glycp_H}{Glycp_H + Km_{tgsyn}^{Glycp_H}} \frac{TG_H^{\max} - TG_H}{(TG_H^{\max} - TG_H) + Km_{tgsyn}^{TG_H}} \frac{Atp_H}{Atp_H + Km_{tgsyn}^{Atp_H}} \quad \text{(S178)}$$

TG degradation (TGDEG)

$$v_{tgdeg}^{TG_H} = Vmax_{tgdeg}^{TG_H} \frac{TG_H}{TG_H + Km_{tgdeg}^{TG_H}} \quad \text{(S179)}$$

Glycerol transporter (GLYCT)

$$v_{glyct}^{Glyc_{BH}} = Vdif_{glyct}^{Glyc_{BH}} \frac{Glyc_B - Glyc_H}{1 + \frac{Glyc_B}{Kdif_{glyct}^{Glyc_{BH}}} + \frac{Glyc_H}{Kdif_{glyct}^{Glyc_H}}} \quad \text{(S180)}$$

Glycerol kinase (GLYK)

$$v_{glyk}^{Glyc_H} = Vmax_{glyk}^{Glyc_H} \frac{Glyc_H}{Glyc_H + Km_{glyk}^{Glyc_H}(1 + \frac{Gap_H}{Ki_{glyk}^{Gap_H}})} \frac{Atp_H}{Atp_H + Km_{glyk}^{Atp_H}} \quad \text{(S181)}$$

TG transporter (TGT)

$$v_{tgt}^{TG_{BH}} = v_{tgt\_a}^{TG_{BH}} + v_{tgt\_d}^{TG_{BH}} \quad \text{(S182)}$$

$$v_{tgt\_d}^{TG_{BH}} = Vdif_{tgt}^{TG_{BH}} \frac{TG_B - TG_H / Keq_{tgt}^{TG_H}}{TG_B + Kdif_{tgt}^{TG_{BH}} + \frac{TG_H}{Keq_{tgt}^{TG_H}}} \quad \text{(S183)}$$

$$v_{tgt\_a}^{TG_{BH}} = Vmax_{tgt}^{TG_{BH}} \frac{TG_B}{TG_B + Km_{tgt}^{TG_H}} \quad \text{(S184)}$$

Glycerol-3-phosphate dehydrogenase (G3PD)

$$v_{g3pd}^{Gap_H} = Vmax_{g3pd}^{Gap_H} \frac{Gap_H Nadh_H - \frac{Glycp_H}{Keq_{g3pd}^{Glycp_H}} Nad_H}{(1 + \frac{Gap_H}{Km_{g3pd}^{Gap_H}})(1 + \frac{Nadh_H}{Km_{g3pd}^{Nadh_H}}) + (1 + \frac{Glycp_H}{Km_{g3pd}^{Glycp_H}})(1 + \frac{Nad_H}{Km_{g3pd}^{Nad_H}}) - 1} \quad \text{(S185)}$$

β-oxidation (BOXID)

$$v_{boxid}^{FFA_H} = Vmax_{boxid}^{FFA_H} \frac{FFA_H}{FFA_H + Km_{boxid}^{FFA_H}} \frac{Atp_H}{Atp_H + Km_{boxid}^{Atp_H}} \frac{Nad_H}{Nad_H + Km_{boxid}^{Nad_H}} \frac{Fad_H}{Fad_H + Km_{boxid}^{Fad_H}} \cdot \frac{Ki_{boxid}^{Accoa_{HM}}}{Accoa_{HM} + Ki_{boxid}^{Accoa_{HM}}} \frac{Ki_{boxid}^{Malcoa_H}}{Malcoa_H + Ki_{boxid}^{Malcoa_H}} \quad \text{(S186)}$$

ATP synthesis from FADH (ATPSYNF)

$$v_{atpsynf}^{Fadh_H} = Vmax_{atpsynf}^{Fadh_H} \frac{Fadh_H}{Fadh_H + Km_{atpsynf}^{Fadh_H}} \frac{Adp_H}{Adp_H + Km_{atpsynf}^{Adp_H}} \quad \text{(S187)}$$

ATP synthesis from NADH (ATPSYNN)

$$v_{atpsynn}^{Nadh_H} = Vmax_{atpsynn}^{Nadh_H} \frac{Nadh_H}{Nadh_H + Km_{atpsynn}^{Nadh_H}} \frac{Adp_H}{Adp_H + Km_{atpsynn}^{Adp_H}} \quad \text{(S188)}$$

ATP utilization (ATPUSE)

$$v_{atpuse}^{Atp_H} = Vmax_{atpuse}^{Atp_H} \frac{Atp_H}{Atp_H + Km_{atpuse}^{Atp_H}} \quad \text{(S189)}$$

Adenosine kinase (AMP regeneration into ADP (AMPREG))

$$v_{ampreg}^{Amp_H} = Vmax_{ampreg}^{Amp_H} \left(\frac{Amp_H}{Amp_H + Km_{ampreg}^{Amp_H}} \frac{Atp_H}{Atp_H + Km_{ampreg}^{Atp_H}} - \frac{Adp_H}{Adp_H + Km_{ampreg}^{Adp_H}} \frac{Adp_H}{Adp_H + Km_{ampreg}^{Adp_H}} \right) \quad \text{(S190)}$$

Uridine diphosphate kinase (UDP regeneration to UDP (UDPREG))

$$v_{udpreg}^{Udp_H} = Vmax_{udpreg}^{Udp_H} \frac{Udp_H Atp_H - \frac{Utp_H Adp_H}{Keq_{udpreg}^{Utp_H}}}{(1 + \frac{Udp_H}{Km_{udpreg}^{Udp_H}})(1 + \frac{Atp_H}{Km_{udpreg}^{Atp_H}}) + (1 + \frac{Utp_H}{Km_{udpreg}^{Utp_H}})(1 + \frac{Adp_H}{Km_{udpreg}^{Adp_H}}) - 1} \quad \text{(S191)}$$

UTP utilization (UTPUSE)

$$v_{utpuse}^{Utp_H} = Vmax_{utpuse}^{Utp_H} \frac{Utp_H}{Utp_H + Km_{utpuse}^{Utp_H}} \quad \text{(S192)}$$

NADH utilization (NADHUSE)

$$v_{nadhuse}^{Nadh_H} = Vmax_{nadhuse}^{Nadh_H} \frac{Nadh_H}{Nadh_H + Km_{nadhuse}^{Nadh_H}} \quad \text{(S193)}$$

FADH utilization (FADHUSE)

$$v_{fadhuse}^{Fadh_H} = Vmax_{fadhuse}^{Fadh_H} \frac{Fadh_H}{Fadh_H + Km_{fadhuse}^{Fadh_H}} \quad \text{(S194)}$$

Creatine kinase (CK)

$$v_{ck}^{Cre_H} = Vmax_{ck}^{Cre_H} \cdot \frac{Cre_H \cdot Atp_H - Crep_H \cdot Adp_H / Keq_{ck}^{Crep_H}}{(1+\frac{Cre_H}{Km_{ck}^{Cre_M}})(1+\frac{Atp_H}{Km_{ck}^{Atp_H}}) + (1+\frac{Crep_H}{Km_{ck}^{Crep_H}})(1+\frac{Adp_H}{Km_{ck}^{Adp_H}}) - 1} \quad \text{(S195)}$$

Flux in brain

Glucose transporter (GLUT3)

$$v_{glut3}^{Glc_{BN}} = Vdif_{glut3}^{Glc_{BN}} \frac{Glc_B - Glc_N}{1+\frac{Glc_B}{Kdif_{glut3}^{Glc_{BN}}} + \frac{Glc_N}{Kdif_{glut3}^{Glc_N}}} \quad \text{(S196)}$$

Hexokinase (HK)

$$v_{hk}^{Glc_N} = Vmax_{hk}^{Glc_N} \frac{Glc_N}{Glc_N + Km_{hk}^{Glc_N}(1+\frac{G6p_N}{Ki_{hk}^{G6p_N}})} \frac{Atp_N}{Atp_N + Km_{hk}^{Atp_N}(1+\frac{G6p_N}{Ki_{hk}^{Atp_N}})} \quad \text{(S197)}$$

Glycogen synthase (GS)

$$v_{gs}^{G6p_N} = Vmax_{gs}^{G6p_N} \frac{G6p_N^{n_{gs}^{G6p_N}}}{G6p_N^{n_{gs}^{G6p_H}} + Km_{gs}^{G6p_N n_{gs}^{G6p_N}}} \frac{(Glygn_N^{\max} - Glygn_N)}{(Glygn_N^{\max} - Glygn_N) + Km_{gs}^{Glygn_N}} \frac{Utp_N}{Utp_N + Km_{gs}^{Utp_N}} \quad \text{(S198)}$$

$Glygn_N^{\max}$ denotes the maximum amount of glycogen that brain can store.

Glycogen degradation (GD) by glycogen phosphorylase (GP)

$$v_{gd}^{Glygn_N} = Vmax_{gd}^{Glygn_N} \frac{Glygn_N}{Glygn_N + Km_{gd}^{Glygn_N}} \frac{Phos_N}{Phos_N + Km_{gd}^{Phos_N}} \quad \text{(S199)}$$

Phosphofructokinase (PFK)

$$v_{pfk}^{G6p_N} = Vmax_{pfk}^{G6p_N} \frac{G6p_N}{G6p_N + Km_{pfk}^{G6p_N}} \frac{Atp_N}{Atp_N + Km_{pfk}^{Atp_N}} \cdot \frac{Ki_{pfk}^{Atp_N}}{Atp_N + Ki_{pfk}^{Atp_N}} \frac{Adp_N}{Adp_N + Km_{pfk}^{Adp_N}} (1 - b_{pfk}^{Gap_N} \frac{Gap_N}{Gap_N + Ki_{pfk}^{Gap_N}}) \quad \text{(S200)}$$

Pyruvate kinase (PK)

$$v_{pk}^{Gap_N} = Vmax_{pk}^{Gap_N} \frac{Gap_N}{Gap_N + Km_{pk}^{Gap_N}} (1 - b_{pk}^{Accoa_{NM}} \frac{Accoa_{NM}}{Accoa_{NM} + Ki_{pk}^{Accoa_{NM}}}) \frac{Adp_N}{Adp_N + Km_{pk}^{Adp_N}} \quad \text{(S201)}$$

Pyruvate transporter (PYRT)

$$v_{pyrt}^{Pyr_{BN}} = Vdif_{pyrt}^{Pyr_{BN}} \frac{Pyr_B - Pyr_N}{1 + \frac{Pyr_B}{Kdif_{pyrt}^{Pyr_{BN}}} + \frac{Pyr_N}{Kdif_{pyrt}^{Pyr_N}}} \quad \text{(S202)}$$

Lactate transporter (LACT)

$$v_{lact}^{Lac_{BN}} = Vdif_{lact}^{Lac_{BN}} \frac{Lac_B - Lac_N}{1 + \frac{Lac_B}{Kdif_{lact}^{Lac_{BN}}} + \frac{Lac_N}{Kdif_{lact}^{Lac_N}}} \quad \text{(S203)}$$

Lactate dehydrogenase (LDH)

$$v_{ldh}^{Pyr_N} = Vmax_{ldh}^{Pyr_N} \frac{Pyr_N \cdot Nadh_N - Lac_N \cdot Nad_N / Keq_{ldh}^{Lac_N}}{(1 + \frac{Pyr_N}{Km_{ldh}^{Pyr_N}})(1 + \frac{Nadh_N}{Km_{ldh}^{Nadh_N}}) + (1 + \frac{Lac_N}{Km_{ldh}^{Lac_N}})(1 + \frac{Nad_N}{Km_{ldh}^{Nad_N}}) - 1} \quad \text{(S204)}$$

Alanine transporter (ALAT)

$$v_{alat}^{Ala_{BN}} = Vdif_{alat}^{Ala_{BN}} \frac{Ala_B - Ala_N}{1 + \frac{Ala_B}{Kdif_{alat}^{Ala_{BN}}} + \frac{Ala_N}{Kdif_{alat}^{Ala_N}}} \quad \text{(S205)}$$

Alanine transaminase (ALAT)

$$v_{alata}^{Pyr_N} = Vmax_{alata}^{Pyr_N} \cdot \frac{Pyr_N - Ala_N / Keq_{alata}^{Ala_N}}{(1 + \frac{Pyr_N}{Km_{alata}^{Pyr_N}}) + (1 + \frac{Ala_N}{Km_{alata}^{Ala_N}}) - 1} \quad \text{(S206)}$$

Pyruvate dehydrogenase (PDH)

$$v_{pdh}^{Pyr_N} = Vmax_{pdh}^{Pyr_N} \frac{Pyr_N}{Pyr_N + Km_{pdh}^{Pyr_N}} \frac{Nad_N}{Nad_N + Km_{pdh}^{Nad_N}} \frac{Km_{pdh}^{Accoa_{NM}}}{Accoa_{NM} + Km_{pdh}^{Accoa_{NM}}} \quad \text{(S207)}$$

TCA cycle (TCA)

$$v_{tca}^{Accoa_{NM}} = Vmax_{tca}^{Accoa_{NM}} \frac{Accoa_{NM}}{Accoa_{NM} + Km_{tca}^{Accoa_{NM}}} \frac{Adp_N}{Adp_N + Km_{tca}^{Adp_N}} \frac{Nad_N}{Nad_N + Km_{tca}^{Nad_N}} \frac{Fad_N}{Fad_N + Km_{tca}^{Fad_N}} \frac{Phos_N}{Phos_N + Km_{tca}^{Phos_N}} \frac{Pyr_N}{Pyr_N + Km_{tca}^{Pyr_N}} \quad \text{(S208)}$$

β-hydroxybutyrate degradation (BHBDEG)

$$v_{bhb\deg}^{Bhb_N} = Vmax_{bhb\deg}^{Bhb_N} \frac{Bhb_N}{Bhb_N + Km_{bhb\deg}^{Bhb_N}} \frac{Nad_N}{Nad_N + Km_{bhb\deg}^{Nad_N}} \frac{Atp_N}{Atp_N + Km_{bhb\deg}^{Atp_N}} \quad \text{(S209)}$$

β-hydroxybutyrate transporter (BHBT)

$$v_{bhbt}^{Bhb_{BN}} = Vdif_{bhbt}^{Bhb_{BN}} \frac{Bhb_B - Bhb_N}{1 + \frac{Bhb_B}{Kdif_{bhbt}^{Bhb_{BN}}} + \frac{Bhb_N}{Kdif_{bhbt}^{Bhb_N}}} \quad \text{(S210)}$$

ATP synthesis from FADH (ATPSYNF)

$$v_{atpsynf}^{Fadh_N} = Vmax_{atpsynf}^{Fadh_N} \frac{Fadh_N}{Fadh_N + Km_{atpsynf}^{Fadh_N}} \frac{Adp_N}{Adp_N + Km_{atpsynf}^{Adp_N}} \quad \text{(S211)}$$

ATP synthesis from NADH (ATPSYNN)

$$v_{atpsynn}^{Nadh_N} = Vmax_{atpsynn}^{Nadh_N} \frac{Nadh_N}{Nadh_N + Km_{atpsynn}^{Nadh_N}} \frac{Adp_N}{Adp_N + Km_{atpsynn}^{Adp_N}} \quad \text{(S212)}$$

ATP utilization (ATPUSE)

$$v_{atpuse}^{Atp_N} = Vmax_{atpuse}^{Atp_N} \frac{Atp_N}{Atp_N + Km_{atpuse}^{Atp_N}} \quad \text{(S213)}$$

Uridine diphosphate kinase (UDP regeneration to UDP (UDPREG))

$$v_{udpreg}^{Udp_N} = Vmax_{udpreg}^{Udp_N} \frac{Udp_N Atp_N - \frac{Utp_N Adp_N}{Keq_{udpreg}^{Utp_N}}}{(1+\frac{Udp_N}{Km_{udpreg}^{Udp_N}})(1+\frac{Atp_N}{Km_{udpreg}^{Atp_N}}) + (1+\frac{Utp_N}{Km_{udpreg}^{Utp_N}})(1+\frac{Adp_N}{Km_{udpreg}^{Adp_N}}) - 1} \quad \text{(S214)}$$

UTP utilization (UTPUSE)

$$v_{utpuse}^{Utp_N} = Vmax_{utpuse}^{Utp_N} \frac{Utp_N}{Utp_N + Km_{utpuse}^{Utp_N}} \quad \text{(S215)}$$

NADH utilization (NADHUSE)

$$v_{nadhuse}^{Nadh_N} = Vmax_{nadhuse}^{Nadh_N} \frac{Nadh_N}{Nadh_N + Km_{nadhuse}^{Nadh_N}} \quad \text{(S216)}$$

FADH utilization (FADHUSE)

$$v_{fadhuse}^{Fadh_N} = Vmax_{fadhuse}^{Fadh_N} \frac{Fadh_N}{Fadh_N + Km_{fadhuse}^{Fadh_N}} \quad \text{(S217)}$$

Creatine kinase (CK)

$$v_{ck}^{Cre_N} = Vmax_{ck}^{Cre_N} \cdot \frac{Cre_N \cdot Atp_N - Crep_N \cdot Adp_N / Keq_{ck}^{Crep_N}}{(1+\frac{Cre_N}{Km_{ck}^{Cre_N}})(1+\frac{Atp_N}{Km_{ck}^{Atp_N}}) + (1+\frac{Crep_N}{Km_{ck}^{Crep_N}})(1+\frac{Adp_N}{Km_{ck}^{Adp_N}}) - 1} \quad \text{(S218)}$$

Cholesterol utilization (CHOLUSE)

$$v_{choluse}^{Chol_B} = k_{choluse}^{Chol_B} Chol_B \quad \text{(S219)}$$

ODE in blood

$$V_B \frac{dIns_B}{dt} = v_{inssyn}^{B} + v_{inssyn}^{Glc_B} + v_{inssyn}^{FFA_B} - v_{insdeg}^{Ins_B} \quad \text{(S220)}$$

$$V_B \frac{dGlc_B}{dt} = v_{meal}^{Glc_B} - v_{glut2}^{Glc_{BL}} - v_{glut4}^{Glc_{BM}} - v_{glut4}^{Glc_{BA}} - v_{glut2}^{Glc_{BG}} - v_{glut2}^{Glc_{BH}} - v_{glut3}^{Glc_{BN}} - v_{glutT}^{Glc_{BT}} \quad \text{(S221)}$$

$$V_B \frac{dPyr_B}{dt} = -v_{pyrt}^{Pyr_{BL}} - v_{pyrt}^{Pyr_{BM}} - v_{pyrt}^{Pyr_{BA}} - v_{pyrt}^{Pyr_{BG}} - v_{pyrt}^{Pyr_{BH}} - v_{pyrt}^{Pyr_{BN}} - v_{pyrt}^{Pyr_{BT}} \quad \text{(S222)}$$

$$V_B \frac{dLac_B}{dt} = -v_{lact}^{Lac_{BL}} - v_{lact}^{Lac_{BM}} - v_{lact}^{Lac_{BA}} - v_{lact}^{Lac_{BG}} - v_{lact}^{Lac_{BH}} - v_{lact}^{Lac_{BN}} - v_{lact}^{Lac_{BT}} \quad \text{(S223)}$$

$$V_B \frac{dAla_B}{dt} = -v_{alat}^{Ala_{BL}} - v_{alat}^{Ala_{BM}} - v_{alat}^{Ala_{BA}} - v_{alat}^{Ala_{BG}} - v_{alat}^{Ala_{BH}} - v_{alat}^{Ala_{BN}} - v_{alat}^{Ala_{BT}} \quad \text{(S224)}$$

$$V_B \frac{dGlyc_B}{dt} = -v_{glyct}^{Glyc_{BL}} - v_{glyct}^{Glyc_{BM}} - v_{glyct}^{Glyc_{BA}} - v_{glyct}^{Glyc_{BG}} - v_{glyct}^{Glyc_{BH}} - v_{glyct}^{Glyc_{BN}} - v_{glyct}^{Glyc_{BT}} + v_{tgt}^{TG_{BL}} + v_{tgt}^{TG_{BM}} + v_{tgt}^{TG_{BA}} + v_{tgt}^{TG_{BG}} + v_{tgt}^{TG_{BH}} + v_{tgt}^{TG_{BN}} \quad \text{(S225)}$$

$$V_B \frac{dTG_B}{dt} = v_{meal}^{TG_B} - v_{tgt}^{TG_{BL}} - v_{tgt}^{TG_{BM}} - v_{tgt}^{TG_{BA}} - v_{tgt}^{TG_{BG}} - v_{tgt}^{TG_{BH}} - v_{tgt}^{TG_{BN}} - v_{tgt}^{TG_{BT}} \quad \text{(S226)}$$

$$V_B \frac{dFFA_B}{dt} = -v_{ffat}^{FFA_{BL}} - v_{ffat}^{FFA_{BM}} - v_{ffat}^{FFA_{BA}} - v_{ffat}^{FFA_{BG}} - v_{ffat}^{FFA_{BH}} - v_{ffat}^{FFA_{BN}} - v_{ffat}^{FFA_{BT}} \quad \text{(S227)}$$

$$V_B \frac{dBhb_B}{dt} = -v_{bhbt}^{Bhb_{BL}} - v_{bhbt}^{Bhb_{BM}} - v_{bhbt}^{Bhb_{BA}} - v_{bhbt}^{Bhb_{BG}} - v_{bhbt}^{Bhb_{BH}} - v_{bhbt}^{Bhb_{BN}} \quad \text{(S228)}$$

$$V_B \frac{dChol_B}{dt} = -v_{cholt}^{Chol_{BL}} - v_{choluse}^{Chol_B} \quad \text{(S229)}$$

ODE in liver

$$V_L \frac{dGlc_L}{dt} = v_{glut2}^{Glc_{BL}} - v_{hk}^{Glc_L} + v_{g6pase}^{G6p_L} \quad \text{(S230)}$$

$$V_L \frac{dG6p_L}{dt} = v_{hk}^{Glc_L} - v_{g6pase}^{G6p_L} - v_{gs}^{G6p_L} + v_{gd}^{Glygn_L} - v_{pfk}^{G6p_L} + \frac{1}{2} v_{fbp}^{Gap_L} - v_{ppp}^{G6p_L} \quad \text{(S231)}$$

$$V_L \frac{dGlygn_L}{dt} = v_{gs}^{G6p_L} - v_{gd}^{Glygn_L} \quad \text{(S232)}$$

$$V_L \frac{dGap_L}{dt} = 2v_{pfk}^{G6p_L} - v_{fbp}^{Gap_L} - v_{pk}^{Gap_L} + v_{pepck}^{Pyr_L} - v_{g3pd}^{Gap_L} \quad \text{(S233)}$$

$$V_L \frac{dPyr_L}{dt} = v_{pk}^{Gap_L} - v_{pepck}^{Pyr_L} + v_{pryt}^{Pyr_{BL}} - v_{ldh}^{Pyr_L} - v_{alata}^{Pyr_L} - v_{pdh}^{Pyr_L} \quad \text{(S234)}$$

$$V_L \frac{dLac_L}{dt} = v_{lact}^{Pyr_{BL}} + v_{ldh}^{Pyr_L} \quad \text{(S235)}$$

$$V_L \frac{dAla_L}{dt} = v_{alat}^{Ala_{BL}} + v_{alata}^{Pyr_L} \quad \text{(S236)}$$

$$V_L \frac{dAccoa_{LM}}{dt} = v_{pdh}^{Pyr_L} - v_{tca}^{Accoa_{LM}} - v_{bhbsyn}^{Accoa_{LM}} + 8 \cdot v_{boxid}^{FFA_L} - v_{accoat}^{Accoa_{LMLC}} \quad \text{(S237)}$$

$$V_L \frac{dBhb_L}{dt} = \frac{1}{2} v_{bhbsyn}^{Accoa_{LM}} + v_{bhbt}^{Bhb_{BL}} \tag{S238}$$

$$V_L \frac{dAccoa_{LC}}{dt} = v_{accoat}^{Accoa_{LMLC}} - v_{lipog1}^{Accoa_{LC}} - v_{cholsyn1}^{Accoa_{LC}} \tag{S239}$$

$$V_L \frac{dMalcoa_L}{dt} = v_{lipog1}^{Accoa_{LC}} - v_{lipog2}^{Malcoa_L} \tag{S240}$$

$$V_L \frac{dHmgcoa_L}{dt} = \frac{1}{3} v_{cholsyn1}^{Accoa_{LC}} - v_{cholsyn2}^{Hmgcoa_L} \tag{S241}$$

$$V_L \frac{dChol_L}{dt} = \frac{1}{6} v_{cholsyn2}^{Hmgcoa_L} + v_{cholt}^{Chol_{BL}} \tag{S242}$$

$$V_L \frac{dFFA_L}{dt} = v_{ffat}^{FFA_{BL}} - 3 \cdot v_{tgsyn}^{FFA_L} + 3 \cdot v_{tgdeg}^{TG_L} - v_{boxid}^{FFA_L} + \frac{1}{8} v_{lipog2}^{Malcoa_L} \tag{S243}$$

$$V_L \frac{dGlyc_L}{dt} = v_{tgdeg}^{TG_L} + v_{glyct}^{Glyc_{BL}} - v_{glyck}^{Glyc_L} \tag{S244}$$

$$V_L \frac{dGlycp_L}{dt} = -v_{tgsyn}^{FFA_L} + v_{glyct}^{Glyc_L} + v_{g3pd}^{Gap_L} \tag{S245}$$

$$V_L \frac{dTG_L}{dt} = v_{tgsyn}^{FFA_L} - v_{tgdeg}^{TG_L} + v_{tgt}^{TG_L} \tag{S246}$$

$$\begin{aligned} V_L \frac{dAtp_L}{dt} = & -v_{hk}^{Glc_L} - v_{pfk}^{G6p_L} + 2v_{pk}^{Gap_L} - 2v_{pepck}^{Pyr_L} + v_{tca}^{Accoa_{LM}} - v_{accoat}^{Accoa_{LMLC}} - v_{glyk}^{Glyc_L} - v_{boxid}^{FFA_L} - v_{lipog1}^{Accoa_{LC}} \\ & + \frac{1}{8} v_{lipog2}^{Malcoa_{LC}} - 2v_{tgsyin}^{FFA_L} - 3v_{cholosyn2}^{Hmgcoa_L} + v_{atpsynf}^{Fadh_L} + 3v_{atpsynn}^{Nadh_L} - v_{ampreg}^{Amp_L} - v_{atpuse}^{Atp_L} - v_{nadhk}^{Nadh_L} \end{aligned} \tag{S247}$$

$$\begin{aligned} V_L \frac{dAdp_L}{dt} = & v_{hk}^{Glc_L} + v_{pfk}^{G6p_L} - 2 \cdot v_{pk}^{Gap_L} + 2 \cdot v_{pepck}^{Pyr_L} - v_{tca}^{Accoa_{LM}} + v_{accoat}^{Accoa_{LMLC}} + v_{glyk}^{Glyc_L} + v_{boxid}^{FFA_L} + v_{lipog1}^{Accoa_{LC}} \\ & - \frac{1}{8} v_{lipog2}^{Malcoa_{LC}} - v_{tgsyin}^{FFA_L} + 3 \cdot v_{cholosyn2}^{Hmgcoa_L} - v_{atpsynf}^{Fadh_L} - 3 \cdot v_{atpsynn}^{Nadh_L} + 2 \cdot v_{ampreg}^{Amp_L} + v_{atpuse}^{Atp_L} + v_{nadhk}^{Nadh_L} \end{aligned} \tag{S248}$$

$$V_L \frac{dAmp_L}{dt} = 3 \cdot v_{tgsyin}^{FFA_L} - v_{ampreg}^{Amp_L} \tag{S249}$$

$$V_L \frac{dNadh_L}{dt} = v_{pk}^{Gap_L} - v_{pepck}^{Pyr_L} - v_{ldh}^{Pyr_L} + v_{pdh}^{Pyr_L} + 3 \cdot v_{tca}^{Accoa_{LM}} - v_{g3pd}^{Gap_L} - \frac{1}{2} v_{bhbsyn}^{Accoa_{LM}} + 7v_{boxid}^{FFA_L} - v_{atpsynn}^{Nadh_L} - v_{nadhuse}^{Nadh_L} \tag{S250}$$

$$V_L \frac{dNad_L}{dt} = -v_{pk}^{Gap_L} + v_{pepck}^{Pyr_L} + v_{ldh}^{Pyr_L} - v_{pdh}^{Pyr_L} - 3v_{tca}^{Accoa_{LM}} + v_{g3pd}^{Gap_L} + \frac{1}{2} v_{bhbsyn}^{Accoa_{LM}} - 7v_{boxid}^{FFA_L} + v_{atpsynn}^{Nadh_L} + v_{nadhuse}^{Nadh_L} \tag{S251}$$

$$V_L \frac{dFadh_L}{dt} = 7v_{boxid}^{FFA_L} + v_{tca}^{Accoa_{LM}} - \frac{1}{6} v_{cholsyn2}^{Hmgcoa_L} - v_{atpsynf}^{Fadh_L} - v_{fadhuse}^{Fadh_L} \tag{S252}$$

$$V_L \frac{dFad_L}{dt} = -7v_{boxid}^{FFA_L} - v_{tca}^{Accoa_{LM}} + \frac{1}{6}v_{cholsyn2}^{Hmgcoa_L} + v_{atpsynf}^{Fadh_L} + v_{fadhuse}^{Fadh_L} \quad \text{(S253)}$$

$$V_L \frac{dGtp_L}{dt} = -v_{pepck}^{Pyr_L} + v_{gdpreg}^{Gdp_L} \quad \text{(S254)}$$

$$V_L \frac{dGdp_L}{dt} = v_{pepck}^{Pyr_L} - v_{gdpreg}^{Gdp_L} \quad \text{(S255)}$$

$$V_L \frac{dUtp_L}{dt} = -v_{gs}^{G6p_L} + v_{udpreg}^{Udp_L} - v_{utpuse}^{Utp_L} \quad \text{(S256)}$$

$$V_L \frac{dUdp_L}{dt} = v_{gs}^{G6p_L} - v_{udpreg}^{Udp_L} + v_{utpuse}^{Utp_L} \quad \text{(S257)}$$

$$V_L \frac{dNadph_L}{dt} = -\frac{14}{8}v_{lipog2}^{Malcoa_L} - \frac{21}{6}v_{cholsyn2}^{Hmgcoa_L} + 2v_{ppp}^{G6p_L} + v_{nadhk}^{Nadh_L} - v_{nadphuse}^{Nadph_L} \quad \text{(S258)}$$

$$V_L \frac{dNadp_L}{dt} = \frac{14}{8}v_{lipog2}^{Malcoa_L} + \frac{21}{6}v_{cholsyn2}^{Hmgcoa_L} - 2v_{ppp}^{G6p_L} - v_{nadhk}^{Nadh_L} + v_{nadphuse}^{Nadph_L} \quad \text{(S259)}$$

$$V_L \frac{dCre_L}{dt} = -v_{ck}^{Cre_L} \quad \text{(S260)}$$

$$V_L \frac{dCrep_L}{dt} = v_{ck}^{Cre_L} \quad \text{(S261)}$$

ODE in skeletal muscle

$$V_M \frac{dGlc_M}{dt} = v_{glut4}^{Glc_{BM}} - v_{hk}^{Glc_M} \quad \text{(S262)}$$

$$V_M \frac{dG6p_M}{dt} = v_{hk}^{Glc_M} - v_{gs}^{G6p_M} + v_{gd}^{Glygn_M} - v_{pfk}^{G6p_M} \quad \text{(S263)}$$

$$V_M \frac{dGlygn_M}{dt} = v_{gs}^{G6p_M} - v_{gd}^{Glygn_M} \quad \text{(S264)}$$

$$V_M \frac{dGap_M}{dt} = 2v_{pfk}^{G6p_M} - v_{pk}^{Gap_M} - v_{g3pd}^{Gap_M} \quad \text{(S265)}$$

$$V_M \frac{dPyr_M}{dt} = v_{pk}^{Gap_M} + v_{pryt}^{Pyr_{BM}} - v_{ldh}^{Pyr_M} - v_{alata}^{Pyr_M} - v_{pdh}^{Pyr_M} \quad \text{(S266)}$$

$$V_M \frac{dLac_M}{dt} = v_{lact}^{Pyr_{BM}} + v_{ldh}^{Pyr_M} \quad \text{(S267)}$$

$$V_M \frac{dAla_M}{dt} = v_{alat}^{Ala_{BM}} + v_{alata}^{Pyr_M} \quad \text{(S268)}$$

$$V_M \frac{dAccoa_{MM}}{dt} = v_{pdh}^{Pyr_M} - v_{tca}^{Accoa_{MM}} + 8 \cdot v_{boxid}^{FFA_M} \quad \text{(S269)}$$

$$V_M \frac{dBhb_M}{dt} = 0 \quad \text{(S270)}$$

$$V_M \frac{dAccoa_{MC}}{dt} = v_{accoat}^{Accoa_{MMMC}} - v_{lipog1}^{Accoa_{MC}} \quad \text{(S271)}$$

$$V_M \frac{dMalcoa_M}{dt} = v_{lipog1}^{Accoa_{MC}} - v_{lipog2}^{Malcoa_M} \quad \text{(S272)}$$

$$V_M \frac{dHmgcoa_M}{dt} = 0 \quad \text{(S273)}$$

$$V_M \frac{dChol_M}{dt} = 0 \quad \text{(S274)}$$

$$V_M \frac{dFFA_M}{dt} = v_{ffat}^{FFA_{BM}} - 3 \cdot v_{tgsyn}^{FFA_M} + 3 \cdot v_{tgdeg}^{TG_M} - v_{boxid}^{FFA_M} \quad \text{(S275)}$$

$$V_M \frac{dGlyc_M}{dt} = v_{tgdeg}^{TG_M} + v_{glyct}^{Glyc_{BM}} - v_{glyck}^{Glyc_M} \quad \text{(S276)}$$

$$V_M \frac{dGlycp_M}{dt} = -v_{tgsyn}^{FFA_M} + v_{glyct}^{Glyc_M} + v_{g3pd}^{Gap_M} \quad \text{(S277)}$$

$$V_M \frac{dTG_M}{dt} = v_{tgsyn}^{FFA_M} - v_{tgdeg}^{TG_M} \quad \text{(S278)}$$

$$V_M \frac{dAtp_M}{dt} = -v_{hk}^{Glc_M} - v_{pfk}^{G6p_M} + 2v_{pk}^{Gap_M} + v_{tca}^{Accoa_{MM}} - v_{glyk}^{Glyc_M} - v_{boxid}^{FFA_M} - 2v_{tgsyin}^{FFA_M} + v_{atpsynf}^{Fadh_M} + 3v_{atpsynn}^{Nadh_M} - v_{ampreg}^{Amp_M} - v_{atpuse}^{Atp_M} \quad \text{(S279)}$$

$$V_M \frac{dAdp_M}{dt} = v_{hk}^{Glc_M} + v_{pfk}^{G6p_M} - 2 \cdot v_{pk}^{Gap_M} - v_{tca}^{Accoa_{MM}} + v_{glyk}^{Glyc_M} + v_{boxid}^{FFA_M} - v_{tgsyin}^{FFA_M} - v_{atpsynf}^{Fadh_M} - 3 \cdot v_{atpsynn}^{Nadh_M} + 2 \cdot v_{ampreg}^{Amp_M} + v_{atpuse}^{Atp_M} \quad \text{(S280)}$$

$$V_M \frac{dAmp_M}{dt} = 3 \cdot v_{tgsyin}^{FFA_M} - v_{ampreg}^{Amp_M} \quad \text{(S281)}$$

$$V_M \frac{dNadh_M}{dt} = v_{pk}^{Gap_M} - v_{ldh}^{Pyr_M} + v_{pdh}^{Pyr_M} + 3 \cdot v_{tca}^{Accoa_{MM}} - v_{g3pd}^{Gap_M} + 7v_{boxid}^{FFA_M} - v_{atpsynn}^{Nadh_M} - v_{nadhuse}^{Nadh_M} \quad \text{(S282)}$$

$$V_M \frac{dNad_M}{dt} = -v_{pk}^{Gap_M} + v_{ldh}^{Pyr_M} - v_{pdh}^{Pyr_M} - 3v_{tca}^{Accoa_{MM}} + v_{g3pd}^{Gap_M} - 7v_{boxid}^{FFA_M} + v_{atpsynn}^{Nadh_M} + v_{nadhuse}^{Nadh_M} \quad \text{(S283)}$$

$$V_M \frac{dFadh_M}{dt} = 7v_{boxid}^{FFA_M} + v_{tca}^{Accoa_{MM}} - v_{atpsynf}^{Fadh_M} - v_{fadhuse}^{Fadh_M} \quad \text{(S284)}$$

$$V_M \frac{dFad_M}{dt} = -7v_{boxid}^{FFA_M} - v_{tca}^{Accoa_{MM}} + v_{atpsynf}^{Fadh_M} + v_{fadhuse}^{Fadh_M} \quad \text{(S285)}$$

$$V_M \frac{dGtp_M}{dt} = 0 \quad \text{(S286)}$$

$$V_M \frac{dGdp_M}{dt} = 0 \quad \text{(S287)}$$

$$V_M \frac{dUtp_M}{dt} = -v_{gs}^{G6p_M} + v_{udpreg}^{Udp_M} - v_{utpuse}^{Utp_M} \quad \text{(S288)}$$

$$V_M \frac{dUdp_M}{dt} = v_{gs}^{G6p_M} - v_{udpreg}^{Udp_M} + v_{utpuse}^{Utp_M} \quad \text{(S289)}$$

$$V_M \frac{dNadph_M}{dt} = 2v_{ppp}^{G6p_M} + v_{nadhk}^{Nadh_M} - v_{nadphuse}^{Nadph_M} \quad \text{(S290)}$$

$$V_M \frac{dNadp_M}{dt} = -2v_{ppp}^{G6p_M} - v_{nadhk}^{Nadh_M} + v_{nadphuse}^{Nadph_M} \quad \text{(S291)}$$

$$V_M \frac{dCre_M}{dt} = -v_{ck}^{Cre_M} \quad \text{(S292)}$$

$$V_M \frac{dCrep_M}{dt} = v_{ck}^{Cre_M} \quad \text{(S293)}$$

ODE in adipose tissue

$$V_A \frac{dGlc_A}{dt} = v_{glut4}^{Glc_{BA}} - v_{hk}^{Glc_A} \quad \text{(S294)}$$

$$V_A \frac{dG6p_A}{dt} = v_{hk}^{Glc_A} - v_{pfk}^{G6p_A} \quad \text{(S295)}$$

$$V_A \frac{dGlygn_A}{dt} = 0 \quad \text{(S296)}$$

$$V_A \frac{dGap_A}{dt} = 2v_{pfk}^{G6p_A} - v_{pk}^{Gap_A} - v_{g3pd}^{Gap_A} \quad \text{(S297)}$$

$$V_A \frac{dPyr_A}{dt} = v_{pk}^{Gap_A} + v_{pryt}^{Pyr_{BA}} - v_{ldh}^{Pyr_A} - v_{alata}^{Pyr_A} - v_{pdh}^{Pyr_A} \quad \text{(S298)}$$

$$V_A \frac{dLac_A}{dt} = v_{lact}^{Pyr_{BA}} + v_{ldh}^{Pyr_A} \quad \text{(S299)}$$

$$V_A \frac{dAla_A}{dt} = v_{alat}^{Ala_{BA}} + v_{alata}^{Pyr_A} \quad \text{(S300)}$$

$$V_A \frac{dAccoa_{AM}}{dt} = v_{pdh}^{Pyr_A} - v_{tca}^{Accoa_{AM}} + 8 \cdot v_{boxid}^{FFA_A} \quad \text{(S301)}$$

$$V_A \frac{dBhb_A}{dt} = 0 \quad \text{(S302)}$$

$$V_A \frac{dAccoa_{AC}}{dt} = v_{accoat}^{Accoa_{AMAC}} - v_{lipog1}^{Accoa_{AC}} \quad \text{(S303)}$$

$$V_A \frac{dMalcoa_A}{dt} = v_{lipog1}^{Accoa_{AC}} - v_{lipog2}^{Malcoa_A} \quad \text{(S304)}$$

$$V_A \frac{dHmgcoa_A}{dt} = 0 \quad \text{(S305)}$$

$$V_A \frac{dChol_A}{dt} = 0 \quad \text{(S306)}$$

$$V_A \frac{dFFA_A}{dt} = v_{ffat}^{FFA_{BA}} - 3 \cdot v_{tgsyn}^{FFA_A} + 3 \cdot v_{tgdeg}^{TG_A} - v_{boxid}^{FFA_A} \quad \text{(S307)}$$

$$V_A \frac{dGlyc_A}{dt} = v_{tgdeg}^{TG_A} + v_{glyct}^{Glyc_{BA}} - v_{glyck}^{Glyc_A} \quad \text{(S308)}$$

$$V_A \frac{dGlycp_A}{dt} = -v_{tgsyn}^{FFA_A} + v_{glyct}^{Glyc_A} + v_{g3pd}^{Gap_A} \quad \text{(S309}$$

$$V_A \frac{dTG_A}{dt} = v_{tgsyn}^{FFA_A} - v_{tgdeg}^{TG_A} \quad \text{(S310)}$$

$$V_A \frac{dAtp_A}{dt} = -v_{hk}^{Glc_A} - v_{pfk}^{G6p_A} + 2v_{pk}^{Gap_A} + v_{tca}^{Accoa_{AM}} - v_{glyk}^{Glyc_A} - v_{boxid}^{FFA_A} - 2v_{tgsyin}^{FFA_A} + v_{atpsynf}^{Fadh_A} + 3v_{atpsynn}^{Nadh_A} - v_{ampreg}^{Amp_A} - v_{atpuse}^{Atp_A} \quad \text{(S311)}$$

$$V_A \frac{dAdp_A}{dt} = v_{hk}^{Glc_A} + v_{pfk}^{G6p_A} - 2 \cdot v_{pk}^{Gap_A} - v_{tca}^{Accoa_{AM}} + v_{glyk}^{Glyc_A} + v_{boxid}^{FFA_A} - v_{tgsyin}^{FFA_A} - v_{atpsynf}^{Fadh_A} - 3 \cdot v_{atpsynn}^{Nadh_A} + 2 \cdot v_{ampreg}^{Amp_A} + v_{atpuse}^{Atp_A} \quad \text{(S312)}$$

$$V_A \frac{dAmp_A}{dt} = 3 \cdot v_{tgsyin}^{FFA_A} - v_{ampreg}^{Amp_A} \quad \text{(S313)}$$

$$V_A \frac{dNadh_A}{dt} = v_{pk}^{Gap_A} - v_{ldh}^{Pyr_A} + v_{pdh}^{Pyr_A} + 3 \cdot v_{tca}^{Accoa_{AM}} - v_{g3pd}^{Gap_A} + 7v_{boxid}^{FFA_A} - v_{atpsynn}^{Nadh_A} - v_{nadhuse}^{Nadh_A} \quad \text{(S314)}$$

$$V_A \frac{dNad_A}{dt} = -v_{pk}^{Gap_A} + v_{ldh}^{Pyr_A} - v_{pdh}^{Pyr_A} - 3v_{tca}^{Accoa_{AM}} + v_{g3pd}^{Gap_A} - 7v_{boxid}^{FFA_A} + v_{atpsynn}^{Nadh_A} + v_{nadhuse}^{Nadh_A} \quad \text{(S315)}$$

$$V_A \frac{dFadh_A}{dt} = 7v_{boxid}^{FFA_A} + v_{tca}^{Accoa_{AM}} - v_{atpsynf}^{Fadh_A} - v_{fadhuse}^{Fadh_A} \quad \text{(S316)}$$

$$V_A \frac{dFad_A}{dt} = -7v_{boxid}^{FFA_A} - v_{tca}^{Accoa_{AM}} + v_{atpsynf}^{Fadh_A} + v_{fadhuse}^{Fadh_A} \quad \text{(S317)}$$

$$V_A \frac{dGtp_A}{dt} = 0 \quad \text{(S318)}$$

$$V_A \frac{dGdp_A}{dt} = 0 \quad \text{(S319)}$$

$$V_A \frac{dUtp_A}{dt} = 0 \quad \text{(S320)}$$

$$V_A \frac{dUdp_A}{dt} = 0 \quad \text{(S321)}$$

$$V_A \frac{dNadph_A}{dt} = 2v_{ppp}^{G6p_A} + v_{nadhk}^{Nadh_A} - v_{nadphuse}^{Nadph_A} \quad \text{(S322)}$$

$$V_A \frac{dNadp_A}{dt} = -2v_{ppp}^{G6p_A} - v_{nadhk}^{Nadh_A} + v_{nadphuse}^{Nadph_A} \quad \text{(S323)}$$

$$V_A \frac{dCre_A}{dt} = -v_{ck}^{Cre_A} \quad \text{(S324)}$$

$$V_A \frac{dCrep_A}{dt} = v_{ck}^{Cre_A} \quad \text{(S325)}$$

ODE in GI tract

$$V_G \frac{dGlc_G}{dt} = v_{glut2}^{Glc_{BG}} - v_{hk}^{Glc_G} \quad \text{(S326)}$$

$$V_G \frac{dG6p_G}{dt} = v_{hk}^{Glc_G} - v_{pfk}^{G6p_G} \quad \text{(S327)}$$

$$V_G \frac{dGap_G}{dt} = 2v_{pfk}^{G6p_G} - v_{pk}^{Gap_G} - v_{g3pd}^{Gap_G} \quad \text{(S328)}$$

$$V_G \frac{dGlygn_G}{dt} = 0 \quad \text{(S329)}$$

$$V_G \frac{dPyr_G}{dt} = v_{pk}^{Gap_G} + v_{pryt}^{Pyr_{BG}} - v_{ldh}^{Pyr_G} - v_{alata}^{Pyr_G} - v_{pdh}^{Pyr_G} \quad \text{(S330)}$$

$$V_G \frac{dLac_G}{dt} = v_{lact}^{Pyr_{BG}} + v_{ldh}^{Pyr_G} \quad \text{(S331)}$$

$$V_G \frac{dAla_G}{dt} = v_{alat}^{Ala_{BG}} + v_{alata}^{Pyr_G} \quad \text{(S332)}$$

$$V_G \frac{dAccoa_{GM}}{dt} = v_{pdh}^{Pyr_G} - v_{tca}^{Accoa_{GM}} + 8 \cdot v_{boxid}^{FFA_G} \quad \text{(S333)}$$

$$V_A \frac{dBhb_A}{dt} = 0 \quad \text{(S334)}$$

$$V_A \frac{dAccoa_{AC}}{dt} = v_{accoat}^{Accoa_{AMAC}} - v_{lipog1}^{Accoa_{AC}} \quad \text{(S335)}$$

$$V_A \frac{dMalcoa_A}{dt} = v_{lipog1}^{Accoa_{AC}} - v_{lipog2}^{Malcoa_A} \quad \text{(S336)}$$

$$V_A \frac{dHmgcoa_A}{dt} = 0 \quad \text{(S337)}$$

$$V_A \frac{dChol_A}{dt} = 0 \quad \text{(S338)}$$

$$V_G \frac{dFFA_G}{dt} = v_{ffat}^{FFA_{BG}} - 3 \cdot v_{tgsyn}^{FFA_G} + 3 \cdot v_{tgdeg}^{TG_G} - v_{boxid}^{FFA_G} \quad \text{(S339)}$$

$$V_G \frac{dGlyc_G}{dt} = v_{tgdeg}^{TG_G} + v_{glyct}^{Glyc_{BG}} - v_{glyck}^{Glyc_G} \quad \text{(S340)}$$

$$V_G \frac{dGlycp_G}{dt} = -v_{tgsyn}^{FFA_G} + v_{glyct}^{Glyc_G} + v_{g3pd}^{Gap_G} \quad \text{(S341)}$$

$$V_G \frac{dTG_G}{dt} = v_{tgsyn}^{FFA_G} - v_{tgdeg}^{TG_G} \quad \text{(S342)}$$

$$V_G \frac{dAtp_G}{dt} = -v_{hk}^{Glc_G} - v_{pfk}^{G6p_G} + 2v_{pk}^{Gap_G} + v_{tca}^{Accoa_{GM}} - v_{glyk}^{Glyc_G} - v_{boxid}^{FFA_G} - 2v_{tgsyin}^{FFA_G} + v_{atpsynf}^{Fadh_G} + 3v_{atpsynn}^{Nadh_G} - v_{ampreg}^{Amp_G} - v_{atpuse}^{Atp_G} \quad \text{(S343)}$$

$$V_G \frac{dAdp_G}{dt} = v_{hk}^{Glc_G} + v_{pfk}^{G6p_G} - 2 \cdot v_{pk}^{Gap_G} - v_{tca}^{Accoa_{GM}} + v_{glyk}^{Glyc_G} + v_{boxid}^{FFA_G} - v_{tgsyin}^{FFA_G} - v_{atpsynf}^{Fadh_G} - 3 \cdot v_{atpsynn}^{Nadh_G} + 2 \cdot v_{ampreg}^{Amp_G} + v_{atpuse}^{Atp_G} \quad \text{(S344)}$$

$$V_G \frac{dAmp_G}{dt} = 3 \cdot v_{tgsyin}^{FFA_G} - v_{ampreg}^{Amp_G} \quad \text{(S345)}$$

$$V_G \frac{dNadh_G}{dt} = v_{pk}^{Gap_G} - v_{ldh}^{Pyr_G} + v_{pdh}^{Pyr_G} + 3 \cdot v_{tca}^{Accoa_{GM}} - v_{g3pd}^{Gap_G} + 7v_{boxid}^{FFA_G} - v_{atpsynn}^{Nadh_G} - v_{nadhuse}^{Nadh_G} \quad \text{(S346)}$$

$$V_G \frac{dNad_G}{dt} = -v_{pk}^{Gap_G} + v_{ldh}^{Pyr_G} - v_{pdh}^{Pyr_G} - 3v_{tca}^{Accoa_{GM}} + v_{g3pd}^{Gap_G} - 7v_{boxid}^{FFA_G} + v_{atpsynn}^{Nadh_G} + v_{nadhuse}^{Nadh_G} \quad \text{(S347)}$$

$$V_G \frac{dFadh_G}{dt} = 7v_{boxid}^{FFA_G} + v_{tca}^{Accoa_{GM}} - v_{atpsynf}^{Fadh_G} - v_{fadhuse}^{Fadh_G} \quad \text{(S348)}$$

$$V_G \frac{dFad_G}{dt} = -7v_{boxid}^{FFA_G} - v_{tca}^{Accoa_{GM}} + v_{atpsynf}^{Fadh_G} + v_{fadhuse}^{Fadh_G} \quad \text{(S349)}$$

$$V_G \frac{dGtp_G}{dt} = 0 \quad \text{(S350)}$$

$$V_G \frac{dGdp_G}{dt} = 0 \quad \text{(S351)}$$

$$V_G \frac{dUtp_G}{dt} = 0 \quad \text{(S352)}$$

$$V_G \frac{dUdp_G}{dt} = 0 \quad \text{(S353)}$$

$$V_G \frac{dNadph_G}{dt} = 2v_{ppp}^{G6p_G} + v_{nadhk}^{Nadh_G} - v_{nadphuse}^{Nadph_G} \quad \text{(S354)}$$

$$V_G \frac{dNadp_G}{dt} = -2v_{ppp}^{G6p_G} - v_{nadhk}^{Nadh_G} + v_{nadphuse}^{Nadph_G} \quad \text{(S355)}$$

$$V_G \frac{dCre_G}{dt} = -v_{ck}^{Cre_G} \quad \text{(S356)}$$

$$V_G \frac{dCrep_G}{dt} = v_{ck}^{Cre_G} \quad \text{(S357)}$$

ODE in heart

$$V_H \frac{dGlc_H}{dt} = v_{glut2}^{Glc_{BH}} - v_{hk}^{Glc_H} \quad \text{(S358)}$$

$$V_H \frac{dG6p_H}{dt} = v_{hk}^{Glc_H} - v_{gs}^{G6p_H} + v_{gd}^{Glygn_H} - v_{pfk}^{G6p_H} \quad \text{(S359)}$$

$$V_H \frac{dGlygn_H}{dt} = v_{gs}^{G6p_H} - v_{gd}^{Glygn_H} \quad \text{(S360)}$$

$$V_H \frac{dGap_H}{dt} = 2v_{pfk}^{G6p_H} - v_{pk}^{Gap_H} - v_{g3pd}^{Gap_H} \quad \text{(S361)}$$

$$V_H \frac{dPyr_H}{dt} = v_{pk}^{Gap_H} + v_{pryt}^{Pyr_{BH}} - v_{ldh}^{Pyr_H} - v_{alata}^{Pyr_H} - v_{pdh}^{Pyr_H} \quad \text{(S362)}$$

$$V_H \frac{dLac_H}{dt} = v_{lact}^{Pyr_{BH}} + v_{ldh}^{Pyr_H} \quad \text{(S363)}$$

$$V_H \frac{dAla_H}{dt} = v_{alat}^{Ala_{BH}} + v_{alata}^{Pyr_H} \quad \text{(S364)}$$

$$V_H \frac{dAccoa_{HM}}{dt} = v_{pdh}^{Pyr_H} - v_{tca}^{Accoa_{HM}} + 8 \cdot v_{boxid}^{FFA_H} \quad \text{(S365)}$$

$$V_H \frac{dBhb_H}{dt} = 0 \quad \text{(S366)}$$

$$V_H \frac{dAccoa_{HC}}{dt} = v_{accoat}^{Accoa_{HMHC}} - v_{lipog1}^{Accoa_{HC}} \quad \text{(S367)}$$

$$V_H \frac{dMalcoa_H}{dt} = v_{lipog1}^{Accoa_{HC}} - v_{lipog2}^{Malcoa_H} \quad \text{(S368)}$$

$$V_H \frac{dHmgcoa_H}{dt} = 0 \quad \text{(S369)}$$

$$V_H \frac{dChol_H}{dt} = 0 \quad \text{(S370)}$$

$$V_H \frac{dFFA_H}{dt} = v_{ffat}^{FFA_{BH}} - 3 \cdot v_{tgsyn}^{FFA_H} + 3 \cdot v_{tgdeg}^{TG_H} - v_{boxid}^{FFA_H} \quad \text{(S371)}$$

$$V_H \frac{dGlyc_M}{dt} = v_{tgdeg}^{TG_M} + v_{glyct}^{Glyc_{BM}} - v_{glyck}^{Glyc_M} \quad \text{(S372)}$$

$$V_H \frac{dGlycp_H}{dt} = -v_{tgsyn}^{FFA_H} + v_{glyct}^{Glyc_H} + v_{g3pd}^{Gap_H} \quad \text{(S373)}$$

$$V_H \frac{dTG_H}{dt} = v_{tgsyn}^{FFA_H} - v_{tgdeg}^{TG_H} \quad \text{(S374)}$$

$$V_H \frac{dAtp_H}{dt} = -v_{hk}^{Glc_H} - v_{pfk}^{G6p_H} + 2v_{pk}^{Gap_H} + v_{tca}^{Accoa_{HM}} - v_{glyk}^{Glyc_H} - v_{boxid}^{FFA_H} - 2v_{tgsyin}^{FFA_H} + v_{atpsynf}^{Fadh_H} + 3v_{atpsynn}^{Nadh_H} - v_{ampreg}^{Amp_H} - v_{atpuse}^{Atp_H} \quad \text{(S375)}$$

$$V_H \frac{dAdp_H}{dt} = v_{hk}^{Glc_H} + v_{pfk}^{G6p_M} - 2 \cdot v_{pk}^{Gap_H} - v_{tca}^{Accoa_{HM}} + v_{glyk}^{Glyc_H} + v_{boxid}^{FFA_H} - v_{tgsyin}^{FFA_H} - v_{atpsynf}^{Fadh_H} - 3 \cdot v_{atpsynn}^{Nadh_H} + 2 \cdot v_{ampreg}^{Amp_H} + v_{atpuse}^{Atp_H} \quad \text{(S376)}$$

$$V_H \frac{dAmp_H}{dt} = 3 \cdot v_{tgsyin}^{FFA_H} - v_{ampreg}^{Amp_H} \quad \text{(S377)}$$

$$V_H \frac{dNadh_H}{dt} = v_{pk}^{Gap_H} - v_{ldh}^{Pyr_H} + v_{pdh}^{Pyr_H} + 3 \cdot v_{tca}^{Accoa_{HM}} - v_{g3pd}^{Gap_H} + 7v_{boxid}^{FFA_H} - v_{atpsynn}^{Nadh_H} - v_{nadhuse}^{Nadh_H} \quad \text{(S378)}$$

$$V_H \frac{dNad_H}{dt} = -v_{pk}^{Gap_H} + v_{ldh}^{Pyr_H} - v_{pdh}^{Pyr_H} - 3v_{tca}^{Accoa_{HM}} + v_{g3pd}^{Gap_H} - 7v_{boxid}^{FFA_H} + v_{atpsynn}^{Nadh_H} + v_{nadhuse}^{Nadh_M} \quad \text{(S379)}$$

$$V_H \frac{dFadh_H}{dt} = 7v_{boxid}^{FFA_H} + v_{tca}^{Accoa_{MM}} - v_{atpsynf}^{Fadh_H} - v_{fadhuse}^{Fadh_H} \quad \text{(S380)}$$

$$V_H \frac{dFad_H}{dt} = -7v_{boxid}^{FFA_H} - v_{tca}^{Accoa_{HM}} + v_{atpsynf}^{Fadh_H} + v_{fadhuse}^{Fadh_H} \quad \text{(S381)}$$

$$V_H \frac{dGtp_H}{dt} = 0 \quad \text{(S382)}$$

$$V_H \frac{dGdp_H}{dt} = 0 \quad \text{(S383)}$$

$$V_H \frac{dUtp_H}{dt} = -v_{gs}^{G6p_H} + v_{udpreg}^{Udp_M} - v_{utpuse}^{Utp_H} \quad \text{(S384)}$$

$$V_H \frac{dUdp_H}{dt} = v_{gs}^{G6p_H} - v_{udpreg}^{Udp_H} + v_{utpuse}^{Utp_H} \quad \text{(S385)}$$

$$V_H \frac{dNadph_H}{dt} = 2v_{ppp}^{G6p_H} + v_{nadhk}^{Nadh_H} - v_{nadphuse}^{Nadph_H} \quad \text{(S386)}$$

$$V_H \frac{dNadp_H}{dt} = -2v_{ppp}^{G6p_H} - v_{nadhk}^{Nadh_H} + v_{nadphuse}^{Nadph_H} \quad \text{(S387)}$$

$$V_H \frac{dCre_H}{dt} = -v_{ck}^{Cre_H} \quad \text{(S388)}$$

$$V_H \frac{dCrep_H}{dt} = v_{ck}^{Cre_H} \quad \text{(S389)}$$

ODE in brain

$$V_N \frac{dGlc_N}{dt} = v_{glut3}^{Glc_{BN}} - v_{hk}^{Glc_N} \quad \text{(S390)}$$

$$V_N \frac{dG6p_N}{dt} = v_{hk}^{Glc_N} - v_{gs}^{G6p_N} + v_{gd}^{Glygn_N} - v_{pfk}^{G6p_N} \quad \text{(S391)}$$

$$V_N \frac{dGlygn_N}{dt} = v_{gs}^{G6p_N} - v_{gd}^{Glygn_N} \quad \text{(S392)}$$

$$V_N \frac{dGap_N}{dt} = 2v_{pfk}^{G6p_N} - v_{pk}^{Gap_N} \quad \text{(S393)}$$

$$V_N \frac{dPyr_N}{dt} = v_{pk}^{Gap_N} + v_{pryt}^{Pyr_{BN}} - v_{ldh}^{Pyr_N} - v_{alata}^{Pyr_N} - v_{pdh}^{Pyr_N} \quad \text{(S394)}$$

$$V_N \frac{dLac_N}{dt} = v_{lact}^{Pyr_{BN}} + v_{ldh}^{Pyr_N} \quad \text{(S395)}$$

$$V_N \frac{dAla_N}{dt} = v_{alat}^{Ala_{BN}} + v_{alata}^{Pyr_N} \quad \text{(S396)}$$

$$V_N \frac{dAccoa_{NM}}{dt} = v_{pdh}^{Pyr_N} - v_{tca}^{Accoa_{NM}} + 2v_{bhbdeg}^{Bhb_N} \quad \text{(S397)}$$

$$V_N \frac{dBhb_N}{dt} = v_{bhbt}^{Bhb_{BN}} - v_{bhbdeg}^{Bhb_N} \quad \text{(S398)}$$

$$V_N \frac{dAccoa_{NC}}{dt} = v_{accoat}^{Accoa_{NMNC}} - v_{lipog1}^{Accoa_{NC}} \quad \text{(S399)}$$

$$V_N \frac{dMalcoa_N}{dt} = v_{lipog1}^{Accoa_{NC}} - v_{lipog2}^{Malcoa_N} \quad \text{(S400)}$$

$$V_N \frac{dHmgcoa_N}{dt} = 0 \quad \text{(S401)}$$

$$V_N \frac{dChol_N}{dt} = 0 \quad \text{(S402)}$$

$$V_N \frac{dFFA_N}{dt} = 0 \quad \text{(S403)}$$

$$V_N \frac{dGlyc_N}{dt} = 0 \quad \text{(S404)}$$

$$V_N \frac{dGlycp_N}{dt} = 0 \quad \text{(S405)}$$

$$V_N \frac{dTG_N}{dt} = 0 \quad \text{(S406)}$$

$$V_N \frac{dAtp_N}{dt} = -v_{hk}^{Glc_N} - v_{pfk}^{G6p_N} + 2v_{pk}^{Gap_N} + v_{tca}^{Accoa_{NM}} - v_{bhb\deg}^{Bhb_N} + v_{atpsynf}^{Fadh_N} + 3v_{atpsynn}^{Nadh_N} - v_{atpuse}^{Atp_N} \quad \text{(S407)}$$

$$V_N \frac{dAdp_N}{dt} = v_{hk}^{Glc_N} + v_{pfk}^{G6p_N} - 2 \cdot v_{pk}^{Gap_N} - v_{tca}^{Accoa_{NM}} - v_{bhb\deg}^{Bhb_N} - v_{atpsynf}^{Fadh_N} - 3 \cdot v_{atpsynn}^{Nadh_N} + v_{atpuse}^{Atp_N} \quad \text{(S408)}$$

$$V_N \frac{dAmp_N}{dt} = 0 \quad \text{(S409)}$$

$$V_N \frac{dNadh_N}{dt} = v_{pk}^{Gap_N} - v_{ldh}^{Pyr_N} + v_{pdh}^{Pyr_N} + 3 \cdot v_{tca}^{Accoa_{NM}} + v_{bhbdeg}^{Bhb_N} - v_{atpsynn}^{Nadh_N} - v_{nadhuse}^{Nadh_N} \quad \text{(S410)}$$

$$V_N \frac{dNad_N}{dt} = -v_{pk}^{Gap_N} + v_{ldh}^{Pyr_N} - v_{pdh}^{Pyr_N} - 3v_{tca}^{Accoa_{NM}} - v_{bhbdeg}^{Bhb_N} + v_{atpsynn}^{Nadh_N} + v_{nadhuse}^{Nadh_N} \quad \text{(S411)}$$

$$V_N \frac{dFadh_N}{dt} = v_{tca}^{Accoa_{NM}} - v_{atpsynf}^{Fadh_N} - v_{fadhuse}^{Fadh_N} \quad \text{(S412)}$$

$$V_N \frac{dFad_N}{dt} = -v_{tca}^{Accoa_{NM}} + v_{atpsynf}^{Fadh_N} + v_{fadhuse}^{Fadh_N} \quad \text{(S413)}$$

$$V_N \frac{dGtp_N}{dt} = 0 \quad \text{(S414)}$$

$$V_N \frac{dGdp_N}{dt} = 0 \quad \text{(S415)}$$

$$V_N \frac{dUtp_N}{dt} = -v_{gs}^{G6p_N} + v_{udpreg}^{Udp_N} - v_{utpuse}^{Utp_N} \quad \text{(S416)}$$

$$V_N \frac{dUdp_N}{dt} = v_{gs}^{G6p_N} - v_{udpreg}^{Udp_N} + v_{utpuse}^{Utp_N} \quad \text{(S417)}$$

$$V_N \frac{dNadph_N}{dt} = 2v_{ppp}^{G6p_N} + v_{nadhk}^{Nadh_N} - v_{nadphuse}^{Nadph_N} \quad \text{(S418)}$$

$$V_N \frac{dNadp_N}{dt} = -2v_{ppp}^{G6p_N} - v_{nadhk}^{Nadh_N} + v_{nadphuse}^{Nadph_N} \quad \text{(S419)}$$

$$V_N \frac{dCre_N}{dt} = -v_{ck}^{Cre_N} \quad \text{(S420)}$$

$$V_N \frac{dCrep_N}{dt} = v_{ck}^{Cre_N} \quad \text{(S421)}$$

References

Ashworth, W.B., Davies, N.A., and Bogle, I.D. (2016). A Computational Model of Hepatic Energy Metabolism: Understanding Zonated Damage and Steatosis in NAFLD. PLoS Comput Biol *12*, e1005105.

Berndt, N., Bulik, S., Wallach, I., Wunsch, T., Konig, M., Stockmann, M., Meierhofer, D., and Holzhutter, H.G. (2018a). HEPATOKIN1 is a biochemistry-based model of liver metabolism for applications in medicine and pharmacology. Nat Commun *9*, 2386.

Berndt, N., Horger, M.S., Bulik, S., and Holzhutter, H.G. (2018b). A multiscale modelling approach to assess the impact of metabolic zonation and microperfusion on the hepatic carbohydrate metabolism. PLoS Comput Biol *14*, e1006005.

Kim, J., Saidel, G.M., and Cabrera, M.E. (2007). Multi-scale computational model of fuel homeostasis during exercise: effect of hormonal control. Ann Biomed Eng *35*, 69-90.

Konig, M., Bulik, S., and Holzhutter, H.G. (2012). Quantifying the contribution of the liver to glucose homeostasis: a detailed kinetic model of human hepatic glucose metabolism. PLoS Comput Biol *8*, e1002577.

Pearson, T., Wattis, J.A., King, J.R., MacDonald, I.A., and Mazzatti, D.J. (2014). A mathematical model of the human metabolic system and metabolic flexibility. Bull Math Biol *76*, 2091-2121.

Zheng, Q., Levitsky, L.L., Mink, K., and Rhoads, D.B. (1995). Glucose regulation of glucose transporters in cultured adult and fetal hepatocytes. Metabolism *44*, 1553-1558.

Supplemental figures

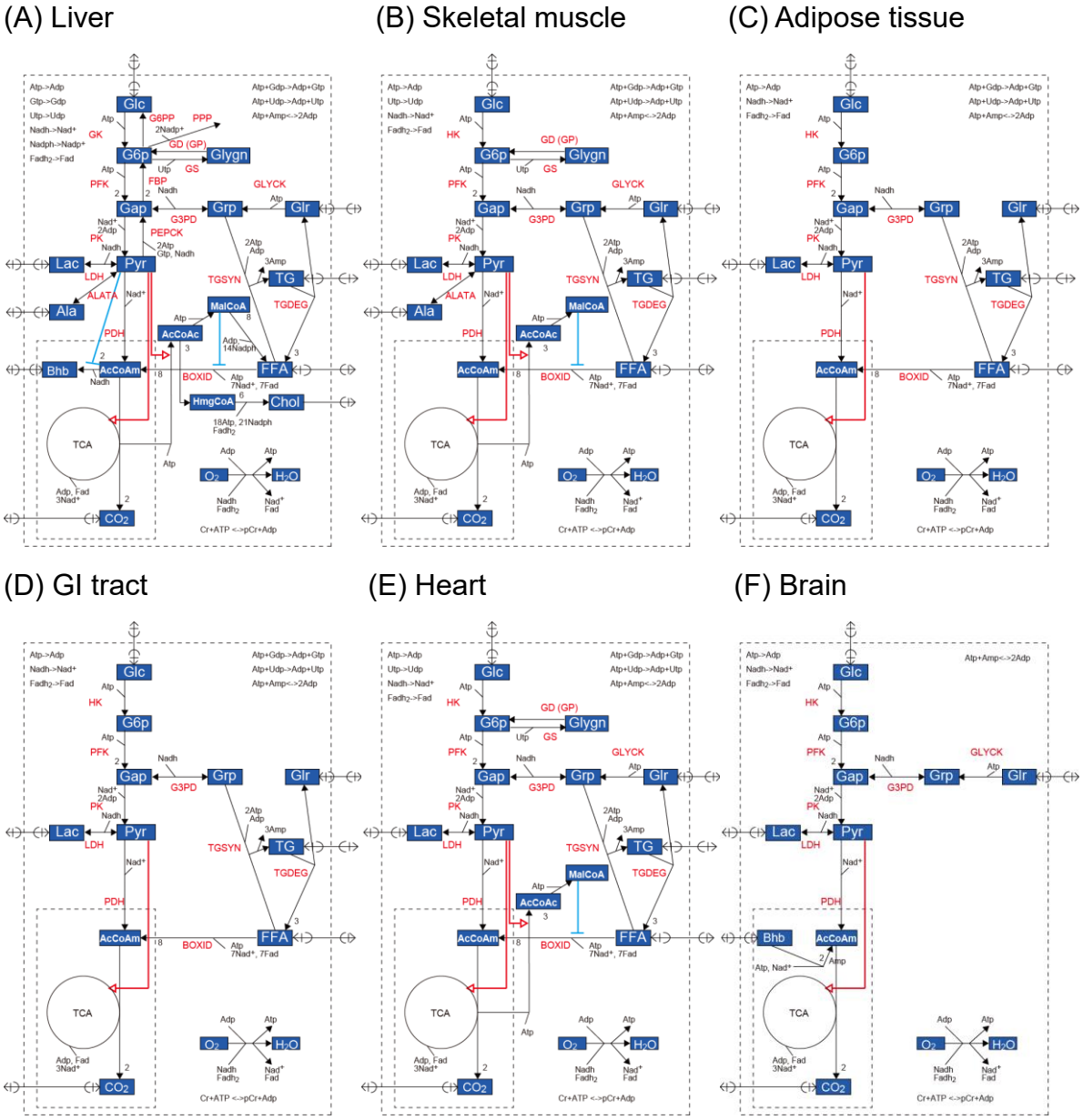

Figure S1 Metabolic network map of each organ, Related to Figure 2

Pancreas module construction

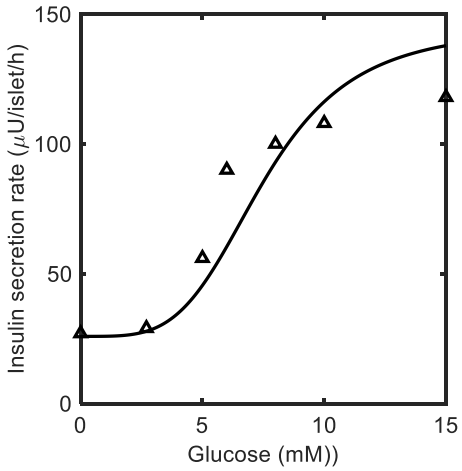

Figure S2 Experimental verification of the simulated insulin secretion rate by the pancreas module, Related to Figure 3

The solid lines indicate the simulated results; the triangles the experimental data (Harrison et al., 1985). Isolated islets from three healthy subjects were cultured in medium (RPMI1640) in 5-ml Petri dishes. The insulin secretion rates from the cultured islets were measured with respect to a glucose concentration from 0 to 20 mM. The values of kinetic parameters regarding the insulin synthesis rate (v_inssyn_Glc_B), which is given by Eqs. **(**S3-S6**)**, was estimated so as to reproduce the experimental insulin secretion rate (μU/islet/h).

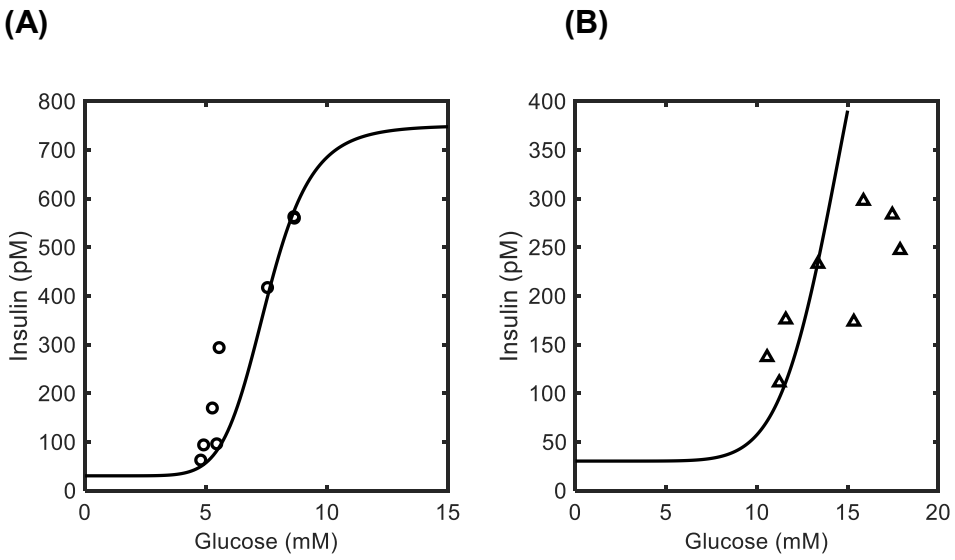

Figure S3 Experimental verification of the simulated insulin response by the pancreas module, Related to Figures 3 and 6

The plasma insulin and glucose concentrations were measured for healthy and T2DM subjects after an overnight fast and following ingestion of 50 g carbohydrate-containing meal. The solid lines indicate the simulated results; the circles and triangles experimental data (Butler and Rizza, 1991).

(A) Healthy subject, Km_inssyn_Glc_B = 7.5 mM.

(B) T2DM subject, Km_inssyn_Glc_B = 11.25 mM. An increase in Km_inssyn_Glc_B well expressed T2DM with β-cell dysfunction.

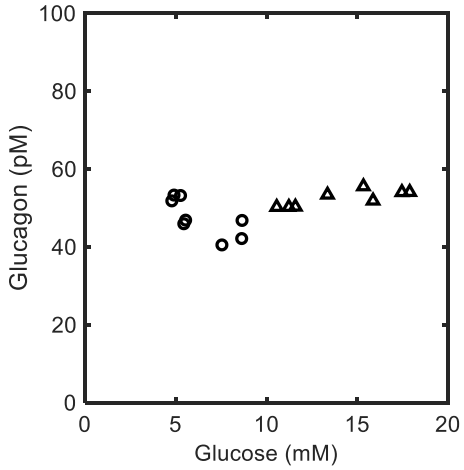

Figure S4 Experimental data of glucagon response to a change in plasma glucose, Related to Figure 2

The plasma glucagon and glucose concentrations were measured for healthy and T2DM subjects after an overnight fast and following ingestion of 50 g carbohydrate-containing meal. The circles (○) indicated the experimental data of healthy subjects; the triangles (△) that of T2DM subjects (Butler and Rizza, 1991).

The experimental glucagon concentration tended to decrease with an increase in plasma glucose for the healthy subject. The glucagon response of T2DM subjects definitely shifted toward a high plasma glucose concentration in the same manner as the insulin response, suggesting that the glucagon response for T2DM becomes insensitive to a change in plasma glucose.

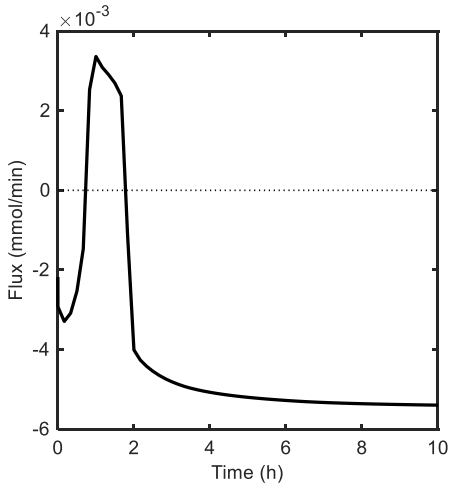

Figure S5 Time course of the G3PD flux in the liver, Related to Figure 3 and Figure S1A

The G3PD flux was simulated after an overnight fast and following a single meal of 87 g carbohydrate and 33 g fat (Time = 0).

The computational model demonstrated the switching of the G3PD reaction, which reflects the remarkable shift from glucose uptake to gluconeogenesis. Negative values show the reaction from Grp to Gap, promoting gluconeogenesis. Positive values show the reaction from Gap to Grp, promoting TG synthesis.

Experimental verification of insulin resistance (IR) in the whole body

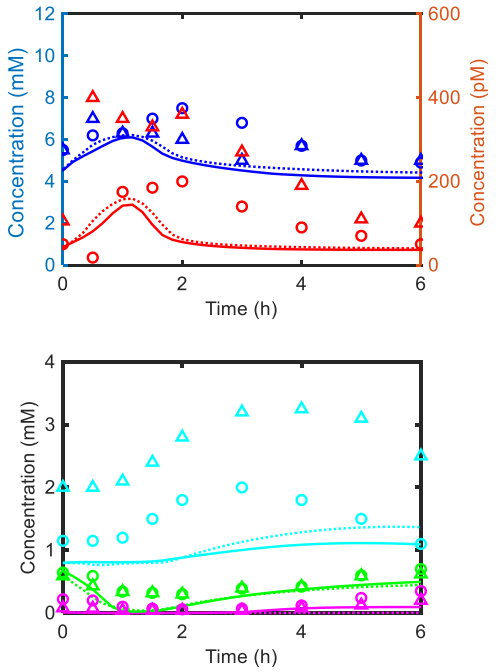

Figure S6 Experimental verification of the simulated time-course of plasma metabolite concentrations of healthy and IR subjects, Related to Figures 3 and 6

IR was built by a combination of insulin resistance for liver (IRL), IR for skeletal muscle (IRM), and IR for adipose tissue (IRA). The time course data of plasma glucose, insulin, β-hydroxybutyrate (Bhb), FFA and TG were measured for 10 healthy subjects and 10 IR subjects (Bickerton et al., 2008). Serial blood samples were taken for 6 h after an overnight fast and following ingestion of a mixed meal containing 40 g carbohydrate and 40 g fat (Time = 0).

Table Legend

metabolite	method	healthy	IR	axis
plasma insulin	simulation	———	----------	right
	experiment	○	△	right
plasma glucose	simulation	———	----------	left
	experiment	○	△	left
plasma TG	simulation	———	----------	
	experiment	○	△	
plasm FFA	simulation	———	----------	
	experiment	○	△	
plasma Bhb	simulation	———	----------	
	experiment	○	△	

This figure verified whether the computational model reproduces the time course of plasma glucose, insulin, Bhb, FFA and TG for healthy and insulin resistance (IR) subjects. The computational model captured the experimental features (Bickerton et al., 2008).:

(1) IR increased plasma insulin.

(2) IR a little increased plasma glucose and plasma TG.

(3) IR decreased plasma Bhb.

Experimental verification of mild T2DM and severe T2DM in the whole body

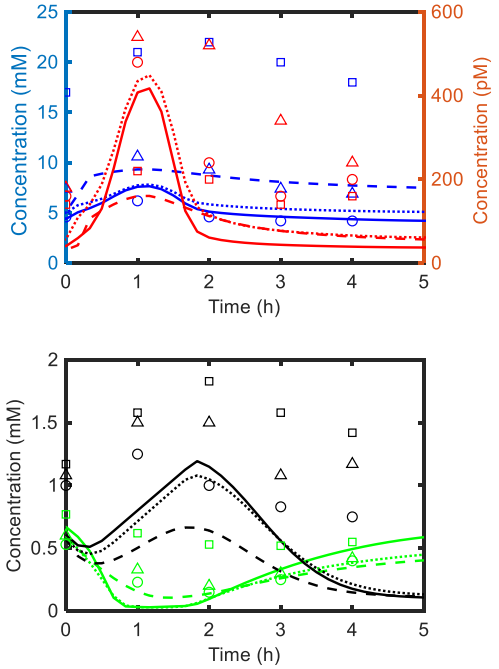

Figure S7 Experimental verification of the simulated time-course of plasma metabolite concentrations of healthy, mild T2DM and sever T2DM subjects, Related to Figures 3 and 6

The time course of plasma insulin, glucose, lactate, and FFA were measured for 9 healthy subjects, 9 mild T2DM, and 9 severe T2DM subjects after an overnight fast and following a meal containing 53 g carbohydrate and 22 g fat (Time = 0) (Reaven et al., 1988).

Table Legend

metabolite	method	healthy	mild T2DM	sever T2DM	axis
plasma insulin	simulation	———	·····	– – –	right
	experiment	○	△	□	right
plasma glucose	simulation	———	·····	– – –	left
	experiment	○	△	□	left
plasma lactate	simulation	———	·····	– – –	
	experiment	○	△	□	
plasm FFA	simulation	———	·····	– – –	
	experiment	○	△	□	

This figure investigated whether the computational model reproduced the T2DM-changed time course of plasma glucose, insulin, lactate, and FFA for healthy, mild T2DM and sever T2DM.

In the computational model, the mild T2DM was built by a combination of IRL, IRM, and IRA; the severe T2DM was constructed by adding β-cell dysfunction to the mild T2DM.
The simulation model reproduced the experimental features (Reaven et al., 1988):
(1) the plasma insulin increased for mild T2DM, while it greatly decreased for severe T2DM due to β-cell dysfunction.
(2) the plasma glucose increased in the order of healthy, mild T2DM, and severe T2DM.
(3) the severe T2DM loosened the dent of the plasma FFA.

Computational verification of the liver module

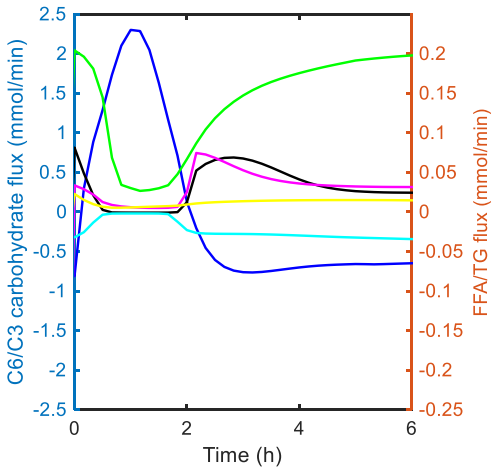

Figure S8 Time course of the exchange fluxes of plasma metabolites between the liver and blood for healthy subjects, Related to Figure 3 and Figure S1A

The metabolite uptake and release fluxes were simulated after an overnight fast and following a single meal of 87 g carbohydrate and 33 g fat (Time = 0). Negative values show the release into plasma.

Legend table

metabolite	method	healthy	axis
glucose uptake	simulation		left
lactate uptake	simulation		left
alanine uptake	simulation		left
glycerol uptake	simulation		left
FFA uptake	simulation		right
TG uptake	simulation		right

This figure indicated the remarkable metabolic shift in the liver. After a meal on Time=0, the glucose uptake flux rapidly increased, while the FFA/lactate/alanine uptake and TG release dramatically decreased, indicating substrate accumulation status. At postabsorptive state, the glucose/TG release increased; the FFA uptake increased; the lactose/alanine/glycerol uptake increased for gluconeogenesis. The liver took up lactate, alanine and glycerol to produce hepatic glucose through gluconeogenesis and to release the glucose into plasma. The resulting glucose was utilized by skeletal muscle and adipose tissue to release alanine and lactose (Figure 3). This indicated that glucose-lactose and glucose-alanine cycles function.

Experimental verification of the liver module

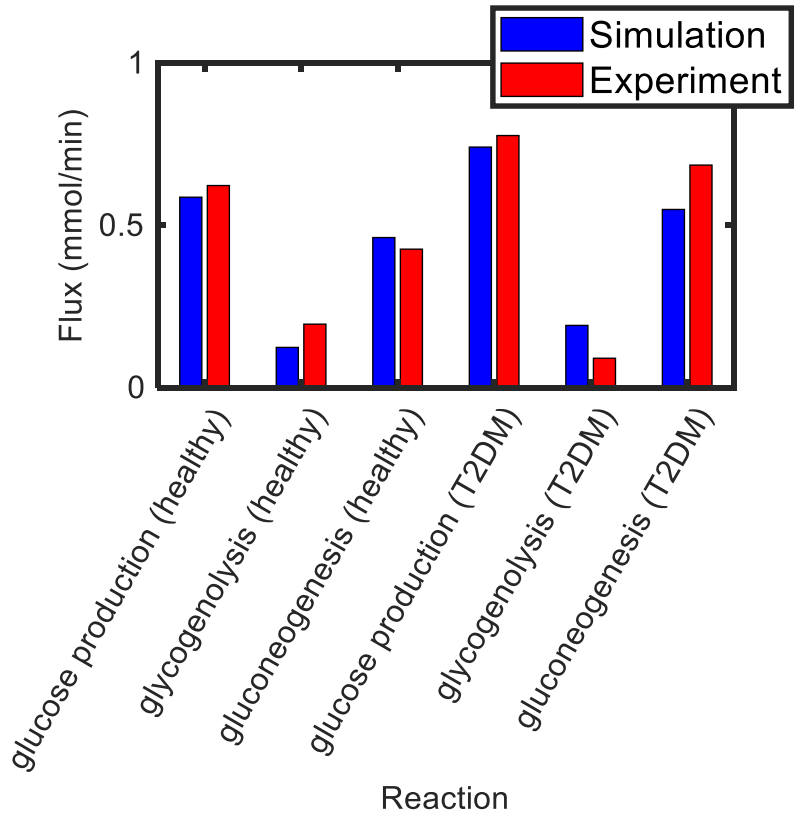

Figure S9 Hepatic glucose production, glycogenolysis, and gluconeogenesis at postabsorptive state for healthy and T2DM subjects, Related to Figure 6 and Figure S1A

These metabolic fluxes were measured and simulated for five healthy subjects and seven T2DM subjects after an overnight fast and following a single meal of 98 g carbohydrate and 17 g fat (Magnusson et al., 1992). The blue bar indicates the simulation results; the red the experimental data.

This figure investigated whether the computational model reproduced the hepatic glucose production, gluconeogenesis and glycogenolysis fluxes for healthy and T2DM subjects. The computational model captured some important features of the experimental data (Magnusson et al., 1992):

(1) the T2DM increased the total glucose production and gluconeogenesis fluxes,

(2) the gluconeogenesis played a major role in glucose production compared to the glycogenolysis.

Experimental verification of the skeletal muscle module

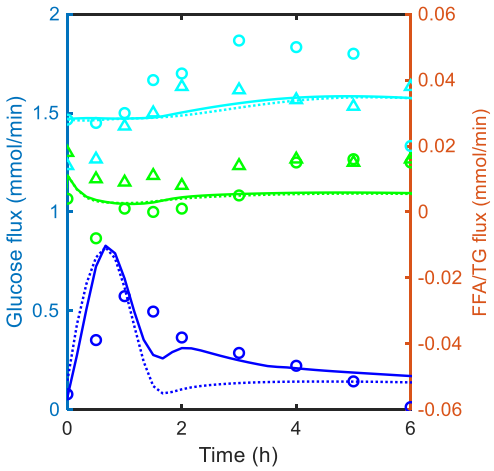

Figure S10 Time course of glucose, FFA and TG uptake fluxes in the skeletal muscle, Related to Figures 3 and 6, and Figure S1B

The glucose uptake flux was measured for 6 h after an overnight fast and following ingestion of a mixed meal containing 87 g carbohydrate and 33 g fat 8 healthy subjects (Frayn et al., 1993). The FFA and TG uptake fluxes were measured for 6 h after an overnight fast and following ingestion of a mixed meal containing 40 g carbohydrate and 40 g fat for 10 healthy subjects and 10 IR subjects (Bickerton et al., 2008).

Legend table

flux	method	healthy	IR	axis
glucose uptake	simulation	———	----------	left
	experiment	○	NA	left
FFA uptake	simulation	———	----------	right
	experiment	○	△	right
TG release	simulation	———	----------	right
	experiment	○	△	right

This figure investigated whether the computational model reproduced the uptake fluxes of glucose, FFA and TG by the skeletal muscle for healthy and T2DM subjects. The computational model captured some important experimental features: an insulin-induced peak response of the glucose uptake flux and the levels of glucose, FFA and TG uptake fluxes.

Experimental verification of the adipose tissue module

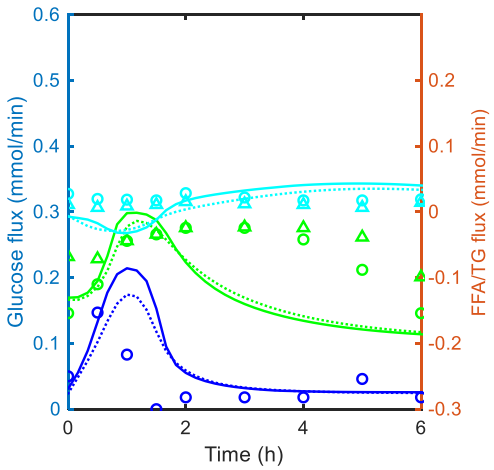

Figure S11 Time course of glucose, FFA and TG uptake fluxes in adipose tissue, Related to Figures 3 and 6, and Figure S1C

The glucose uptake flux was measured for 6 h after an overnight fast and following ingestion of a mixed meal containing 87 g carbohydrate and 33 g fat 8 healthy subjects (Frayn et al., 1993). The FFA and TG uptake fluxes were measured for 6 h after an overnight fast and following ingestion of a mixed meal containing 40 g carbohydrate and 40 g fat for 10 healthy subjects and 10 IR subjects (Bickerton et al., 2008).

Legend table

flux	method	healthy	IR	axis
glucose uptake	simulation	———	----------	left
	experiment	○	NA	left
FFA uptake	simulation	———	----------	right
	experiment	○	△	right
TG release	simulation	———	----------	right
	experiment	○	△	right

This figure investigated whether the computational model reproduced the uptake fluxes of glucose, FFA and TG by adipose tissue for healthy and T2DM subjects. The computational model captured the important experimental features: the insulin-induced peak response of the glucose uptake flux and the levels of the FFA and TG uptake flux after the meal. The computational model showed an insulin-induced peak response of FFA and TG, while the experimental data showed a gradual response. It suggests some hidden mechanisms of FFA and TG exchanges in adipose tissue.

Computational simulation of the GI module

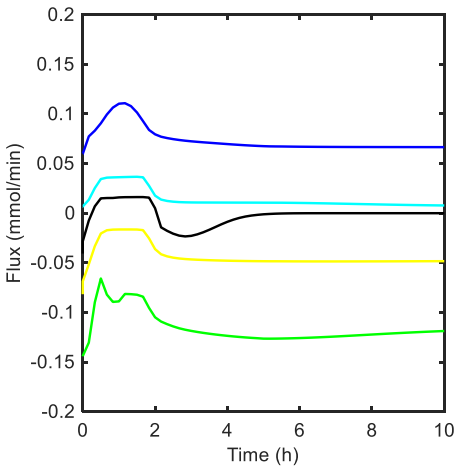

Figure S12 Time course of glucose, lactate, glycerol, FFA, and TG exchange fluxes in the GI tract, Related to Figure 3 and Figure S1D

The time courses of these exchange fluxes were simulated after an overnight fast and following a single meal of 87 g carbohydrate and 33 g fat for a healthy subject. A negative value of the flux indicates the release into plasma. The experimental data is not available.

Legend table

metabolite	method	healthy
glucose uptake	simulation	
lactate uptake	simulation	
glycerol release	simulation	
FFA release	simulation	
TG uptake	simulation	

After a meal on 0 h, the glucose and TG uptake increased due to insulin action and their increased plasma concentrations (Figure 3); the FFA and glycerol release decreased because they were utilized for TG synthesis. According to the previous model (Kim et al., 2007; Pan and Hussain, 2012), the computational model assumed that the GI degrades accumulated TG in its cytoplasm into FFA and glycerol to release them into plasma (Kim et al., 2007).

Computational simulation of the heart module

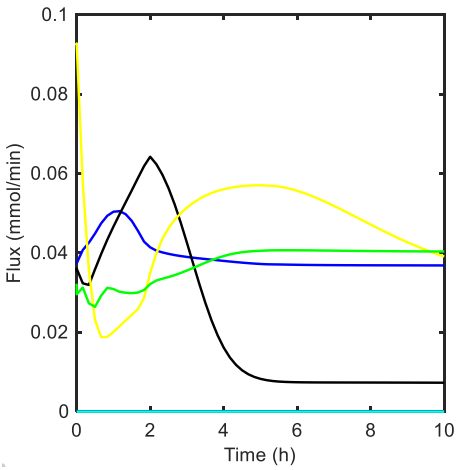

Figure S13 Time course of glucose, lactate, glycerol, FFA, and TG uptake fluxes in heart, Related to Figure 3 and Figure S1E

The time courses of these metabolite uptakes were simulated after an overnight fast and following a single meal of 87 g carbohydrate and 33 g fat for a healthy subject.

Legend table

metabolite	method	healthy
glucose uptake	simulation	
lactate uptake	simulation	
glycerol uptake	simulation	
FFA uptake	simulation	
TG uptake	simulation	

The heart took up plasma glucose, lactate, glycerol, and FFA. After a meal on 0 h, the glucose and lactate uptake increased due to their increased plasma concentrations (Figure 3); the FFA and glycerol uptake decreased due to their decreased plasma concentration.

Computational simulation of the brain module

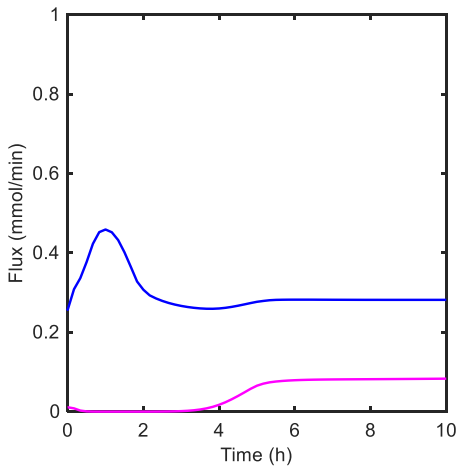

Figure S14 Time course of glucose and Bhb uptake fluxes in the brain, Related to Figure 3 and Figure S1F

The time courses of glucose and Bhb uptak were simulated after an overnight fast and following a single meal of 87 g carbohydrate and 33 g fat for a healthy subject.

Legend table

metabolite	method	healthy
glucose uptake	simulation	
Bhb uptake	simulation	

The brain utilized the plasma glucose and liver-produced Bhb. After a meal on 0 h, the glucose uptake increased due to its increased plasma concentration. The Bhb uptake occurred late, because its synthesis by the liver needs some fasting conditions.

Compuataional simulation of plasma glucose, Bhb and FFA concentration under a fasted condition

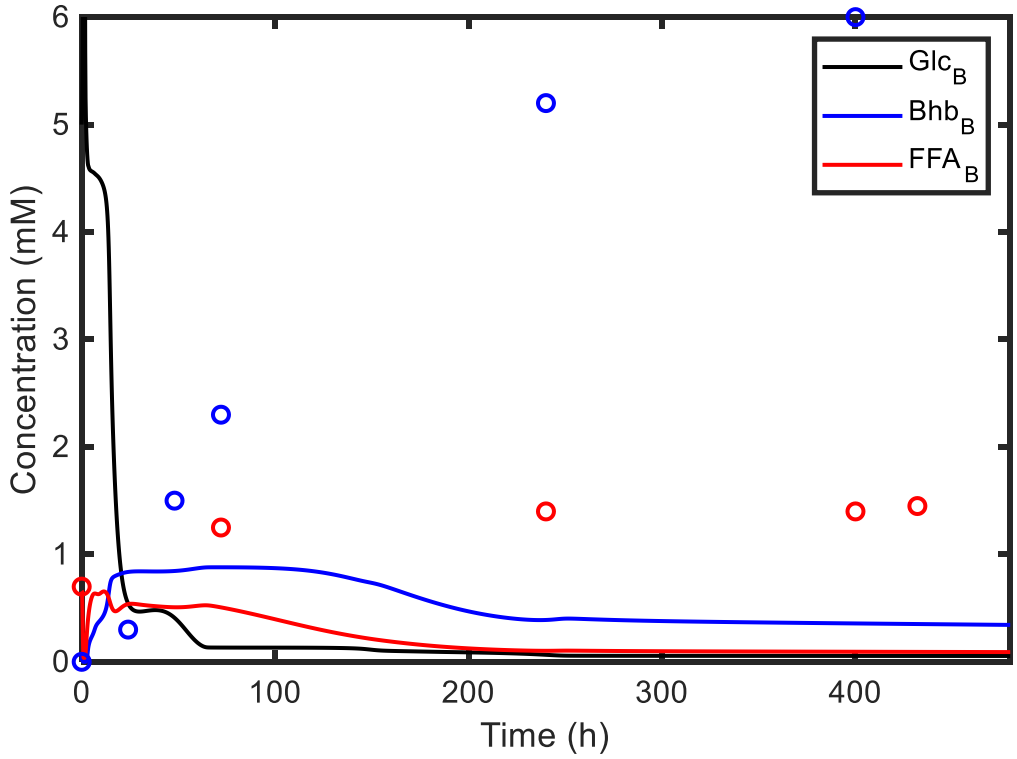

Figure S15 Time-course of plasma glucose, Bhb and FFA concentrations under a fasted condition, Related to Figure 5

The proposed model was simulated during 480 h after an overnight fast and following a single meal of 87 g glucose and 33 g fat. The blue circles and blue lines indicate the experimental and simulated concentrations of plasma Bhb, respectively. The red circles and red lines indicate the experimental and simulated concentrations of plasma FFA, respectively. The black line indicates the plasma glucose concentration.

Computational simulation of metformin administration

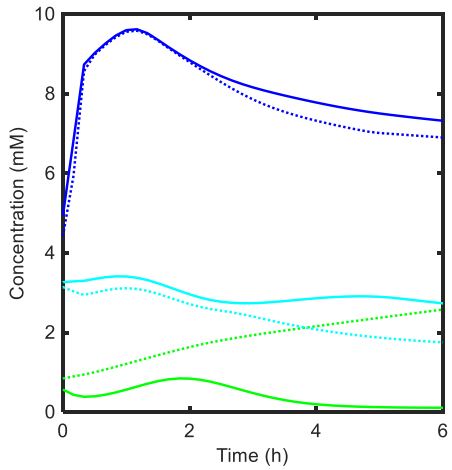

Figure S16 Effect of metformin on metabolite concentrations of a T2DM model, Related to Figure 7

Time courses of the concentration of plasma glucose, lactate and hepatic TG for T2DM and T2DM with metformin were simulated after an overnight fast and following a single meal of 87 g carbohydrate and 33 g fat. The LDH inhibition by metformin administration is provided by Vmax_ldh_Pyr_L = 0.

Legend table

metabolite	method	T2DM	T2DM+metformin
plasma glucose	simulation		
plasma lactate	simulation		
hepatic TG	simulation		

The LDH inhibition by metformin decreased plasma glucose and hepatic TG, while increasing plasma lactate.

References

Bickerton, A.S., Roberts, R., Fielding, B.A., Tornqvist, H., Blaak, E.E., Wagenmakers, A.J., Gilbert, M., Humphreys, S.M., Karpe, F., and Frayn, K.N. (2008). Adipose tissue fatty acid metabolism in insulin-resistant men. Diabetologia *51*, 1466-1474.

Butler, P.C., and Rizza, R.A. (1991). Contribution to postprandial hyperglycemia and effect on initial splanchnic glucose clearance of hepatic glucose cycling in glucose-intolerant or NIDDM patients. Diabetes *40*, 73-81.

Frayn, K.N., Coppack, S.W., Humphreys, S.M., Clark, M.L., and Evans, R.D. (1993). Periprandial regulation of lipid metabolism in insulin-treated diabetes mellitus. Metabolism *42*, 504-510.

Harrison, D.E., Christie, M.R., and Gray, D.W. (1985). Properties of isolated human islets of Langerhans: insulin secretion, glucose oxidation and protein phosphorylation. Diabetologia *28*, 99-103.

Kim, J., Saidel, G.M., and Cabrera, M.E. (2007). Multi-scale computational model of fuel homeostasis during exercise: effect of hormonal control. Ann Biomed Eng *35*, 69-90.

Magnusson, I., Rothman, D.L., Katz, L.D., Shulman, R.G., and Shulman, G.I. (1992). Increased rate of gluconeogenesis in type II diabetes mellitus. A 13C nuclear magnetic resonance study. J Clin Invest *90*, 1323-1327.

Pan, X., and Hussain, M.M. (2012). Gut triglyceride production. Biochim Biophys Acta *1821*, 727-735.

Reaven, G.M., Hollenbeck, C., Jeng, C.Y., Wu, M.S., and Chen, Y.D. (1988). Measurement of plasma glucose, free fatty acid, lactate, and insulin for 24 h in patients with NIDDM. Diabetes *37*, 1020-1024.